AN ANALYSIS OF THE SOLAR ENERGETIC PARTICLE PROPAGATION OF THE MAXIMUM SOLAR FLARE ON 24TH SOLAR CYCLE.

KARMA TSHERING

A Thesis Submitted to the Graduate School of Naresuan University
in Partial Fulfillment of the Requirements
for the Master of Science in (Physics)
2020

Copyright by Naresuan University

AN ANALYSIS OF THE SOLAR ENERGETIC PARTICLE PROPAGATION OF THE MAXIMUM SOLAR FLARE ON 24TH SOLAR CYCLE.

KARMA TSHERING

A Thesis Submitted to the Graduate School of Naresuan University
in Partial Fulfillment of the Requirements
for the Master of Science in (Physics)
2020

Copyright by Naresuan University

Thesis entitled "An analysis of the solar energetic particle propagation of the maximum solar flare on 24th solar cycle."

By KARMA TSHERING

has been approved by the Graduate School as partial fulfillment of the requirements

for the Master of Science in Physics of Naresuan University

Oral Defense Committee

..... Chair
(Assistant Professor Charuangrit Channok, Ph.D.)

..... Advisor
(Assistant Professor Thiranee Khumlumlert, Ph.D.)

..... Internal Examiner
(Associate Professor Pornrad Srisawad, Ph.D.)

Approved

.....
(Professor Paisarn Muneesawang, Ph.D.)

Dean of the Graduate School

Title AN ANALYSIS OF THE SOLAR ENERGETIC PARTICLE PROPAGATION OF THE MAXIMUM SOLAR FLARE ON 24TH SOLAR CYCLE.

Author KARMA TSHERING

Advisor Assistant Professor Thiranee Khumlumlert, Ph.D.

Academic Paper Thesis M.S. in Physics, Naresuan University, 2020

Keywords solar energetic particles, solar flare, coronal mass ejection, Sun, solar cycle, space weather

ABSTRACT

This research studies the propagation of solar energetic particles (SEPs) from the strongest solar flare in the 24th solar cycle. The particle propagation was simulated for the solar event on September 6, 2017. The X-ray class of the selected solar event is X9.3, the solar flare position on the sun is S10W30, and the solar wind speed is 575 km/s at 12:02 UTC for 17 minutes. We used data from the Solar Isotope Spectrometer instrument on ACE (Advanced Composition Explorer) spacecraft. The propagation of the solar energetic particles was simulated by the Ruffolo (1995, 1998) transport equation and solved by finite different method. The injection duration was estimated by the curve-fitting technique of piecewise-linear least square with the simulated results and the data from spacecraft. The fitting results between the spacecraft data and the simulation results found the mean free path roughly constant for each particle. The element with a small atomic mass such as helium, carbon, oxygen and nitrogen have the larger mean free path as compare to the high atomic mass element iron. The results showed the injection time is from 39-743 minutes, which corresponded to the energy range of particles. The coronal mass injection was detected at the end time of this flare that affects in increasing the injection time. This solar event didn't affect the Earth's magnetic field as the value of kp index is 4 at the end of solar flare. The value of kp index has increased to 8 on 7th September, 2017 due to another solar event occurred from same sunspot region.

ACKNOWLEDGEMENTS

The completion of my thesis couldn't have been accomplished without the support of many kind hearted people. In particular, I would like to express my deep and sincere gratitude to my advisor Asst. Prof. Dr. Thiranee Khumlumlert. Her immeasurable support and guidance helped me to carry out the research efficiently without any obstacles. I am thankful to my friend Mrs. Dechen Peldon, MS.c Physics, Naresuan university for her frequent help and support.

I am very grateful to Professor Dr. David Ruffolo, Department of Physics, Mahidol University, for the transport equation and simulation program used in this research. I also would like to thank Thailand International Cooperation Agency (TICA) and Royal Government of Bhutan for supporting the budget for this research. Nevertheless, I would like to thank staffs in department of Physics, Naresuan university for necessary documentation and encouragement.

KARMA TSHERING

TABLE OF CONTENTS

Page

ABSTRACT C

ACKNOWLEDGEMENTS ..... D

TABLE OF CONTENTS ..... E

List of tables ..... H

List of figures I

CHAPTER I INTRODUCTION 1

1.1 Background and Significance of the Study 1

1.2 Research objectives 2

1.3 Scope of the Study 2

1.4 Research operation guidelines 2

1.5 Operation plan 3

1.6 Expected Benefits 4

1.7 Related Works and Studies 4

CHAPTER II THEORY AND RESEARCH RELATED 7

2.1 The structure of the Sun 7

2.1.1 The Sun is divided into three layers which are; 7

2.1.2 The atmosphere of the Sun is divided into 3 layers which are; 8

2.2 Solar flare 8

2.3 Solar Cycle 11

2.4 Coronal Mass Ejection (CMEs) 12

2.5 Spiral magnetic field 13

2.6 Data analysis of high energy particles from solar eruption 19

2.7 Transport equations that describe the motion of high energy particles 20

2.8 ACE (Advanced Composition Explorer) spacecraft 42

2.9 Time profile of injection near the Sun 45

CHAPTER III METHODOLOGY 48
3.1 Tools used in research operations 48
3.1.1 Data from the ACE spacecraft 48
3.1.2 Program written in C++ for the simulation of particle motion from Ruffolo's transport equation 48
3.2 Numerical methods used in research operations 49
3.2.1 explicit method 51
3.2.2 Implicit methods 53
3.2.3 Crank-Nicolson method 54
3.3 Study of solar eruptions to select the solar event 55
3.4 Download basic information collected from the ACE spacecraft 59
3.4.1 Go to website www.srl.caltech.edu/ACE 59
3.4.2 Select Online Data to access the online data download. 60
3.4.3 Select Level 2 (Verified) the type of measuring instrument 60
3.4.4 Select SIS Data to select the data from the instrument SIS 61
3.4.5 Select SIS Data to select data from the instrument SIS 61
3.4.6 Select the required element for simulation. 62
3.5 Procedure for preparing data from the spacecraft for simulation 63
3.5.1 Determination of the data error due to spacecraft 63
3.5.2 Determination of the true mass of each particle. 65
3.5.3 Determination of the average energy value for each energy level (E_K) ... 66
3.5.4 Determination of the distance of the magnetic field lines drawn by the solar wind (R) 66
3.5.5 Determination of the distance between the position of the spacecraft and the Sun (USERR) 67
3.5.6 Determination of the momentum of energy levels for each element 67
3.5.7 Determination of the ratio of solar wind speed to light speed 67
3.5.8 Determination of the Spectrum 67
3.5.9 Determination of the constant value for the particle decay. 68

3.5.10 Determination of the maximum distance of particles in each energy level from the relationship.....68
3.6 Simulation of particle motion and fitting data.....70
3.7 Fit to compare data.....70
3.8 Determine the period of release of particles.....71
3.9 Space condition analysis.....73
CHAPTER IV RESULT ANALYSIS.....75
4.1 The simulation result for the SEP propagation.....75
4.2 Distribution simulation of particles over time at average mean free path λ.....76
4.3 Comparison fitting between the spacecraft data and simulation result.....77
CHAPTER V CONCLUSION.....90
REFERENCES.....92
APPENDIX.....93
BIOGRAPHY.....104

List of tables

Page

Table 1 Action plan.....3

Table 2 The classification of solar flare.....10

Table 3 Description of each term of transport equation.....42

Table 4 Physical characteristics of the event on 6 September 2017.....56

Table 5 Shows an example of data measured from the SIS instruments on the ACE spacecraft of helium particle erupted on 6th September 2017.....64

Table 6 Energy value of element He.....66

Table 7 Shows the values in the data preparation process for the element Fe.....69

Table 8 Data for the solar eruption in September.....73

Table 9 The potential impact of solar activity on the kp index.....74

Table 10 The simulation results of helium, carbon, oxygen, nitrogen and iron. 87

List of figures

Page

Figure 1 Structure of the Sun 7

Figure 2 The eruption on the Sun's surface 9

Figure 3 The number of Sunspots on the Sun between 2008-2019 for 24th solar cycle. 12

Figure 4 Eruption of corona mass ejection 13

Figure 5 Spherical Coordinates 14

Figure 6 Shows the characteristics of the magnetic field that emits from the Sun in a spherical coordinate. 16

Figure 7 Early diffusion of particles 19

Figure 8 Later diffusion of the particles 20

Figure 9 Examples of mean free path of high-energy particles that can move before scattering due to the change of the magnetic field lines, with particle A having less mean free path than particle B. 20

Figure 10 Systematic flux conduction 21

Figure 11 Random flux conduction 22

Figure 12 Shows the pitch angle θ between the velocity of the particle and magnetic field line direction. 23

Figure 13 Fixed reference frame 25

Figure 14 Solar wind reference frame. 25

Figure 15 The characteristics of magnetic field lines. 26

Figure 16 The relation of perpendicular velocity and parallel velocity to magnetic field lines 28

Figure 17 The magnetic field acting on the radial line from the Sun 31

Figure 18 Advance Composition Explorer Spacecraft (ACE) 43

Figure 19 Solar Isotope Spectrometer 44

Figure 20 Illustration of the deconvolution technique for a piecewise linear injection function near the Sun. The transport equation is solved for an instantaneous injection of particles. The resulting Green's function is convolved with (a) triangular injection profiles to (b) yield response functions. Linear, least squares fitting yields (d) the linear combination of response functions that best fits the data and (c) the corresponding best-fit piecewise linear injection profile 47

Figure 21 Flow of particles through cells 50

Figure 22 The solar eruption on 6th September, 2017 56

Figure 23 X-ray severity values on 6th September 2017 57

Figure 24 Shows the X-ray emission eruption from 4-6 September 2017. 58

Figure 25 The graph showing the solar wind speed on 6th September 2017. 58

Figure 26 Homepage www.srl.caltech.edu/ACE 59

Figure 27 Homepage www.srl.caltech.edu/ACE 60

Figure 28 Shows a page for Online Data 60

Figure 29 Shows a page level 2 (Verified) measurement tools for research 61

Figure 30 Shows the date range setting for the data to be studied 61

Figure 31 Website page that can choose to download only the desired information. . 62

Figure 32 Shows an example of the He element downloaded from SIS. 63

Figure 33 The density of He particles related with time 64

Figure 34 The graph shows the relationship between momentum log values and flux spectrum log values of He Particle. 68

Figure 35 Shows a graph of the relationship between $x2$ and the mean free path 71

Figure 36 Shows the injection profile of helium at an energy level of 4.032 MeV/n. 71

Figure 37 shows the kp index value on 6-8 September 2017. 74

Figure 38 The simulation results of carbon particles distribution over time at different energy levels from 7.443– 28.883 MeV/n. 75

Figure 39 Simulation result of carbon particle distribution at various mean free path on a 12.267 MeV/n energy level 76

Figure 40 Shows the spacecraft data of He at 4.032 MeV/n for the solar event on 6th September, 2017. 77

Figure 41 Shows the simulation result of He at 4.032 MeV/n for the solar event on 6th September, 2017. 77

Figure 42 Shows the simulation result of He at 4.032 MeV/n for the solar event on 6th September, 2017. 78

Figure 43 Shows the injection profile of He at 4.032 MeV/n for the solar event on 6th September, 2017. 78

Figure 44 Shows the spacecraft data of C at 7.443 MeV/n for the solar event on 6th September, 2017. 79

Figure 45 Shows the simulation result of C at 7.443 MeV/n for the solar event on 6th September, 2017. 79

Figure 46 Shows the fitting result of C at 7.443 MeV/n for the solar event on 6th September, 2017. 80

Figure 47 Shows the injection profile of C at 7.443 MeV/n for the solar event on 6th September, 2017. 80

Figure 48 Shows the spacecraft data of O at 8.538 MeV/n for the solar event on 6th September, 2017. 81

Figure 49 Shows the simulation result of O at 8.538 MeV/n for the solar event on 6th September, 2017. 81

Figure 50 Shows the fitting result of O at 8.538 MeV/n for the solar event on 6th September, 2017. 82

Figure 51 Shows the injection profile of O at 8.538 MeV/n for the solar event on 6th September, 2017. 82

Figure 52 Shows the spacecraft data of N at 8.009 MeV/n for the solar event on 6th September, 2017. 83

Figure 53 Shows the simulation result of N at 8.009 MeV/n for the solar event on 6th September, 2017. 83

Figure 54 Shows the fitting result of N at 8.009 MeV/n for the solar event on 6th September, 2017. 84

Figure 55 Shows the injection profile of N at 8.009 MeV/n for the solar event on 6th September, 2017. 84

Figure 56 Shows the spacecraft data of Fe at 13.002 MeV/n for the solar event on 6th September, 2017. 85

Figure 57 Shows the simulation result of Fe at 13.002 MeV/n for the solar event on 6th September, 2017. 85

Figure 58 Shows the fitting result of Fe at 13.002 MeV/n for the solar event on 6th September, 2017. 86

Figure 59 Shows the injection profile of Fe at 13.002 MeV/n for the solar event on 6th September, 2017. 86

Figure 60 Best mean free path of He, C, O, N and Fe at various energy range of the solar event on September 6,2017. 88

Figure 61 Injection time of He, C, O, N and Fe at various energy range of the solar event on September 6,2017..... 89

CHAPTER I
INTRODUCTION

1.1 Background and Significance of the Study

The life on the Earth is exclusive influenced by the phenomenon of the Sun's activities. The Sun is spontaneously emitting the steam of charged particles in the form of electromagnetic waves and high energy particles to the Earth. The eruption on the Sun will occur more or less in accordance with the solar cycle. If the eruption is larger or more violent than normal phenomena it is referred as solar flare that releases energy in many forms such as X-ray and radiation of other radio wave including cosmic rays. This phenomenon is likely to occur most often in the middle of the solar cycle.

The solar cycle or one cycle of the Sun is approximately 11 years and currently we are in the 25th cycle (2019-2030). The eruptions will occur near dark spots where magnetic fields are unstable causing solar storms with the release of high energy particles. These particles are charged particles moving in a spiral magnetic field (Archimedean spiral magnetic field) allows high-energy particles from the Sun to move along the magnetic field into the Earth. If the Sun's eruption is violent, it may damage the satellite, can disrupt radio transmission line facilities and electrical line facilities resulting in potentially massive and long- lasting power outages.

Therefore, this research study the physical characteristics of the solar event and eruptions on the Sun's surface including the analysis of the motion of high energy particles from the Sun by using the distribution data obtained from the Advanced Composition Explorer (ACE) spacecraft. The study is mainly focused on the solar event on 6th September 2017 because, it is a violent event based on the X-rays intensity of X9.3 at 12:02 UTC and it is the strongest solar flare of the 24th solar cycle. The research analysis the helium, carbon, oxygen, nitrogen and iron elements and simulates particle motion with transport equation and solve the motion equation by

using the numerical methods written in the C++ programming on the Ubuntu operating system. So that, we can analyze the timing of high energy particles released from the Sun to Earth and compare with actual time of eruption. Therefore, such data are used to predict and warn about space conditions to reduce the damage that caused by the high energy particles moving from Sun to Earth.

1.2 Research objectives

- To study the physical characteristics of strongest solar flare erupted at the solar minimum on 24th Solar cycle and its space environment.
- To download the data of high energetic particles recorded by ACE (Advanced Composition Explorer) spacecraft on 6th September 2017 and prepare for the simulation.
- To simulate the propagation of high energy particle coming from the Sun to Earth with the equation of motion and solve problem using numerical methods in Ubuntu operating system.
- To calculate and compare the injection time of particles between simulation and actual value.

1.3 Scope of the Study

- This research studies the physical characteristics of the solar energetic particle from the violent solar flare.
- The simulation of the propagation of the high energetic particle that are erupted on 6th September, 2017.
- The data obtained from ACE spacecraft is used to simulate with transport equations written in C++ programming to analyze the time for particles erupted and compare with the actual eruption.

1.4 Research operation guidelines

- Study the theoretical background and research related to the 24th solar cycle and the movement of high energetic particles.

- Study of research related to the movement of high energy particles from the Sun and changes that occur in the solar cycle.
- Select the event of the eruption of high energetic particles that occur during the 24th cycle and get information on the distribution of high energetic particles from the ACE spacecraft and the information necessary to use in the simulation.
- Simulate particle motion with transport equations using a program written in C language on the Ubuntu operating system.
- Analyze the data obtained from simulations and compare with the actual data from spacecraft.
- Summary, analyze the findings and write a thesis book.

1.5 Operation plan

Table 1 Action plan

Activities	Month																	
	1	2	3	4	5	6	7	8	9	10	11	12	13	14	15	16	17	18
Study background of the thesis and selection of topic.	✓	✓	✓	✓	✓	✓	✓											
Study of research related to the movement of high energy particles from the Sun and changes that occur in the solar cycle.					✓	✓	✓	✓	✓									
Simulate the transport of particles and fitting the data in C language on the Ubuntu operating system.							✓	✓	✓	✓	✓	✓						
Analyze the data obtained from simulations and actual data from spacecraft.										✓	✓	✓	✓	✓				
Summary, analyze the findings and write a book.													✓	✓	✓	✓	✓	✓

1.6 Expected Benefits

- Gain knowledge about the physical characteristics of the Sun's eruption and the release of high energetic particles.
- Understand and explain the movement of high energetic particles by transport equation and the use of numerical methods to solve physics problems.
- State the effect of the high energetic particles on earth due to eruption on the Sun.
- Gain skills in using computers to solve physics problems and knowledge on operating C++ programming.

1.7 Related Works and Studies

Relativistic proton levels from region AR 12673 (GLE#72) and the heliospheres current sheet as a Sun − earth magnetic connection (Augusto et al., 2018). The study is about the solar event on 10th September 2017, an X8.2-class which was the second strongest solar flare in the 24th solar cycle. The solar flare erupted from the active region AR 12673 when it was located at the edge of the west solar disks. The research present five solar blasts that has happened at the western edge of the solar limb, three of them from the active region 12673 at the time of the blast which was no longer seen from the Earth and two cases where the SEPs and HCS structures are correlated. When Earth crosses the HCS sector, a fraction of these particles can reach Earth with a harder energetic particle flux, triggering a ground-level enhancement (GLE). The signals detected by spacecraft detectors on 10th September 2017 correspond to two different phases of the solar flare. The energy released during the impulsive phase of the flare, was observed as an increase of gamma rays and hard X-rays registered by the RHESSI and Fermi GBM and peaking at ~ 15:57 UT. While the energy released in the gradual phase of the flare was observed as an increase of soft X-rays registered by GOES and peaking at 16:06 UT. The proton particles from the Sun are accelerated by shockwaves to a speed of about 948 km/s. This means that SEPs propagation and HCS are closely related.

The solar energetic particle propagation of solar flare events on 24th solar cycle., J. Phys.: Conf. Ser. 901, 012016 (Paluk, Khumlumlert, Kanlayaprasit, & Aiemsa-ad, 2017). They studied about the violent explosion at the solar atmosphere and releases the high energy ion from the Sun to the interplanetary medium. The particle scattering is approximately energy independent, but the level of scattering varies with time. The selected solar flare events are on August 9, 2011, January 27, 2012, and November 3, 2013 in 24^{th} solar cycle. The transport equation of SEPs was solved by the numerical technique of finite different method in the C program by using the data for each solar flare was obtained from SIS instrument on ACE spacecraft. It is found that mean free path is roughly constant for each event but there are some fluctuations. Overall, the injection duration of the higher energy is shorter than the lower energy particles. The injection duration time from the data fitting of the solar event is more than the injection time from spacecraft because of the irregularity of the magnetic field from the Sun to the Earth affects the particle propagation.

Solar Flares, CMEs and Solar Energetic Particle Events during Solar Cycle 24. Advances in Space Research (Pande, Pande, Chandra, & Mathpal, 2018). The study is about the emission of solar energetic particle in the year 2010 - 2014 which is obtained from the satellites GOES and SOHO/ERNE (Energetic and Relativistic Nuclei and Electron) for proton intensity greater than 1 pfu and less than equal to 1 pfu respectively. The observed SEPs are divided into three categories based on the intensity of proton flux unit(pfu): weak (proton intensity $\leq$ 1 pfu), minor (1 pfu <proton intensity <10 pfu) and major (10 proton intensity 10 pfu). It is found that 54% were major, 29% were minor and 1% SEPs were weak. The majority of SEP events source regions are located in the western hemisphere while some from the eastern part due to the deflection from the radial direction of the eruptions from coronal holes or due to the interaction of CMEs. The study has found that the correlation between X-ray flux and SEP intensity is slow and increased in the correlation between CME speed and SEP intensity.

Deconvolution of interplanetary transport of solar energetic particles, Journal of geophysical research (D Ruffolo, Khumlumlert, & Youngdee, 1998). The study is about the energetic particles produced by solar activity and to apply such state-of-the-art transport simulations and develop semi-automated fitting techniques to accurately determine the injection of particles near the Sun as a function of energy and time as well as the interplanetary scattering mean free path. The techniques for fitting are determined by piecewise linear profile and Reid profile methods using the proton data measured by ISEE3 (International Sun-Earth Explorer 3) on the solar flare events of July 20, 1981 (gradual flare), and January 2, 1982 (impulsive flare). It is found that both deconvolution techniques yielded good fits and consistent result but prefer piecewise profile which takes less time for protons of high energy levels (75-147MeV). This result suggests that release of CMEs from corona can cause shock wave and accelerate the particles about 100MeV after covering certain distance from the Sun.

Analysis of extreme solar activity in early september 2017 (Tassev, Velinov, Tomova, & Mateev, 2017) . The paper analysed the extreme solar activity in early 2017 at minimum of solar cycle 24. It is found that the Active region AR2673 which produced four powerful eruption class X9.3 on 6th September 2017 and severe geomagnetic storm on 7-8 September 2017 with A_p=106. Three space regions are investigated 1. Sun – photosphere and solar corona 2. Interplanetary space with S_w and its basic parameters velocity (V) density (N), Temperature (T_p) and Intensity of magnetic field (B) 3. Earth and its magnetosphere to calculate the solar wind from SOHO and DSCOV space probe in the point of Lagrange, kinetic energy density E_k, thermal energy density E_t and magnetic energy density E_m during 2-15 September 2017. Two interesting phenomena are found which are tunnel effect in the earth's environment and specific distribution of the solar wind energy density during and after the CME. It is likely that both kinetic and magnetic energies can be used as predictors of strong geomagnetic storms.

CHAPTER II

THEORY AND RESEARCH RELATED

2.1 The structure of the Sun

The Sun is the closest star to our planet, about 4.6 x10^9 years old. The Sun is about 1.39 × 10^6 km in diameter, 1.496 × 10^8 km away from Earth and has a mass of 1.989 x 10^{30} kg. The structure of the Sun is divided into 2 parts, which consists of Sun's body and the atmosphere of the Sun as shown in Figure 1.

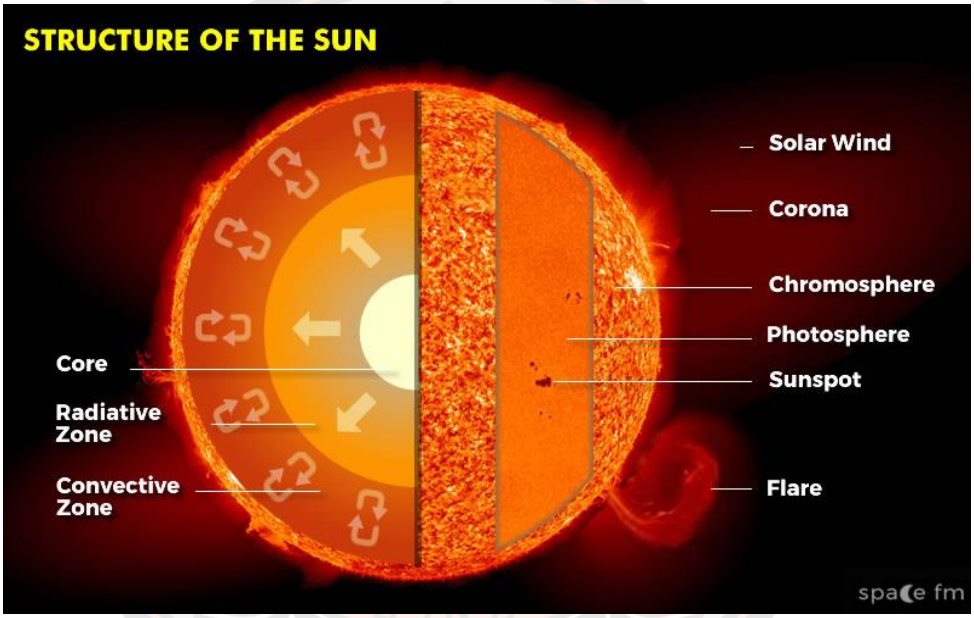

Figure 1 Structure of the Sun

Source: https://www.space.fm/astronomy/EarthmoonSun/structure.html

2.1.1 The Sun is divided into three layers which are;

i. The core or fusion core is at the center of the Sun up to 25% of solar radius. The gravitational force of the Sun causes the mass to compress together until the temperature at the center reaches 1.5 x 10^7 K. The nuclear reaction takes place where it fuses the hydrogen atoms into helium and releases large amount of energy.

ii. The radiative zone is the area of 25-70% of the Sun's radius. The energy generated by nuclear fusion in the core is brought to the upper layer by photon particles.

iii. The convection zone is the outer-most layer of 70-100% of the Sun's radius. The resulting energy cannot directly radiate into space. Since the mass of the Sun is full of hydrogen gas which is moving in a spiral by the convection process, energy from the inside is then released to the surface by the swirling of hot gas.

2.1.2 The atmosphere of the Sun is divided into 3 layers which are;

i. Photosphere is a lower layer of the Sun that we see as a light. It is only 400 km thick and has a temperature of about 5.8 x 10^3 K.
ii. Chromosphere is a middle layer of the Sun with a temperature of almost 2.5x10^4 K. Normally, we cannot see the chromosphere because the lower atmosphere called photosphere is much brighter.
iii. Corona is the uppermost layer with the temperature up to 2x10^6 K. The shape changes according to the magnetic field of the Sun. This atmosphere can be seen only when a full solar eclipse occurs (Learning center for Earth Science and Astronomy, 2020, November 10).

2.2 Solar flare

The solar flares are large explosion of electromagnetic radiation with intense variation in brightness on the Sun lasting from minutes to hours. A solar flare occurs when magnetic energy that has built up in the solar atmosphere is suddenly released. The energy released during a flare is ten million times greater that the energy released from the volcanic explosion. The intensity of solar flare depends on the solar cycle and if the eruption is violent it may damage the satellite, can disrupt radio transmission line facilities and electrical grid. The process of solar flare eruption has 3 stages.

i. The precursor stage is the stage where magnetic energy is triggered. In this phase low energy X- rays (soft X-rays) are radiated.
ii. The impulsive stage is the stage where protons and electrons are accelerated to have kinetic energy greater than 1 million electron volt (MeV). In this phase hard X-rays, radio waves and gamma rays are radiated.

iii. Decay stage is where the gradual builds up and decay of soft x-rays can be detected (Su, 2007).

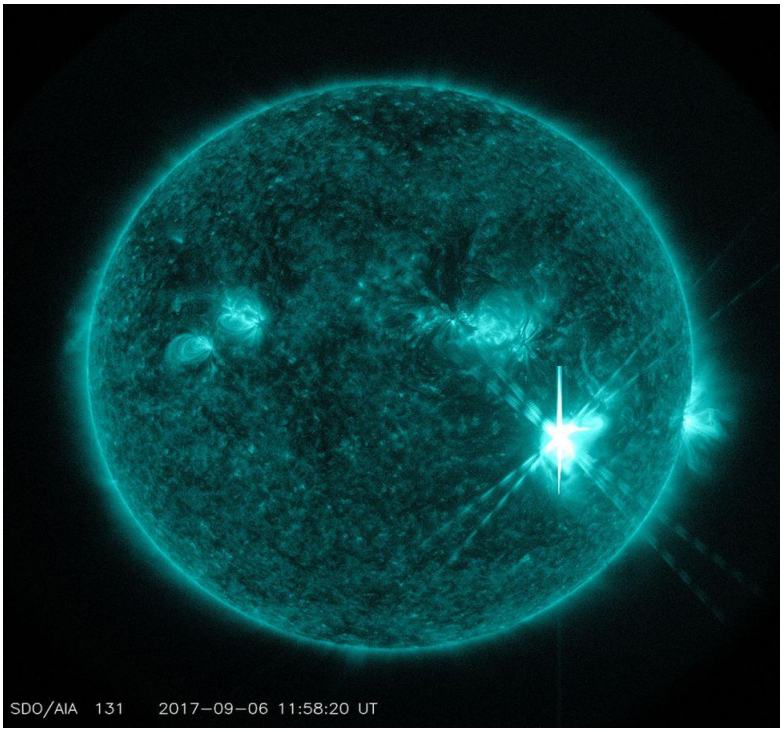

Figure 2 The eruption on the Sun's surface

Source: https://www.space.com/38066-monster-solar-flare-photos-september-2017.html

Solar flares usually take place in active regions, which are areas on the Sun marked by the presence of strong magnetic fields, typically associated with Sunspot groups. As these magnetic fields evolve, they can reach a point of instability and release energy in a various form. These include electromagnetic waves in all frequencies from the waves with long wavelength such as radio waves, light that the human eyes see, X – rays and to the short waves such as gamma rays. Generally, an eruption on the Sun releases at the energy level of 10^{20} J/s and for sever eruption it may reach 10^{25} J/s.

The eruption on the Sun is divided into 2 types owing to its physical characteristics, which are impulsive solar flares and gradual solar flares**.**

i. Impulsive solar flares are the eruptions which release a high amount of electron particles with an eruption duration less than 1 hour. The density of the particles increases rapidly when these particles move through the Earth. The increase in Fe/O and the $^{3}He/^{4}He$ ratios is 4 times the value found in corona and will not release corona mass ejection (CMEs) from the corona layer after the eruption and has normal speed and intensity. As a result, there is no shock wave phenomenon.

ii. Gradual solar flares erupt with the release of high energy particles such as protons. This type of eruption causes accelerating particles in the interplanetary medium, known as corona mass ejection from the corona layer. The solar wind has more speed and intensity than normal until it becomes solar storm. Gradual eruption will take very long time to release the particle which is more than 1hour.

We classify the violent eruption of the solar flares from the intensity of X-ray class as shown in table 2.

Table 2 The classification of solar flare

Eruption (Class)	Intensity (W/m^2)
A	$10^{-8} – 10^{-7}$
B	$10^{-7} – 10^{-6}$
C	$10^{-6} – 10^{-5}$
M	$10^{-5} – 10^{-4}$
X	Greater than 10^{-4}

At each level, the eruption on the Sun may affect the world depending upon intensity as follows;

- X class flare is extremely violent. Most of the radio waves are generated throughout the eruption and have long release period time with the intensity greater than 10^{-4} W/m^2.

- M class flare is a medium level of violence which generally emits short radio waves with the intensity range of 10^{-5} - 10^{-4} W/m^2.
- C class flare is a mild level which doesn't affect the Earth much. The intensity is in the range of 10^{-6}-10^{-5} W/m^2.
- B class flare is very mild level which rarely affect the Earth. The intensity is in the range of 10^{-7} – 10^{-6} W/m^2.
- A class flare is a normal level which doesn't affect the Earth. The intensity is in the range of 10^{-8}-10^{-7} W/m^2 (SpaceWeatherlive.com, 202, November 9).

2.3 Solar Cycle

Solar cycle mainly referred to the cyclic variation of number of Sunspots visible on the photosphere of the Sun. The number of Sunspots increases and decreases over a time in a regular, approximately 11- year cycle, called the solar or Sunspot's cycle. However, the exact length of the cycle can vary from one cycle to the other. More Sunspots may be directly associated with increased solar activity such as solar flares and CMEs. The duration in which highest number of Sunspots in any given cycle are recorded is designated as the solar maximum, while the lowest number is termed as solar minimum. Our Sun is a huge ball of electrically-charged hot gas. This charged gas moves, generating a powerful magnetic field. The Sun's magnetic field goes through a cycle therefore, every 11 years the Sun's magnetic field completely flips which is commonly known as polar field reversal. This means that the Sun's north and south poles switch places. Then it takes about another 11 years for the Sun's north and south poles to flip back again.

The solar cycle affects activity on the surface of the Sun, such as Sunspots which are caused by the Sun's magnetic fields. As the magnetic fields change, so does the amount of activity on the Sun's surface. The giant eruptions on the Sun, such as solar flares and coronal mass ejections also increases during the solar cycle. These eruptions send powerful bursts of energy and material into space. This activity can have effects on Earth. For example, eruptions can cause lights in the sky called aurora, impact radio communications and extreme eruptions can even affect electricity grids on the Earth.

Some cycles have lots of Sunspots and activity where as some cycles can have very less Sunspots and activity. Scientists work hard to improve our ability to predict the strength and duration of solar cycles. These predictions can help them forecast these solar conditions which is called space weather (Space place, 2020, November 11).

Solar cycle 24 was the most recent solar cycle since 1755. It began in December 2008 and ends at the end of 2019 as shown in Figure 3.

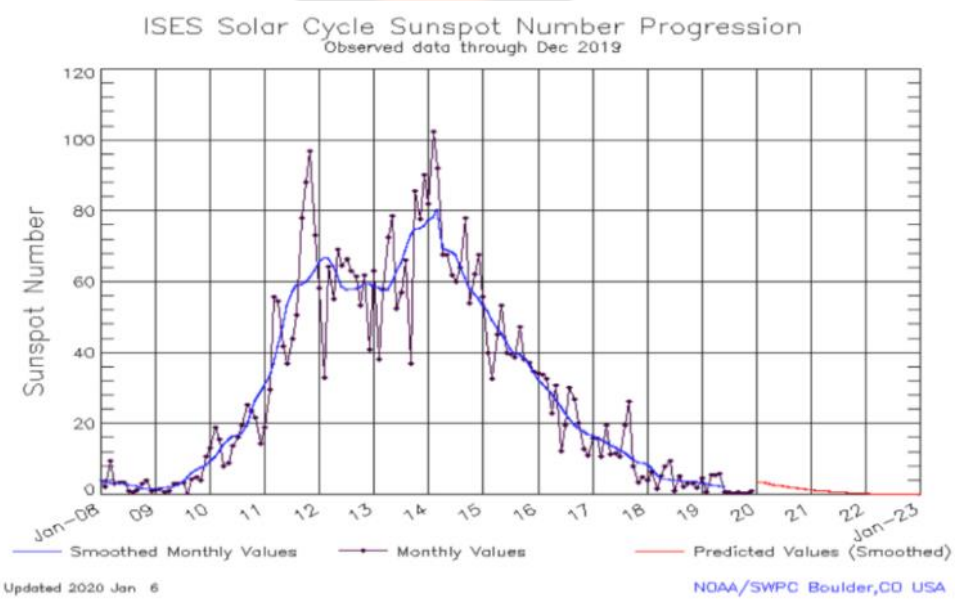

Figure 3 The number of Sunspots on the Sun between 2008-2019 for 24th solar cycle.

Source: https://www.swpc.noaa.gov/products/solar-cycle-progression

2.4 Coronal Mass Ejection (CMEs)

Coronal mass ejection (CMEs) are large expulsions of plasma and magnetic field from the Sun's corona atmosphere. The materials that are released from corona tends to coincide with the gradual eruption of the Sun's surface but sometimes it may occur alone without a surface eruption.

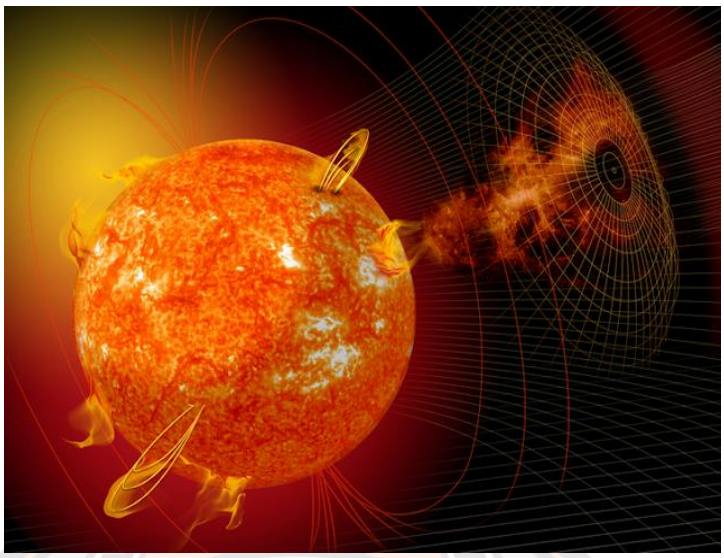

Figure 4 Eruption of corona mass ejection

Source: http://www.Earthquakepredict.com/2017/07/what-is-coronal-mass-ejection-cme.html

The coronal emission begins with the pair of magnetic fields from the solar hole, which expands into the corona layer. After that, some magnetic field lines are connected again. The connected points gradually expand within the magnetic field lines due to increase of particle inside. Finally, the pressure within the magnetic field lines overcomes the magnetic field and releases the millions of tons of material with a speed of millions of miles per hour. CMEs travel outward from the Sun at the speeds ranging from slower than 250 km/s to as fast as near 3000 km/s. The fastest Earth-directed CMEs can reach our planet in as little as 15-18 hours while the slower CMEs will take several days to arrive. CMEs travelling faster than the background solar wind speed can generate shock wave in the inter-planetary medium. These shock wave can accelerate charged particles ahead of them causing increased radiation storm (Earthquake Preduction, 2017,July 2).

2.5 Spiral magnetic field

The eruption on the Sun releases large amount of high energy particles into the interplanetary medium. The charge particles move along the magnetic field drawn

from the Sun by the conduction of the solar wind. The magnetic field that is drawn out are twisted into a spiral shape, also known as Archimedean spiral (David Ruffolo et al., 2006). As the Sun rotates on its axis, we consider this magnetic line in the spherical coordinates (Figure 5) along the radius of the magnetic field line

Where; $$\vec{dl} \times \vec{B} = 0 \quad (2.1)$$

$$\vec{\nabla} \times \vec{B} = 0 \quad (2.2)$$

Where $\vec{dl}$ is a spherical coordinate and $\vec{B}$ is a magnetic field with zero electric force because the charged particles move parallel to the magnetic field.

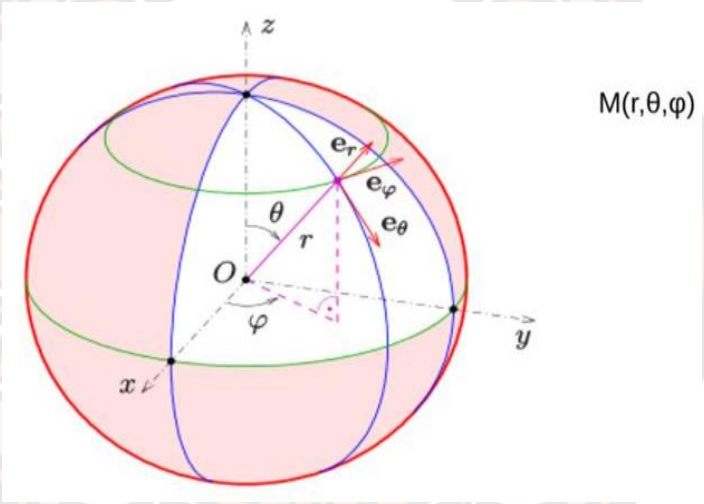

Figure 5 Spherical Coordinates

Source: https://www.wikiwand.com/en/Spherical_coordinate_system

From the equation (2.1) when considering the magnetic field of the Sun in the spherical coordinates in figure 5.

$$\vec{dl} = dr\,\hat{e_r} + rd\theta\,\hat{e}_\theta + r\sin\theta d\varphi \hat{e}_\varphi \quad (2.3)$$

Then magnetic field is

$$\vec{B}(r,\theta,\varphi) = B_r\hat{e}_r + B_\theta\hat{e}_\theta + B_\varphi\hat{e}_\varphi \quad (2.4)$$

From $d\vec{l} \times \vec{B} = 0$ then;

$$d\vec{l} \times \vec{B} = \left(rd\theta B_{\varphi} - B_{\theta} r\sin\theta d\varphi\right)\hat{e}_r + \left(B_r \sin\theta d\varphi - B_{\varphi} dr\right)\hat{e}_{\theta} + \left(B_{\theta} dr - B_r rd\theta\right)\hat{e}_{\varphi} \quad (2.5)$$

Consider the elements along the line $\hat{e}_r$ to get;

$$rd\theta B_{\varphi} = B_{\theta} r\sin\theta d\varphi$$

$$\frac{rd\theta}{B_{\theta}} = \frac{r\sin\theta d\varphi}{B_{\varphi}} \quad (2.6)$$

Consider the elements along the line $\hat{e}_{\theta}$ to get;

$$B_r r\sin\theta d\varphi = B_{\varphi} dr$$

$$\frac{r\sin\theta d\varphi}{B_{\varphi}} = \frac{dr}{B_r} \quad (2.7)$$

Consider the elements along the line $\hat{e}_{\varphi}$ to get;

$$B_{\theta} dr = B_r rd\theta$$

$$\frac{dr}{B_r} = \frac{rd\theta}{B_{\theta}} \quad (2.8)$$

Comparing the equation (2.6), (2.7) and (2.8) we get;

$$\frac{dr}{B_r} = \frac{rd\theta}{B_{\theta}} = \frac{r\sin\theta\, d\varphi}{B_{\varphi}} \quad (2.9)$$

From the equation (2.9) write $\vec{B}$ in various element in the form of $B_r(r,\theta,\varphi)$

$$B_r(r,\theta,\varphi) = B_r(r,\theta,\varphi)$$

$$B_{\theta}(r,\theta,\varphi) = r\frac{d\theta}{dr} B_r(r,\theta,\varphi) \quad (2.10)$$

$$B_{\varphi}(r,\theta,\varphi) = r\sin\theta \frac{d\varphi}{dr} B_r(r,\theta,\varphi)$$

From the above in the simulation of Parker spiral, let B_{θ}=0 because we consider the magnetic field in the equatorial plane. Therefore, the relation of $\vec{B}(r,\theta,\varphi)$ various elements is the following equation;

$$B_r(r,\theta,\varphi) = B_r(r,\theta,\varphi)$$

$$B_{\theta}(r,\theta,\varphi) = 0 \qquad (2.11)$$

$$B_{\varphi}(r,\theta,\varphi) = r\sin\theta \frac{d\varphi}{dr} B_r(r,\theta,\varphi)$$

Next, consider the rate of change of the angle 'φ' and the radius 'r' of the magnetic field that is emitted from the Sun.

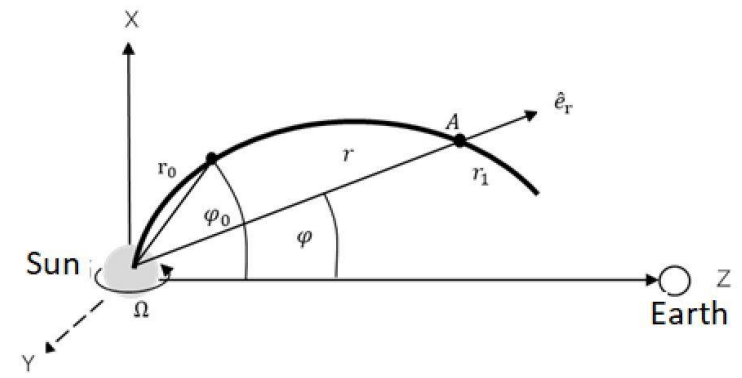

Figure 6 Shows the characteristics of the magnetic field that emits from the Sun in a spherical coordinate.

The Sun revolves around itself at an angular velocity (Ω) which is related to the angle (φ) in the magnetic field that acts at radius (r) as equation (2.12). From angular velocity, which is the angular displacement that changes in unit time.

$$\Omega = \frac{\varphi_0 - \varphi}{t} = -\frac{\Delta\varphi}{\Delta t} \qquad (2.12)$$

so $-|\Delta\varphi|$ shows that if the value of φ is large it will take less time and if the value of φ is small it will take more time. When $\Delta\varphi = \varphi - \varphi_0$ and $\Delta t = t - t_0$.

Consider the radius of the particles moving according to the solar wind speed. From the equation;

$$r = v_{sw}t$$

$$\frac{dr}{dt} = v_{sw}$$

$$r - r_0 = v_{sw}(t - t_0)$$

$$\Delta r = v_{sw}\Delta t \tag{2.13}$$

Substitute Δt from Equation (2.12) into Equation (2.13) we get;

$$\Delta r = v_{sw}\frac{\varphi_0 - \varphi}{\Omega}$$

$$\Delta r = -\frac{v_{sw}\Delta\varphi}{\Omega}$$

$$\frac{\Delta r}{\Delta\varphi} = -\frac{v_{sw}}{\Omega}$$

$$\frac{dr}{d\varphi} = -\frac{v_{sw}}{\Omega} \tag{2.14}$$

Where;
φ is the angle that the magnetic field interacts with the radius when time t at position r1 (rad).

φ_0 is the angle that the magnetic field acts on the radius of the initial time t_0 (rad).

r is the distance from the Sun to A (m).

v_{sw} is the speed of the solar wind (km/s).

Ω is the angular velocity of the Sun's rotation = 2.7x10-6 rad sec^{-1}.

Substitute the equation (2.14) into the equation (2.11) to get the magnetic field in the direction $\hat{e}_\varphi$ are;

$$B_\varphi(r,\theta,\varphi) = r\sin\theta\left(-\frac{\Omega}{v_{sw}}\right)B_r(r,\theta,\varphi) \tag{2.15}$$

Therefore, magnetic field $\vec{B}$ becomes

$$\vec{B}(r,\theta,\varphi) = B_r(r,\theta,\varphi)\hat{e}_r - \frac{\Omega}{v_{sw}} r\sin\theta B_r(r,\theta,\varphi)\hat{e}_\varphi$$

$$\vec{B}(r,\theta,\varphi) = B_r(r,\theta,\varphi)\left(\hat{e}_r - \frac{\Omega}{v_{sw}} r\sin\theta\hat{e}_\varphi\right) \qquad (2.16)$$

From the Maxwell electromagnetic equation $\vec{\nabla}\cdot\vec{B} = 0$ when, considering the theory of divergence of magnetic field is obtained. The $\vec{\nabla}\cdot\vec{B}$ in the spherical coordinates is

$$\vec{\nabla}\cdot\vec{B} = \frac{\partial\vec{B}}{\partial r} + \frac{\partial\vec{B}}{\partial\theta} + \frac{\partial\vec{B}}{\partial\varphi} = 0 \qquad (2.16)$$

The divergence of the vector field in the spherical coordinate system is shown as follows;

$$\frac{1}{r^2}\frac{\partial r^2}{\partial r}B_r + \frac{1}{r\sin\theta}\frac{\partial}{\partial\theta}\sin\theta B_\theta + \frac{1}{r\sin\theta}\frac{\partial B_\varphi}{\partial\varphi} = 0 \qquad (2.17)$$

From the above condition $B_\theta = 0$ and substituting B_φ from equation (2.11) into (2.17) we get;

$$\frac{1}{r^2}\frac{\partial r^2}{\partial r}B_r - \frac{1}{r\sin\theta}\frac{\partial}{\partial\varphi}\left(\frac{\Omega}{v_{sw}} r\sin\theta B_r\right) = 0$$

$$\frac{1}{r^2}\frac{\partial r^2}{\partial r}B_r - \left(\frac{\Omega}{v_{sw}}\right)\frac{\partial B_r}{\partial\varphi} = 0 \qquad (2.18)$$

From the equation (2.18) we get B_r independent of φ and value of $r^2 B_r$ is constant and do not depend on r but depend on θ therefore,

$$B_r = \frac{A(\theta)}{r^2} \qquad (2.19)$$

consider r_1 is a magnetic reference point $B_r = B_1$ so,

$$A(\theta) = B_1 r^2{}_1$$

Substitute $A(\theta)$ into the equation (2.19) we get;

$$B_r = \frac{B_1 r^2{}_1}{r^2} \tag{2.20}$$

Substituting the equation (2.20) into the equation (2.16) we get;

$$\vec{B}(r,\theta,\phi) = \frac{B_1 r^2{}_1}{r^2}\left(\hat{e}_r - \frac{\Omega}{v_{sw}} r\sin\theta\hat{e}_\phi\right) \tag{2.21}$$

In the equation (2.21) the equation shows the characteristics of the magnetic field that exists in spiral or Parker spiral in a spherical coordinate. The characteristics of the magnetic field in various components are as in the following equation.

$B_r = \frac{B_1 r^2{}_1}{r^2}$ Show the characteristics of the magnetic field in the radius.

$B_\theta = 0$ No magnetic field in the line θ.

$B_\varphi = -\frac{B_1 \Omega r^2{}_1 \sin\theta}{v_{sw} r}$ Shows the characteristics of vertical magnetic field φ.

2.6 Data analysis of high energy particles from solar eruption

For the analysis of high-energy particle data, it is considered the diffusion of particles at various times from the simulation, $f[t, \mu, z, p]$. The characteristic of diffusion of particles as in the figure 7 and 8.

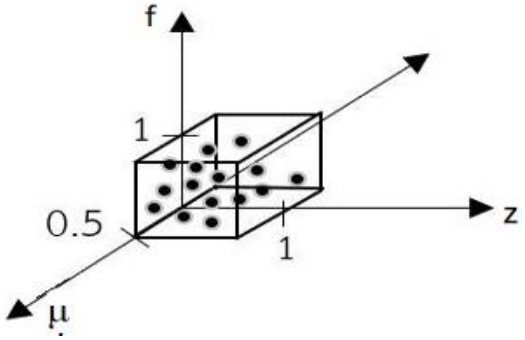

Figure 7 Early diffusion of particles

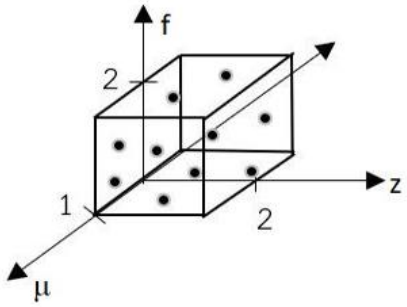

Figure 8 Later diffusion of the particles

We analyze the mean free path($\boldsymbol{\lambda}$) of high energy particles to determine the high energy particles that can move through magnetic field lines before high energy particles are scattered due to the unstable magnetic field lines resulting from the solar wind. It has the characteristic of diffusion of particles as shown in figure 9.

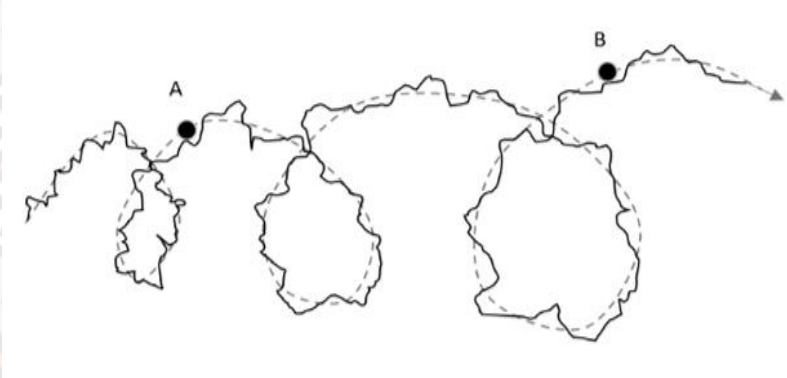

Figure 9 Examples of mean free path of high-energy particles that can move before scattering due to the change of the magnetic field lines, with particle A having less mean free path than particle B.

2.7 Transport equations that describe the motion of high energy particles

High energy particles coming out of the Sun are charged and neutral electrical particles. In describing the motion of particles in space that are moving along a magnetic field line that is not stable and can be explained from the diffusion-conduction equation. Let us consider the distribution of particles in 1 dimension which can be defined as:

$$f(x,t) = \frac{dN}{dx}$$

$$dN = f(x,t)dx \tag{2.22}$$

Where, N is the number of particles in the cell. Let, S be flux and is defined as, number of particles (N) moving through a point at unit time t. Mathematically;

$$S = \frac{N}{\Delta t} \tag{2.23}$$

Substituting, equation (2.22) in equation (2.23), we get;

$$S = vf(x,t) \tag{2.24}$$

We have;

$$N = f(x,t)\Delta x \tag{2.25}$$

As the particles moves through the cell in the x-direction the relationship between equation (2.24) and equation (2.25) can be written as:

$$\frac{\partial}{\partial t}(f \cdot \Delta x) = S\left(x - \frac{\Delta x}{2}\right) - S\left(x + \frac{\Delta x}{2}\right)$$

As, $\Delta x \to 0$ $$\frac{\partial f(x,t)}{\partial t} = -\frac{\partial S(x,t)}{\partial x} \tag{2.26}$$

The distribution of particles over time consists of systematic processes and random processes. The systematic process is when the particles move in the cell in the same direction and at the same speed as shown in figure 10.

Mathematically, the systematic or convective change is:

$$S(x,t)_{convective} = \left(\frac{\Delta x}{\Delta t}\right) f(x,t) \tag{2.27}$$

Random changes are the particles moving randomly or disordered manner as shown in the figure 11. From the figure, the flux of the left particle is denser than the right.

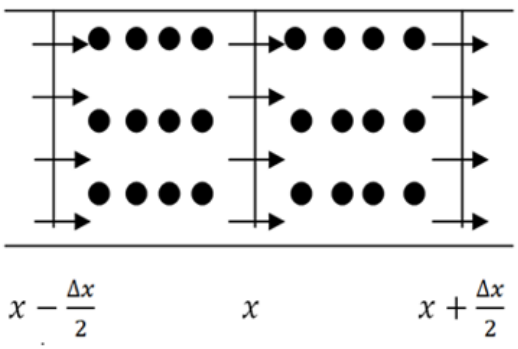

Figure 10 Systematic flux conduction

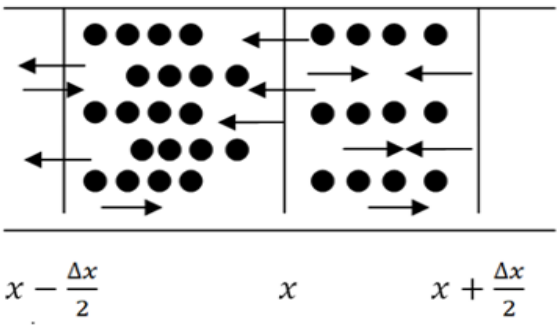

Figure 11 Random flux conduction

$$S(x,t)_{diffusive} \propto -\left(\frac{\partial f(x,t)}{\partial x}\right) \tag{2.28}$$

$$S(x,t)_{diffusive} = -D\left(\frac{\partial f(x,t)}{\partial x}\right) \tag{2.29}$$

Substituting equations (2.27) and equation (2.29) in equation (2.26), we get;

$$\frac{\partial f(x,t)}{\partial t} = -\frac{\partial}{\partial x}\underbrace{\left[\frac{\Delta x}{\Delta t} f(x,t)\right]}_{\text{Systematic first order}} + \frac{\partial}{\partial x}\underbrace{\left[D\frac{\partial f(x,t)}{\partial x}\right]}_{\text{Random process of diffusion second order term}} \tag{2.30}$$

The motion of particles that decay over time can be explained by the diffusion equation, which has the form of partial differential equation as follows:

$$D\frac{\partial^2 F}{\partial x^2} - \frac{\partial F}{\partial t} = 0 \tag{2.31}$$

Where; D is the diffusion coefficient, ∂x is the period position in which the particle moves through, ∂t is the time period in which the particles move through the distance ∂x, $\frac{\partial^2 F}{\partial x^2}$ is the flux of particles per unit volume that flows through the phase ∂x and $\frac{\partial F}{\partial t}$ is the distribution of particles over time consisting of systemic change and random change.

The motion of particles is simulated using Fokker Planck equation based on the time particle distribution equation. It was developed by Ruffolo 1998, an equation describing the transport of high energy particles from the Sun.

$$\frac{\partial F}{\partial t} + \frac{\partial (\dot{a}_i F)}{\partial a_i} = Q \qquad (2.32)$$

Where;

Q is the particle release function (Source term).

F is the particle diffusion function (Distribution function).

$\frac{\partial F}{\partial t}$ is the distribution of the flux of particles over time.

a_i are parameters of various independent variables related to movement or independent variable in terms $t, \mu, z,$ and p.

Where, t is the time the particle to travel from the Sun to the Earth (seconds), μ is the direction of the movement of the particles moving in or out of the Sun, z is the distance along the magnetic field from the Sun to the Earth (AU) and p is the momentum of the particle (MeV/c).

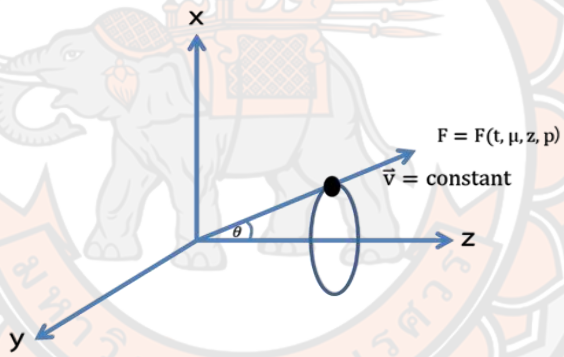

Figure 12 Shows the pitch angle θ between the velocity of the particle and magnetic field line direction.

From Figure 12, when considering independent variables that affect the motion of high energy particles from the Sun, it can be seen that high energy particles are charged particles. Therefore, the motion of particles moves along the magnetic field lines at the speed $\vec{v}$. Considering the independent variables in terms of systemic change, the changed variables can be as follows:

1. Change of distance along the magnetic field lines in the z-axis.
2. Change of momentum.
3. The change of μ, where μ is a variable that shows the direction of particle motion.

We know;

$\mu = \cos\theta$; θ is the angle between the velocity of the particle and the direction of the magnetic field which is also known as spiral phase. When;

$\theta > 90°, \mu < 0$ the particles move towards the Sun.

$\theta < 90°, \mu > 0$ the particles will move out of the Sun.

When F is the flux of the particle

$$F(t, \mu, z, p) = \frac{d^3N}{dz d\mu dp} \tag{2.33}$$

z distance along the magnetic field line to Earth (AU).

p is the momentum of a particle (MeV/c).

$\mu = \cos\theta$ where, θ = pitch angle.

N is the number of particles.

a is arbitory variable.

Q is the source term.

Since, the magnetic field lines on the Sun fluctuates due to solar wind, we consider the independent variables of particle motion in terms of random changes. The independent variables in terms of random changes are changes in μ along the line of the magnetic field that has fluctuations and the density of the particles in the distance along the magnetic field lines in the z-axis with the velocity v. When considering various independent variables, it follows that the equation is:

$$\frac{\partial F(t, \mu, z, p)}{\partial t} = -\frac{\partial}{\partial z}\left(\frac{\Delta z}{\Delta t}F\right) - \frac{\partial}{\partial \mu}\left(\frac{\Delta \mu}{\Delta t}F\right) - \frac{\partial}{\partial p}\left(\frac{\Delta p}{\Delta t}F\right) + \frac{\partial}{\partial \mu}\left[\frac{\varphi\mu}{2}\frac{\partial}{\partial \mu}\left(\frac{E'}{E}F\right)\right] \tag{2.34}$$

We define velocity of particles in fixed frame v and in solar wind frame as v'.

Conservative velocity in fixed frame is given as in the equation;

$$v = v' + v_{sw} \tag{2.35}$$

Where;

v_{sw} solar wind speed.

$v_{||}$ velocity parallel to the magnetic field lines in the fixed frame.

$v_{\perp}$ velocity perpendicular to the magnetic field lines in the fixed frame.

$v'_{||}$ velocity parallel to the magnetic field lines in the solar wind frame.

$v'_{\perp}$ velocity perpendicular to the magnetic field lines in the solar wind frame.

If considered in the reference frame of the solar wind and in the stationary reference frame, the particles will be moving in the solar wind frame(v_{sw}) speed is equal to the as given in equation;

$$v' = v - v_{sw} \tag{2.36}$$

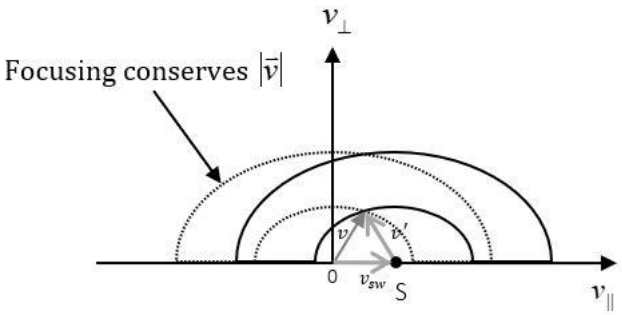

Figure 13 Fixed reference frame.

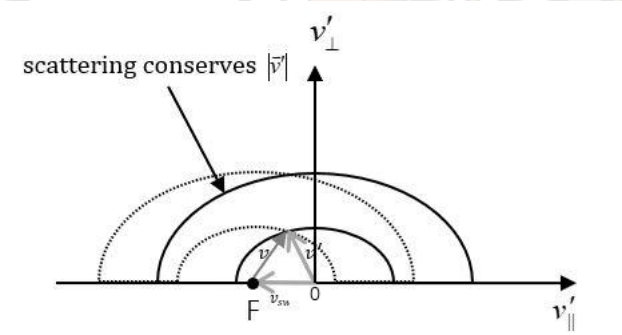

Figure 14 Solar wind reference frame.

The rate of deceleration will cause the velocity of the particle to decrease in the solar wind frame under scattering and focusing according to the equation.

$$\dot{v}' = \frac{dv'}{d\mu}\Big|_v \dot{\mu} \tag{2.37}$$

Where;

μ direction of motion of the particle ($\mu = \cos\theta$).

$\dot{\mu}$ rate of change in the direction of particle movement over time.

v velocity of particles in fixed frame.

v' velocity of particles in solar wind frame.

$\dot{v}'$ rate of change of the velocity over time in the solar wind reference frame.

Consider the magnetic field lines that are released from the Sun in fixed reference frame as in figure 15.

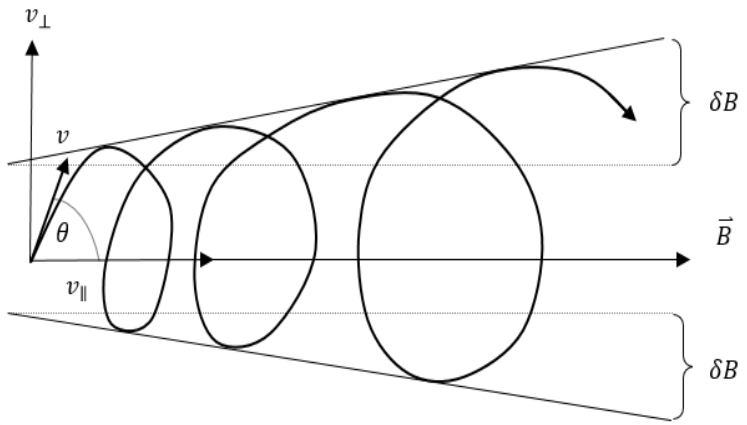

Figure 15 The characteristics of magnetic field lines.

The intensity of magnetic field of the Sun decreases as the distance increases when the particles move along the distance z-axis. According to the definition of the focusing length as follow;

$$\frac{1}{L(z)} = -\frac{1}{B}\frac{dB}{dz} \tag{2.38}$$

$L_{(z)}$ is the length field line along z-axis (Au).

B is the magnetic field (T).

Z is the distance of particles from the Sun to Earth (Au).

The particles travel between the Sun and the intermediate planets create force due to magnetic field according to the law of the Lorentz force;

$$\vec{F} = q\left(\vec{E} + \frac{\vec{v}}{c} \times \vec{B}\right) \tag{2.39}$$

Where;

$\vec{F}$ force due to the magnetic field in N.

q charged particle in C.

$\vec{v}$ velocity of the particle in m/s.

$\vec{B}$ magnetic field is in T.

$\vec{E}$ electric field in V/m.

c Speed of light 3 x10^8 m/s.

We do not consider the electric field in the inter-planetary medium; $\vec{E} = 0$, and the particles move at a speed close to the speed of light. Therefore, the force arising from the flux of the magnetic field lines perpendicular is as follows;

$$\Delta F = \frac{ev_\perp}{c}\delta B \tag{2.40}$$

And from the centripetal force

$$\frac{mv_\perp^2}{R} = \frac{ev_\perp}{c}\delta B$$

$$R = \frac{mv_\perp c}{eB} \tag{2.41}$$

When $p_\perp = mv_\perp$ will get; $R = \frac{p_\perp c}{eB}$

When R is the radius of curvature of the magnetic field lines from the equation (2.41).

let $\vec{F} = m\vec{a}$ will get;

$$ma = \frac{ev_\perp}{c}\delta B$$

$$a = \frac{ev_\perp}{mc}\delta B$$

$$\frac{\partial v_z}{\partial t} = \frac{ev_\perp}{mc}\delta B$$

When $v_z = v\cos\theta = v\mu$ will get; $\frac{\partial(v\mu)}{\partial t} = \frac{ev_\perp}{mc}\delta B$

Where v is constant $\dot{\mu} = \frac{ev_\perp}{mcv}\delta B$ (2.42)

From the Maxwell equation $\vec{\nabla}\cdot\vec{B} = 0$

$$\vec{\nabla}\cdot\vec{B} = \frac{\partial B_x}{\partial x} + \frac{\partial B_y}{\partial y} + \frac{\partial B_z}{\partial z} = 0$$

Since, it is considered the motion of the particles along the magnetic field lines in the z axis

When $\vec{B}\ \alpha\ \frac{1}{r^2}$

From the definition of the focusing of magnetic field

$$\frac{1}{L(z)} = -\frac{1}{B}\frac{dB}{dz} \tag{2.43}$$

$$\frac{1}{L(z)} = -r^2\frac{d}{dz}\left(\frac{1}{r^2}\right)$$

$$\frac{1}{L(z)} = \frac{1}{B}\frac{dB}{dz} = \frac{2}{r}$$

Substitute $\frac{\partial B_x}{\partial x} = \frac{\partial B_y}{\partial y}$ in Maxwell equation we get;

$$\frac{\partial B_y}{\partial y} + \frac{\partial B_y}{\partial y} + \frac{\partial B_z}{\partial z} = 0$$

$$\frac{2\,\partial B_y}{\partial y} = -\frac{\partial B_z}{\partial z}$$

$$\frac{\partial B_y}{\partial y} = -\frac{\partial B_z}{2\,\partial z}$$

Therefore, the combine relation of magnetic field line with the radius we get;

$$\delta B = -\frac{1}{2}\frac{\partial B_z}{\partial z} R \qquad (2.44)$$

substitute equation (2.41) and (2.43) in (2.42) we get;

$$\dot{\mu} = \frac{e v_\perp}{mcv}\left(-\frac{1}{2}\frac{\partial B_z}{\partial z}\frac{m v_\perp c}{eB}\right)$$

$$\dot{\mu} = -\frac{1}{2B}\frac{\partial B_z}{\partial z}\frac{v_\perp^2}{v}$$

And from Figure 13 the relation of the solar wind speed perpendicular and parallel to the magnetic field, as shown in Figure 16.

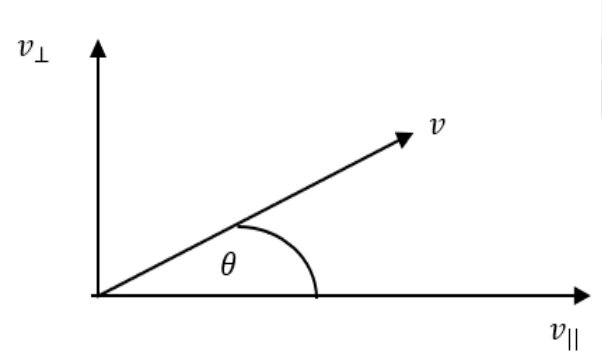

Figure 16 The relation of perpendicular velocity and parallel velocity to magnetic field lines.

From Figure 16 the relationship can be written as;

$$v_\perp = v \sin\theta$$

$$v_\perp^2 = v^2 \sin^2\theta$$

$$v_\perp^2 = v^2(1 - \cos^2\theta)$$

$$v_{\perp}^2 = v^2(1-\mu^2)$$

And from $\frac{1}{L(z)} = -\frac{1}{B}\frac{dB}{dz}$ Will get;

$$\dot{\mu} = \frac{1}{2L(z)}\frac{v^2(1-\mu^2)}{v}$$

$$\dot{\mu} = \frac{v(1-\mu^2)}{2L(z)} \quad (2.45)$$

Where; z is the length of the arc that the particle travels from the Sun to the Earth along the line magnetic field line and $L(z)$ is length of the magnetic field.

The particle moving at a velocity $\vec{v}$ with an angle θ of magnetic field lines in the z axis.

The velocity in solar wind frame v' is as given in following equation.

$$v' = \sqrt{v'^2_{||} + v'^2_{\perp}} \quad (2.46)$$

when $$v'_{||} = v_{||} - v_{sw} \quad (2.47)$$

The velocity perpendicular in fixed reference frame and the solar wind frame are equal. $v'_{\perp} = v_{\perp}$ Then substitute the equation (2.47) into the equation (2.46), will get;

$$v' = \sqrt{(v_{||} - v_{sw})^2 + v_{\perp}^2}$$

$$v' = \sqrt{v_{||}^2 - 2v_{||}v_{sw} + v_{sw}^2 + v_{\perp}^2}$$

when $v^2 = v_{||}^2 + v_{\perp}^2$ will get;

$$v' = \sqrt{v^2 - 2v_{||}v_{sw} + v_{sw}^2}$$

When $v_{||} = v\cos\theta = v\mu$ then;

$$v' = \sqrt{v^2 - 2v\mu v_{sw} + v_{sw}^2} \quad (2.48)$$

Take equation (2.45) and equation (2.48) instead into equation (2.37) to find the rate of change of velocity in the frame of the solar wind to get;

$$\dot{v}' = \frac{dv'}{d\mu}\Big|_v \dot{\mu}$$

$$\dot{v}' = \left[\frac{d}{d\mu}(v^2 - 2v\mu v_{sw} + v_{sw}^2)^{\frac{1}{2}}\Big|_v\right] \cdot \left[\frac{v(1-\mu^2)}{2L(z)}\right]$$

$$\dot{v}' = \left[\frac{1}{2}(v^2 - 2v\mu v_{sw} + v_{sw}^2)^{-\frac{1}{2}} \frac{d}{d\mu}(v^2 - 2v\mu v_{sw} + v_{sw}^2)\right] \cdot \left[\frac{v(1-\mu^2)}{2L(z)}\right]$$

$$\dot{v}' = \left[\frac{-vv_{sw}}{(v^2 - 2v\mu v_{sw} + v_{sw}^2)^{\frac{1}{2}}}\right] \cdot \left[\frac{v(1-\mu^2)}{2L(z)}\right]$$

velocity in the frame of the solar wind to get;

When: $v' = \sqrt{v^2 - 2v\mu v_{sw} + v_{sw}^2}$ will get;

$$\dot{v}' = \left[-\frac{vv_{sw}}{v'}\right] \cdot \left[\frac{v(1-\mu^2)}{2L(z)}\right]$$

$$\dot{v}' = -\frac{v^2 v_{sw}(1-\mu^2)}{v' 2L(z)}$$

Due to the conservation of velocity considerations $\vec{v}$, so $v = v'$ will get;

$$\dot{v}' = -\frac{v' v_{sw}(1-\mu^2)}{2L(z)}$$

Therefore, the rate of change of velocity in the frame of the solar wind is according to the equation;

$$\dot{v}' = -\frac{v_{sw} v'}{2L(z)}(1-\mu^2) \tag{2.49}$$

And from $p = mv$ will get;

$$\dot{p}' = -\frac{v_{sw} p'}{2L(z)}(1-\mu^2) \tag{2.50}$$

From the equation (2.50) the rate of change in momentum in the solar wind frame due to the decreasing momentum in the solar wind according to the adiabatic focusing. The rate of change of momentum depends on the length of the magnetic

field line (z) and the value of the solar wind velocity at different position (v_{sw}^{c}) which is called differential convection.

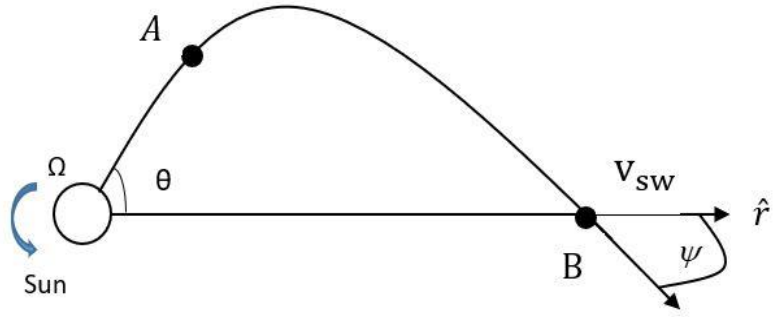

Figure 17 The magnetic field acting on the radial line from the Sun

$$v_{sw}^{c} = V_{sw} - \Omega\, r \sin\theta$$

$$\dot{p}' = -\frac{p' v_{sw} \sec\psi}{2L(z)}(1-\mu'^{2}) \tag{2.51}$$

From figure 17, the relationship is as follows;

$$\cos\psi = \frac{v_{sw}}{v_{sw}^{c}}$$

$$v_{sw}^{c} = v_{sw} \sec\psi$$

Substitute v_{sw}^{c} in equation (2.51) we get;

$$\dot{p}' = -\frac{p' v_{sw} \sec\psi}{2L(z)}(1-\mu'^{2}) \tag{2.54}$$

$$\dot{p}' = -\frac{v_{sw}^{c} p'}{2L(z)}(1-\mu^{2}) \tag{2.53}$$

From the equation (2.47) when we consider the relationship as follows;

$$v_{||} = v'_{||} + v_{sw}^{c}$$

when $E = mc^{2}$ we get;

$$m = \frac{E}{c^{2}}$$

Therefore, the momentum along the magnetic field line due to the solar wind speed in various coordinates is;

$$p_{||} = p'_{||} + \left(\frac{E}{c^2}\right) v^c_{sw}$$

$$p'_{||} = p_{||} - \left(\frac{E}{c^2}\right) v^c_{sw} \tag{2.54}$$

The decreasing momentum of the particles in solar wind from point A to B and from the equation (2.54), will get;

$$p'_{||}, A = p_{||} - \left(\frac{E}{c^2}\right) v^c_{sw,A} \tag{2.55}$$

$$p'_{||}, B = p_{||} - \left(\frac{E}{c^2}\right) v^c_{sw,B} \tag{2.56}$$

From the equation (2.55) and equation (2.56) we will get;

$$\Delta\, p'_{||} = -\frac{E}{c^2} \Delta v^c_{sw}$$

$$\Delta\, p'_{||} = -\frac{E}{c^2} \Delta v_{sw} \sec\psi$$

The relationship between the radius (r) to the axis (z), which is the angle ψ.

$$\cos\psi = \frac{dr}{dz}$$

$$dr = \cos\psi\, dz$$

Where;

z is length along the spiral of the magnetic field lines.

Δz is distance along the magnetic field lines from point A to point B.

Δt is time taken.

$$\Delta p'_{||} = -\frac{E}{c^2} \Delta v_{sw} \left(\frac{d}{dz} \sec\psi\right) \Delta z$$

When $\Delta z = v_{||} \Delta t$ will get;

$$\Delta p'_{||} = -\frac{E}{c^2} v_{sw} \left(\frac{dr}{dz} \frac{d(\sec\psi)}{dr}\right) v_{||} \Delta t$$

$$\Delta p'_{||} = -\frac{E}{c^2} v_{sw} \left(\cos\psi \frac{d(\sec\psi)}{dr} \right) v_{||} \Delta t$$

Where $m = \frac{E}{c^2}$ and $v_{||} = v\mu$ will get;

$$\dot{p}'_{||} = -p'_{||} v_{sw} \left(\cos\psi \frac{d(\sec\psi)}{dr} \right) \tag{2.57}$$

The equation (2.57) is an equation shows the change in momentum from one point to another along a magnetic field line which is in terms of the particle transport equation Ruffolo (1995,1998).

Due to the momentum in the framework of the solar wind(p') depends on the conduction of the solar wind particles. Therefore, $p'_{\perp} = 0$ then $p_{||} v_{sw} = p' v_{sw}$ we can calculate the rate of decreasing momentum according to the change of solar wind (v_{sw}^{c}) from

$$\dot{p}' = \frac{p'_{||} \dot{p}'_{||}}{p'} \tag{2.58}$$

Substituting $p'_{||} = p'\mu'$ in equation (2.58), we get;

$$\dot{p}' = \mu' p'_{||}$$

Substituting $\dot{p}'_{\parallel}$ in equation (2.58), we get;

$$\dot{p}' = \mu' \left[-p'_{||} v_{sw} \left(cos\,\psi \frac{d(sec\,\psi)}{dr} \right) \right]$$

when $p_{||} = p\mu$ and $\mu = \mu'$ will get;

$$\dot{p}' = -p v_{sw} \left(\cos\psi \frac{d(\sec\psi)}{dr} \right) \mu'^2 \tag{2.59}$$

Combine the equation (2.53) with the equation (2.59) to get;

$$\dot{p}' = -\frac{p' v_{sw} \sec\psi}{2L(z)} (1 - \mu'^2) - p v_{sw} (\cos\psi \frac{d(\sec\psi)}{dr}) \mu'^2 , p = p'$$

$$\dot{p}' = -p' v_{sw} \left[\frac{\sec\psi}{2L(z)} (1 - \mu'^2) + \left(\cos\psi \frac{d\sec\psi}{dr} \right) \mu'^2 \right] \tag{2.60}$$

The equation (2.60) is the rate of momentum change in the solar wind frame which is a consequence of the total deceleration.

Consider the effects of solar wind on the movement of particles in the interplanetary medium on z and μ.

$$v_{||} = v'_{||} + v^c_{sw}$$

$$E = mc^2 = pc$$

And From;

$$p'_{||} = p'\mu'$$

$$v^c_{sw} = v_{sw}\sec\psi$$

Therefore, we can write the relationship between the fixed reference frame and the solar wind frame as follows

$$\frac{E}{c^2}v_{||} = p'_{||} + \frac{E}{c^2}v^c_{sw}$$

$$\frac{E}{c^2}v_{||} = p'\mu' + \frac{E}{c^2}v^c_{sw}$$

When $p' = m'v'$ will get;

$$\frac{E}{c^2}v_{||} = m'v'\mu' + \frac{E}{c^2}v^c_{sw}$$

$$v_{||} = \frac{m'v'\mu'c^2}{E} + v^c_{sw} \qquad , v_{||} = \dot{z}$$

$$\dot{z} = \frac{m'v'\mu'c^2}{E} + v_{sw}\sec\psi \quad , m'c^2 = E'$$

$$\dot{z} = v'\mu'\frac{E'}{E} + v_{sw}\sec\psi \tag{2.61}$$

Find $\frac{E'}{E}$ from the equation (2.57) $p_{||} = p'_{||} + \frac{E}{c^2}v^c_{sw}$ so $p_{||} = p'_{||}$ will get

$$cp_{||} = cp'_{||} + \frac{E}{c}v^c_{sw}$$

$$E = E' + \frac{E}{c}v^c_{sw}$$

$$E = pE' + pv^c_{sw} \qquad , p_{||} = p'_{||}$$

$$E' = E - p'_{||} v^c_{sw}$$

$$E' = E\left(1 - \frac{p'_{||} v^c_{sw}}{E}\right)$$

$$\frac{E'}{E} = 1 - \frac{p'_{||} v^c_{sw}}{E}$$

$$\frac{E'}{E} = 1 - \frac{m v'_{||} v^c_{sw}}{mc^2} \qquad , v'_{||} = v'\mu'$$

$$\frac{E'}{E} = 1 - \frac{v'\mu' v^c_{sw}}{c^2}$$

Substitute $\frac{E'}{E}$ in equation (2.61) to get;

$$\dot{z} = v'\mu'\left[1 - \frac{v'\mu' v^c_{sw}}{c^2}\right] + v_{sw}\sec\psi$$

$$\dot{z} = v'\mu'\left[1 - \frac{v'\mu' v_{sw}\sec\psi}{c^2}\right] + v_{sw}\sec\psi$$

$$\dot{z} = v'\mu' - \frac{v'^2\mu'^2}{c^2} v_{sw}\sec\psi + v_{sw}\sec\psi$$

$$\dot{z} = v'\mu' + \left(1 - \frac{v'^2\mu'^2}{c^2}\right) v_{sw}\sec\psi \qquad (2.62)$$

From the equation (2.62), the change of distance along the magnetic field with time in 2 terms, streaming and convection in the transport equation Ruffolo (1995,1998). The first term is the term of streaming which describes the movement of the particles from one point to another point which doesn't have the effect of solar wind speed. The second term expression is the convection, which describes the movement of particles along the magnetic field having the effect of the solar wind.

Consider the change of μ based on time in the fixed reference frame and the frame of the solar wind.

Consider the change of μ in a fixed frame from the adiabatic focus from the equation (2.45) we got;

$$\dot{\mu} = \frac{1}{2L(z)} v(1 - \mu^2)$$

Consider the change of μ in the frame of the solar wind and by using the chain rule.

$$\frac{d\mu'}{dt} = \left.\frac{d\mu'}{d\mu}\right|_p \frac{d\mu}{dt}$$

$$\dot{\mu}' = \left.\frac{d\mu'}{d\mu}\right|_p \dot{\mu} \qquad (2.63)$$

From $p'_{||} = p'\mu'$ (2.64)

And From $p'_{||} = p_{||} - \frac{E}{c^2} v_{sw}^c$ (2.65)

When; $p_\perp = p'_\perp$

So that; $p' = \sqrt{p'^2_{||} + p'^2_\perp}$ (2.66)

Since, the momentum is perpendicular to the magnetic field line, it doesn't affect the motion of the particles. So, $p'_\perp = 0$ substitute the equation (2.65) in equation (2.66), we will get;

$$p' = \sqrt{p'^2_{||} - 2p_{||}\frac{E}{c^2}v_{sw}^c + \left(\frac{E}{c^2}v_{sw}^c\right)^2}$$

The equation (2.66) will be;

$$\mu' = \frac{p_{||} - \frac{E}{c^2}v_{sw}^c}{\sqrt{p'^2_{||} - 2p_{||}\frac{E}{c^2}v_{sw}^c + \left(\frac{E}{c^2}v_{sw}^c\right)^2}}, p_{||} = p\mu$$

$$\mu' = \frac{p\mu - \frac{E}{c^2}v_{sw}^c}{\sqrt{p'^2_{||} - 2p_{||}\frac{E}{c^2}v_{sw}^c + \left(\frac{E}{c^2}v_{sw}^c\right)^2}}, p_{||}^2 = p'^2$$

$$\mu' = \frac{p\mu - \frac{E}{c^2}v_{sw}^c}{\sqrt{p'^2 - \frac{2E}{c^2}p\mu v_{sw}^c + \left(\frac{E}{c^2}v_{sw}^c\right)^2}}$$

$$\mu' = \left[p\mu - \frac{E}{c^2}v_{sw}^c\right]\left[p'^2 - \frac{2E}{c^2}p\mu v_{sw}^c + \left(\frac{E}{c^2}v_{sw}^c\right)^2\right]$$

$$\frac{d\mu'}{d\mu} = \left[p\mu - \frac{E}{c^2}v_{sw}^c\right]\left\{-\frac{1}{2}\left[p'^2 - \frac{2E}{c^2}p\mu v_{sw}^c + \left(\frac{E}{c^2}v_{sw}^c\right)^2\right]^{-3/2}\left[-\frac{2E}{c^2}pv_{sw}^c\right]\right\} + \left[p'^2 - \frac{2E}{c^2}p\mu v_{sw}^c + \left(\frac{E}{c^2}v_{sw}^c\right)^2\right]^{-\frac{1}{2}}p$$

$$\frac{d\mu'}{d\mu} = \frac{-\frac{1}{2}\left[p\mu - \frac{E}{c^2}v_{sw}^c\right]\left[-\frac{2E}{c^2}pv_{sw}^c\right]}{\left[p'^2 - \frac{2E}{c^2}p\mu v_{sw}^c + \left(\frac{E}{c^2}v_{sw}^c\right)^2\right]^{3/2}} + \frac{p}{\left[p'^2 - \frac{2E}{c^2}p\mu v_{sw}^c + \left(\frac{E}{c^2}v_{sw}^c\right)^2\right]^{1/2}}$$

From $$p' = \sqrt{p_{||}'^2 - 2p_{||}\frac{E}{c^2}v_{sw}^c + \left(\frac{E}{c^2}v_{sw}^c\right)^2}$$

$$\frac{d\mu'}{d\mu} = \frac{-\frac{1}{2}\left[-\frac{2E}{c^2}p^2\mu v_{sw}^c + \frac{2E^2}{c^4}p(v_{sw}^c)^2\right]}{p'^3} + \frac{p}{p'}$$

$$\frac{d\mu'}{d\mu} = \frac{Ep^2\mu v_{sw}^c}{c^2p'^3} - \frac{E^2p(v_{sw}^c)^2}{c^4p'^3} + \frac{p}{p'} \qquad (2.67)$$

Substitute equation (2.67) into equation (2.63)

$$\dot{\mu}' = \left[\frac{Ep^2\mu v_{sw}^c}{c^2p'^3} - \frac{p}{p'^3}\left(\frac{Ev_{sw}^c}{c^2}\right)^2 + \frac{p}{p'}\right]\left[\frac{1}{2L(z)}v(1-\mu^2)\right]$$

$$\dot{\mu}' = \frac{v}{2L(z)}(1-\mu^2)\frac{Ep^2\mu v_{sw}^c}{c^2p'^3} - \frac{p}{p'^3}\left(\frac{Ev_{sw}^c}{c^2}\right)^2\frac{v}{2L(z)}(1-\mu^2) + \frac{v}{2L(z)}(1-\mu^2)\frac{p}{p'}$$

$$\dot{\mu}' = \frac{v}{2L(z)}(1-\mu^2)\frac{p^3\mu v_{sw}^c}{p'^3c} - \frac{p^3}{p'^3}\left(\frac{v_{sw}^c}{c}\right)^2\frac{v}{2L(z)}(1-\mu^2) + \frac{v}{2L(z)}(1-\mu^2)\frac{p}{p'}$$

We consider the ratio of $\frac{v_{sw}^c}{c}$ in order 1

$$\dot{\mu}' = \frac{v}{2L(z)}(1-\mu^2)\frac{p^3 \mu v_{sw}^c}{p'^3 c} + \frac{v}{2L(z)}(1-\mu^2)\frac{p}{p'^3}$$

From $E = mc^2 = pc = mvc$ will get;

$$\therefore v = \frac{E}{mc} = \frac{pc}{mc} = \frac{pc^2}{E}$$

Substitute $v = \frac{pc^2}{E}$equation of $\dot{\mu}'$ will get;

$$\dot{\mu}' = \frac{1}{2L(z)}(1-\mu^2)\left(\frac{pc^2}{E}\right)\left(\frac{\mu v_{sw}^c}{c}\right) +$$

$$\frac{1}{2L(z)}(1-\mu^2)\left(\frac{pc^2}{E}\right)$$

$$\dot{\mu}' = \frac{1}{2L(z)}(1-\mu^2)\left[\mu v_{sw}^c + \frac{pc^2}{E}\right]$$

Take $\frac{E'v'}{p'c^2} = 1$ multiplying with the last term

$$\dot{\mu}' = \frac{1}{2L(z)}(1-\mu^2)\left[\mu v_{sw}^c + \left(\frac{pc^2}{E}\right)\left(\frac{E'v'}{p'c^2}\right)\right]$$

$$\dot{\mu}' = \frac{1}{2L(z)}(1-\mu^2)\left[\mu v_{sw}^c + \frac{E'v'}{E}\right] \ , p = p'$$

$$\dot{\mu}' = \frac{v'}{2L(z)}(1-\mu^2)\left[\frac{\mu v_{sw}^c}{v'} + \frac{E'}{E}\right]$$

Substitute $\frac{E'}{E} = 1 - \frac{\mu' v' v_{sw}^c}{c^2}$ to get;

$$\dot{\mu}' = \frac{v'}{2L(z)}(1-\mu^2)\left[\frac{\mu v_{sw}^c}{v'} + 1 - \frac{\mu' v' v_{sw}^c}{c^2}\right]$$

When $v_{sw}^c = v_{sw}\sec\psi$ we get;

$$\dot{\mu}' = \frac{v'}{2L(z)}(1-\mu'^2)\left[\frac{\mu' v_{sw}\sec\psi}{v'} + 1 - \frac{\mu' v' v_{sw}\sec\psi}{c^2}\right]$$

$\mu = \mu'$

$$\dot{\mu} = \frac{v}{2L(z)}\left[1 + \frac{\mu v_{sw}\sec\psi}{v} - \frac{\mu v v_{sw}\sec\psi}{c^2}\right](1-\mu^2) \qquad (2.68)$$

Equation (2.67) in the term of the focusing of the transport equation Ruffolo (1995,1998). Consider the momentum perpendicular to the magnetic field lines in the solar wind frame does not affect the motion of the particles.

$$\begin{aligned} d(p'_{\perp}) &= 0 \\ &= d(p'^2 \sin^2\theta) \\ &= d\left(p'^2(1-\cos^2\theta)\right) \\ &= d\left(p'^2(1-\mu'^2)\right) \\ &= p'^2 d\left(1-\mu'^2\right) + \left(1-\mu'^2\right) d\left(p'^2\right) \\ &= p'^2\left(-2\mu'\right) d\mu' + \left(1-\mu'^2\right)\left(2p'\right) dp' \end{aligned}$$

$$d\mu' = -\frac{\left(1-\mu'^2\right)\left(2p'\right)dp'}{\left(-2\mu'\right)p'^2}$$

$$d\mu' = -\frac{\left(1-\mu'^2\right)dp'}{\left(-\mu'\right)p'}$$

$$\dot{\mu}' = \frac{\left(1-\mu'^2\right)\dot{p}'}{\mu' p'} \qquad (2.69)$$

From the equation (2.59) can be rewritten as;

$$\frac{\dot{p}'}{p'} = -v_{sw}\left(\cos\psi \frac{d(\sec\psi)}{dr}\right)\mu'^2$$

Substitute $\frac{\dot{p}'}{p'}$ in equation (2.69) we get;

$$\dot{\mu}' = -v_{sw}\left(\cos\psi \frac{d}{dr}(\sec\psi)\right)\mu'\left(1-\mu'^2\right) \qquad (2.70)$$

From the equation (2.70) is the rate of change of μ over time, regardless of the divergent magnetic field in the solar wind. Which is one of the terms in the transport equation Ruffolo (1995,1998), which is called the differential convection.

From the equation (2.68) and the equation (2.70) when combined, the rate of change μ of time t in the focusing term and the differential convection in the transportation equation in the following equation

$$\dot{\mu} = \frac{v}{2L(z)}\left[1 + \frac{\mu v_{sw}\sec\psi}{v'} - \frac{\mu v v_{sw}\sec\psi}{c^2}\right](1-\mu^2) \quad \text{focusing}$$

$$-v_{sw}\left(\cos\psi\frac{d}{dr}\sec\psi\right)\mu'(1-\mu'^2) \quad \text{Differential convection}$$

$$\dot{p'} = -p'v_{sw}\left[\frac{\sec\psi}{2L(z)}(1-\mu'^2) - \cos\psi\frac{d(\sec\psi)}{dr}\mu'^2\right] \quad \text{Deceleration}$$

$$\dot{z} = \underbrace{v'\mu'}_{\text{Streaming}} \underbrace{- \frac{v'^2\mu'^2}{c^2}v_{sw}\sec\psi + v_{sw}\sec\psi}_{\text{convection}}$$

From the Fokker Planck equation first term order and second term order

$$\frac{\partial F}{\partial t} + \frac{\partial}{\partial z}\left(\frac{\Delta z}{\Delta t}F\right) + \frac{\partial}{\partial \mu}\left(\frac{\Delta \mu}{\Delta t}F\right) + \frac{\partial}{\partial p}\left(\frac{\Delta p}{\Delta t}F\right) + \frac{\partial}{\partial \mu}\left(\frac{\Delta \mu}{\Delta t}F\right) = 0$$

$$\frac{\partial F(t,\mu,z,p)}{\partial t} = -\frac{\partial}{\partial z}\left(\frac{\Delta z}{\Delta t}F\right) - \frac{\partial}{\partial \mu}\left(\frac{\Delta \mu}{\Delta t}F\right) - \frac{\partial}{\partial p}\left(\frac{\Delta p}{\Delta t}F\right) + \underbrace{\frac{\partial}{\partial \mu}\left[\frac{\varphi\mu}{2}\frac{\partial}{\partial \mu}\left(\frac{E'}{E}F\right)\right]}_{\text{Pitch angle scattering random term}}$$

To simulate the movement of high energy particles that emitted from the Sun using the basic equation of Fokker Planck, which are combined with various influences caused by an intermediary between the planets. The change in the magnetic fluxes and the effects of the solar wind in various considerations will give us the transport equation that describes the movement of high energy particles according to the transport equation of Ruffolo,1995, which is a form of the equation is:

$$\frac{\partial \vec{F}(t,\mu,z,p)}{\partial t} = -\frac{\partial}{\partial z}\mu v\,\vec{F}\,(t,\mu,z,p) \quad \text{(streaming)}$$

$$-\frac{\partial}{\partial z}(1-\mu^2\frac{v^2}{c^2})v_{sw}\sec\Psi\,\vec{F}\,(t,\mu,z,p) \quad \text{(convection)}$$

$$-\frac{\partial}{\partial u}\frac{v}{2L(z)}1+\left[1+\mu\frac{v_{sw}}{v}\sec\Psi-\mu\frac{v_{sw}v}{c^2}\sec\Psi\right](1-\mu^2)\,\vec{F}\,(t,\mu,z,p)$$

(focusing)

$$+\frac{\partial}{\partial u}v_{sw}\left(\cos\Psi\frac{d}{dr}\sec\Psi\right)\mu(1-\mu^2)\,\vec{F}\,(t,\mu,z,p)$$

(differential convection)

$$+\frac{\partial}{\partial u}\frac{\phi(\mu)}{2}\frac{\partial}{\partial \mu}(1-\mu\frac{v_{sw}v}{c^2}\sec\Psi)\,\vec{F}\,(t,\mu,z,p) \quad \text{(scattering)}$$

$$+\frac{\partial}{\partial p}pv_{sw}\left[\frac{\sec\Psi}{2L(z)}(1-\mu^2)+\cos\Psi\frac{d}{dr}(\sec\Psi)\mu^2\right]\vec{F}\,(t,\mu,z,p)$$

(deceleration)

The table below explains the meaning of each term in brief from the above complete Ruffolo's transport equation:

Table 3 Description of each term of transport equation

Terms	Descriptions
Streaming	It describes the motion of particles along the magnetic field lines in the z-axis.
Convection	It describes the movement of particles along the magnetic field lines caused by solar convection.
Focusing	It describes the movement of particles resulting from the adiabatic focusing considered in the stationary reference frame and the frame of the solar wind.
Differential convection	It shows the change in solar velocity by position. By considering the rate of change 'μ' with respect to time 't' in the frame of the solar wind which has no effect on focussing.
Scattering	It is a term that shows the scattering of particles in the framework of the solar wind in random changes.
Deceleration	It is a term for the rate of change of momentum that depends on the rate of change of velocity along the line of the magnetic field in the frame of the solar wind.

2.8 ACE (Advanced Composition Explorer) spacecraft

In this research, we have used the data from the ACE spacecraft. The ACE spacecraft was launched on August 25, 1997 and it is used to observe and measure various particles that comes from the Sun and particles from other sources to the Earth. The spacecraft is about 1.6 m in width and has a height of about 1 m. The weight of the spacecraft is combined with the fuel tank and is approximately 758 kg. The image of ACE spacecraft and its component is shown in Figure 18.

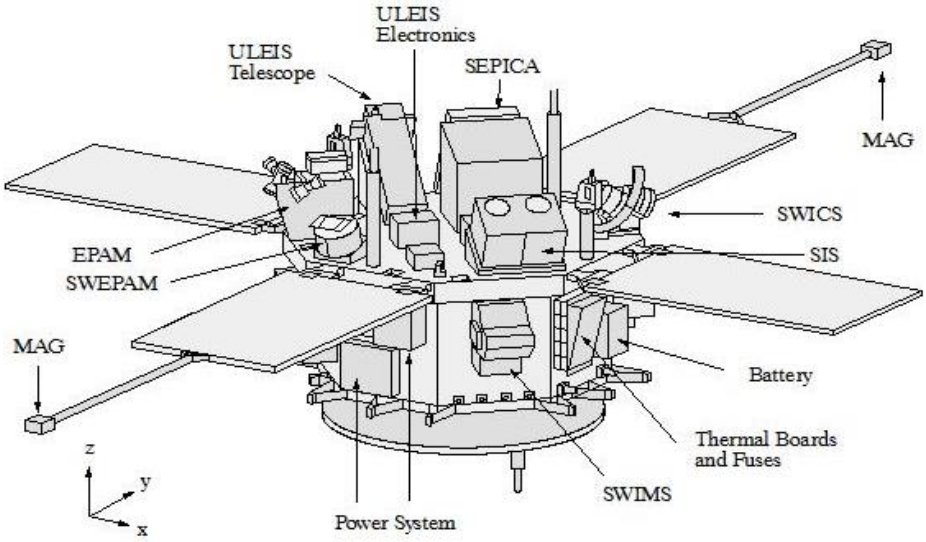

Figure 18 Advance Composition Explorer Spacecraft (ACE).

Source: https://directory.eoportal.org/web/eoportal/satellite-missions/content/-/article/ace

There are total of nine instruments installed on the ACE spacecraft, six high resolution sensors and three monitoring instruments.

i. CRIS (Cosmic Ray Isotope Spectrometer) is a tool used to measure and study isotopes of cosmic rays with energy levels in the range 100-600 MeV / n.

ii. SIS (Solar Isotope Spectrometer) is designed to provide high resolution measurements of the isotopic composition of energetic nuclei from He to Ni over the energy range from ~10 to ~100 MeV/n.

iii. ULEIS (Ultra-Low Energy Isotope Spectrometer) is instrument for measuring the low energy particles released from the Sun with energy levels in the range of 0.2-10 MeV/n.

iv. SWEPAM (Solar Wind Electron, Proton and Alpha Monitor) is a tool for measuring of electron and ion fluxes in the low energy solar wind range.

v. MAG (Magnetic Field Experiment) is an instrument that measures the direction and magnitude of the interplanetary magnetic field.

vi. EPAM (Electron, Proton, and Alpha Monitor) is a tool that shows the density and the energy of protons, alpha particles and electrons by measuring the energy of particles with energy levels in the range of 0.3-0.4 MeV / n.

vii. SWIMS (Solar Wind Ion Mass Spectrometer) is a tool that SWIMS measure the chemical and isotopic composition of the solar wind for every element between He and Ni, up to 10 keV/e.

viii. SWICS (Solar Wind Ionic Charge Spectrometer) is tool for measuring the ionic-charge composition, temperature and mean speeds of all major solar wind ions.

ix. SEPICA (The Solar Energetic Particle Ionic Charge Analyzer) is a tool for measurement of the ionic charge state, energy and the nuclear charge of ions coming from the Sun (Sharing Earth Observation Resources, 2020, November 13).

All instruments are used to measure particle's charge, mass, energy and direction of movement according to the time which is very much useful in research. It also enhances the understanding of the origin of particles and evolution of the solar system. ACE spacecraft is mainly used to study electrons and groups of high energy isotopes. In this research we used a SIS instrument to obtained the data.

Figure 19 Solar Isotope Spectrometer

Source: http://www.srl.caltech.edu/ACE/CRIS_SIS/sis.html

The SIS instrument is designed to provide high resolution measurements of the isotopic composition of energetic nuclei from He to Ni (Z=2 to 28) over the energy range from ~10 to ~100 MeV/n. During large solar events, when particle fluxes can increase over quiet-time values by factors of up to 10000, SIS will measure the isotopic composition of the solar corona, while during solar quiet times SIS will measure the isotopes of low-energy Galactic cosmic rays and the composition of the anomalous cosmic rays which are thought to originate in the nearby interstellar medium. The solar energetic particle measurements are useful in understanding of the Sun, while also providing a baseline for comparison with the Galactic cosmic ray measurements carried out by CRIS. SIS has a geometry factor of ~40 cm^2-sr, which is significantly larger than previous satellite solar particle isotope spectrometers. It is also designed to provide excellent mass resolution during the extremely high particle flux conditions which occur during large solar particle events.

The first two detectors, M1 and M2, are position-sensitive "matrix" devices that form the horoscope measuring the trajectory and energy loss of incident nuclei. The matrix detectors are octagonal in shape, 70 to 80 μm in thickness, and have 34cm^2 active areas that are divided into 64 strips. Each of the strips on M1 and M2 is individually pulse-height analyzed with its own 12-bit ADC (Analog Digital Converter) when an event occurs so that the trajectory of heavy ions traversing the system can be separated from the tracks of low energy H or He that might happen to hit one of these detectors at the same time. Detectors M1 and M2 are separated by 6 cm so, the resulting rms angular resolution of the system is ~0.25 degrees averaged over all angles (California Institute of Technology, 2007,November 28).

2.9 Time profile of injection near the Sun

The two techniques were developed for deconvolving the effects of interplanetary transport in order to determine the underlying time profile of injection near the Sun, which in turn yields the injected spectrum as well as the best fit value of the interplanetary scattering mean-free path. These techniques solve the inversion problem

$$R(t) = \int_0^t G(t - t')I(t')dt' \qquad (2.71)$$

where I(t') is the injection of particles versus time near the Sun, G(t- t') is the Green's function, or the response to δ-function injection, which is calculated by the transport simulation, and R(t) is the "response," that is the measured intensity or anisotropy times intensity at the spacecraft. Both techniques are semi-automated in that a computer program finds injection parameter values that minimize the x^2 of the fit between R(t) and the observational data (minus background). Results for different values of λ are then compared, and the overall best fit is used as the final result.

The deconvolution technique finds the optimal piecewise linear injection function for a given set of "joints," t_i. The times of the joints in the piecewise linear injection function, I(t'), are chosen a priori, and the injection function is constrained to be zero at the first and final joints (figure 20 c). Then I(t') is a linear combination of triangular injections, Ii(t') (figure 20 a).

The first triangular function starts from 0 at the first joint, rises linearly to 1 at the next joint, and falls linearly to 0 at the following joint (in units of 10^{26} sr^{-1} s^{-1} MeV^{-1}, that is 10^{26} per unit solid angle of the solar surface, time, and energy). The peak time of this function is then the start time of the next function and so on. We then convolve G (t- t'), the intensity predicted by the transport simulation for an instantaneous injection, with each $I_i(t')$, which yields the predicted response, $R_i(t)$, due to each triangular injection (Figure 20 b). Now we want to consider the response, R(t), to a general linear combination of the triangular injections. Because the transport equation is linear in F, the response to a linear combination of injections, $I(t') = \sum_i a_i I_i(t')$ is the linear combination of responses, $R(t)= \sum_i a_i R_i(t)$. Therefore, we can use linear least-squares fitting to find the linear combination that minimizes the x^2 between R(t) and the observed data (Figure 20 d). Because each $I_i(t')$ has a peak value of one, the coefficients, a_i, are the values of the injection function at each joint t_i (Figure 20 c), the least squares fit also directly yields the statistical errors of these values. Initially, we set t_0 to the peak time of the H α flare, set t_1 and t_2 so that t_2-t_1 and t_1-t_0 were equal to the width of the time bins of the data, and set further t_i so that each interval was twice the preceding interval (D Ruffolo et al., 1998).

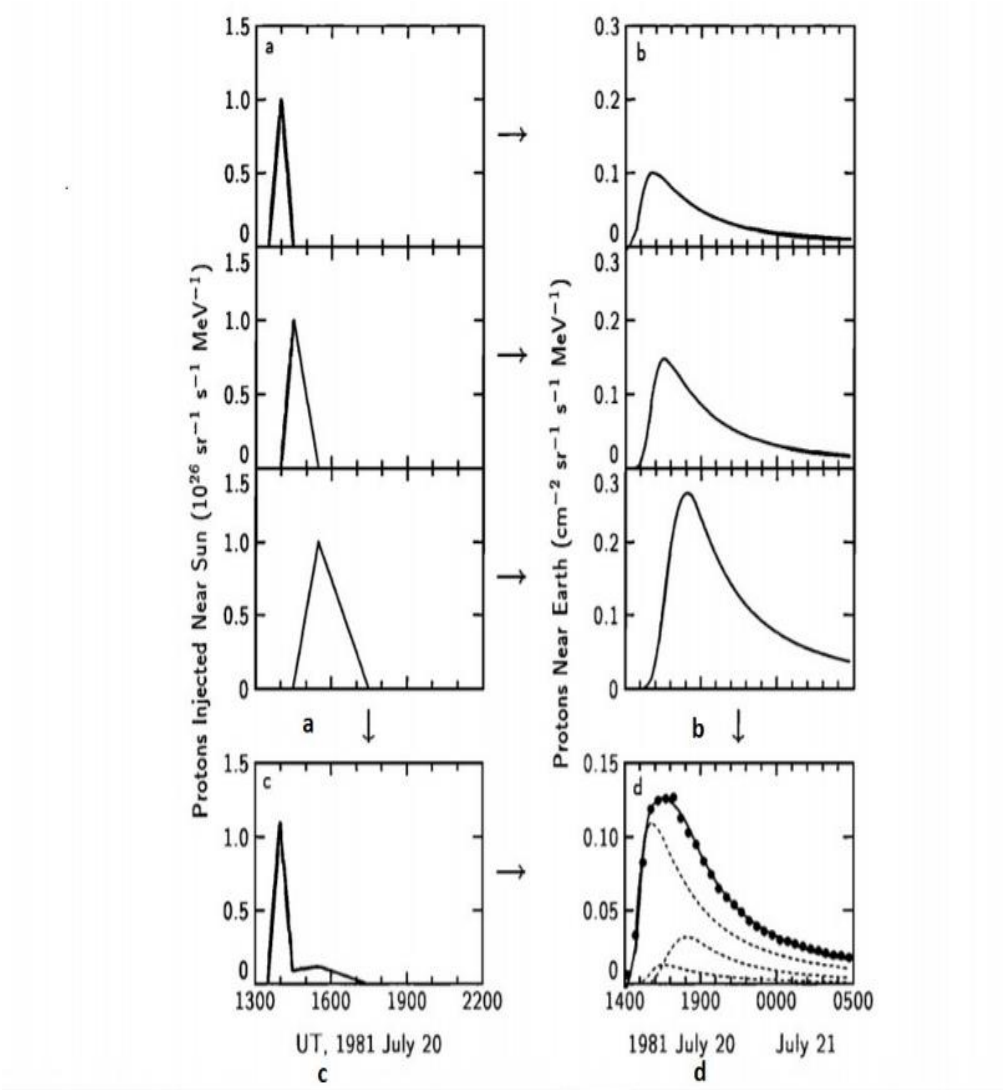

Figure 20 Illustration of the deconvolution technique for a piecewise linear injection function near the Sun. The transport equation is solved for an instantaneous injection of particles. The resulting Green's function is convolved with (a) triangular injection profiles to (b) yield response functions. Linear, least squares fitting yields (d) the linear combination of response functions that best fits the data and (c) the corresponding best-fit piecewise linear injection profile

CHAPTER III
METHODOLOGY

In this chapter, we will discuss the research methods of simulation on the motion of particles from the Sun's eruption along the magnetic field lines to Earth. The details are as follows

3.1 Tools used in research operations

In this research, two types of research tools are used, which are

3.1.1 Data from the ACE spacecraft

The ACE spacecraft is a NASA spacecraft for studying the composition of the solar wind. This spacecraft launch to the Lagrange point L1 which is 1.5 million kilometers away from Earth. It is the point where the gravity of Earth and the Sun are well balanced. When the spacecraft reaches L1 after traveling for about 3 months, it will begin to study the elements and isotopes that blow from the Sun and from other sources in space. The researchers can download the information from the website. http://www.srl.caltech.edu/ACE/ as this website is completely free to access and download the information.

3.1.2 Program written in C++ for the simulation of particle motion from Ruffolo's transport equation

The researcher uses C++ programming language to simulate particle motion from Ruffolo's transport equation, which is processed on the operating system. In which the program was written in C language to simulate particle’s motion that consists of 9 programs which are;

i. wind.c is the main program for the simulation of particle motion which the program will receive various variable values from the data used to simulate the movement and retrieve files from other programs. To do processing the variables that are used to simulate particle motion are in the file named in, which has the following variables:

starts	is the starting distance in the simulation (AU).
stops	is the final distance of the simulation (AU).
s. step	is the increment of distance (AU).
prints	is the printing between (AU).

nmu is the number of points of μ.

length is the length of the simulation (AU).

np is the amount of momentum.

p [1 ... np] is the momentum of each energy.

m is the mass of the particle.

beta of sw is the ratio of solar wind speed to light speed.

lambda (λ) is the average free distance.

q is the index of particle scattering.

printextra is to print the information on the screen or not.

ii. decel.c is a program for processing in terms of the gradual decomposition of the particle Ruffolo transport equation.

iii. field.c is a program for processing the motion of particles along a magnetic field line in an intermediate planet. It will calculate the coefficient of scattering in terms of the flaring of the magnetic field, as well as the effect of the solar wind on interplanetary medium.

iv. initial.c is a program that determines the particle distribution source for use in processing particle motion simulation, by comparing the maximum particle distribution in the smallest energy to the default value. Due to the maximum number of particles the flux of the particles at the higher energy levels is calculated proportionally respectively to determine the maximum flux at each energy level.

v. inject.c is a program used to calculate particle release.

vi. nrutil.c is a program used to reserve space in memory.

vii. printout.c is a program for the display of required information.

viii. stream.c is a program that considers the movement of particles along the z-axis by the convection of the solar wind.

ix. tridag.c is a program for solving matrix equations.

3.2 Numerical methods used in research operations

The Ruffolo transport equation is in the form of a partial differential equation (PDE) with many independent variables. Therefore, it is difficult for us to find the answer or the solution directly. Since the Ruffolo transport equation is a linear PDE

and can know the boundary condition. Therefore, the finite difference method can be used to find the solution of transport equations. There are 3 ways to find a solution that are explicit method, implicit method and Crank-Nicholson method.

From the particle diffusion equation when $f(x_i, t_n)$ is as shown in the following equation

when $$\frac{\partial f}{\partial t} = -\frac{\partial S}{\partial x}$$

$$S = -D\frac{\partial f}{\partial x}$$

Substitute S into the equation to get

$$\frac{\partial f}{\partial t} = -\frac{\partial}{\partial x}\left(-D\frac{\partial f}{\partial x}\right)$$

$$= D\frac{\partial^2 f}{\partial^2 x}$$

Where;

S is a flux or number of particles moving through a point in time t.

f is the particle flux.

D is the coefficient of diffusion.

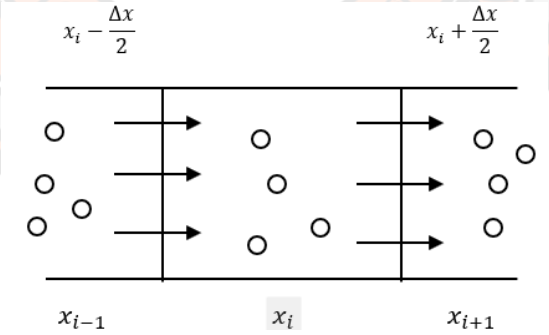

Figure 21 Flow of particles through cells

Net number of particles = inflow particles - outflow particles

$$\frac{\partial}{\partial t}(f \cdot \Delta x) = s\left(x_i - \frac{\Delta x}{2}\right) - s\left(x_i + \frac{\Delta x}{2}\right) \quad (3.1)$$

particle flow rate

$$\frac{\partial f}{\partial t} = \frac{f^{n+1}(x_i) - f^n(x_i)}{\Delta t} = \frac{s\left(x_i - \frac{\Delta x}{2}\right) - s\left(x_i + \frac{\Delta x}{2}\right)}{\Delta x} \quad (3.2)$$

when n = 0,1,2, …

$$\frac{f^{n+1}(x_i)-f^n(x_i)}{\Delta t} = \frac{-D\left(x_i-\frac{\Delta x}{2}\right)[f(x_i)-f(x_{i-1})]+D\left(x_i+\frac{\Delta x}{2}\right)[f(x_{i+1})-f(x_i)]}{(\Delta x)^2} \quad (3.2)$$

where $r = \frac{D\Delta t}{(\Delta x)^2}$ when x = 1

$$f^{n+1}(x_i) - f^n(x_i) = -r[f(x_i) - f(x_{i-1})] + r[f(x_{i+1}) - f(x_i)]$$

$$= -rf(x_i) + rf(x_{i-1}) + rf(x_{i+1}) - rf(x_i)$$

$$f^{n+1}(x_i) = f^n(x_i) + r[f(x_{i-1}) - 2f(x_i) + f(x_{i+1})] \quad (3.3)$$

Equation (3.3) is the main equation for solving transport equation for solving by using explicit method, implicit method and Crank-Nicholson method.

3.2.1 explicit method

The principle is from the equation (3.3) to put all the old values on the right-hand side by assigning n + 1 to the new value as time increases and n is the old value at the beginning time and in the left-hand expression of the equation (3.3) Set all f power to n.

From the initial equation, the equation (3.3) will get the equation as

$$f^{n+1}(x_i) - f^n(x_i) = r[f(x_{i-1}) - 2f(x_i) + f(x_{i+1})]$$

$$f^{n+1}(x_i) = f^n(x_i) + r[f(x_{i-1}) - 2f(x_i) + f(x_{i+1})]$$

So, $$f^{n+1}(x_i) = rf^n(x_{i-1}) + (1-2r)f^n(x_i) + rf^n(x_{i+1}) \quad (3.4)$$

when i = 1,2, 3…., N-1

From the equation (3.4) to solve the equation by using the matrix to solve the equation by substituting the value of i but each value into the equation will get;

$$i = 1, \quad f^{n+1}(x_1) = rf^n(x_0) + (1-2r)f^n(x_1) + rf^n(x_2)$$

$$i = 2, \quad f^{n+1}(x_2) = rf^n(x_1) + (1-2r)f^n(x_2) + rf^n(x_3)$$

$$i = 3, \quad f^{n+1}(x_3) = rf^n(x_2) + (1-2r)f^n(x_3) + rf^n(x_4)$$

$$\vdots$$

$$i = N-1, \quad f^{n+1}(x_{N-1}) = rf^n(x_{N-2}) + (1-2r)f^n(x_{N-1}) + rf^n(x_N)$$

Error analysis

From the initial equation;

$$f^{n+1}(x_i) - f^n(x_i) = r[f(x_{i-1}) - 2f(x_i) + f(x_{i+1})]$$

Consider $f(x_{i-1}) - 2f(x_i) + f(x_{i+1})$

using the Taylor series distribution method

$$f(x_{i-1}) = f(x_{i-1}) \quad (3.5)$$

$$f(x_i) = f(x_{i-1}) + \Delta x f'(x_{i-1}) + \frac{(\Delta x)^2 f''(x_{i-1})}{2} + \frac{(\Delta x)^3 f'''(x_{i-1})}{6} + \cdots \quad (3.6)$$

$$f(x_{i+1}) = f(x_{i-1}) + 2\Delta x f'(x_{i-1}) + \frac{(2\Delta x)^2 f''(x_{i-1})}{2} + \frac{(2\Delta x)^3 f'''(x_{i-1})}{6} + \cdots \quad (3.7)$$

Substitute the equation (3.5), (3.6) and the equation (3.7) into $f(x_{i-1}) - 2f(x_i) + f(x_{i+1})$, we get;

$$f(x_{i-1}) - 2f(x_i) + f(x_{i+1}) = f(x_{i-1}) - 2f(x_{i-1}) - 2\Delta x f'(x_{i-1}) - (\Delta x)^2 f''(x_{i-1}) - \frac{1}{3}(\Delta x)^3 f'''(x_{i-1}) + \cdots + f(x_{i-1}) + 2\Delta x f'(x_{i-1}) + 2(\Delta x)^2 f''(x_{i-1}) + \frac{2}{3}(\Delta x)^3 f'''(x_{i-1}) \quad (3.8)$$

$$f(x_{i-1}) - 2f(x_i) + f(x_{i+1}) \approx -(\Delta x)^2 f''(x_{i-1}) - \frac{1}{3}(\Delta x)^3 f'''(x_{i-1}) + \cdots + 2(\Delta x)^2 f''(x_{i-1}) + \frac{2}{3}(\Delta x)^3 f'''(x_{i-1}) + \cdots$$

So, $f(x_{i-1}) - 2f(x_i) + f(x_{i+1}) \approx f''(x_{i,t}) + 0(\Delta x)^2$

when $0(\Delta x)^2$ is the error that is in order of 2 from the initial equation considered in the expression $f^{n+1}(x_i) - f^n(x_i)$

Therefore, $\frac{f^{n+1}(x_i) - f^n(x_i)}{\Delta t} = \frac{\partial f(x_i)}{\partial t} \approx 0(\Delta t)$

when $0(\Delta t)$ is the error in x in order 2 as shown in equation (3.9).

$$\text{error} \propto 0(\Delta t) + 0(\Delta x)^2 \quad (3.9)$$

3.2.2 Implicit methods

The principle of this method is to reset all values to the right from the initial equation in the equation (3.3) by assigning n + 1 to the new value as time increases and n is the old value at the initial time. Set all f power to n + 1.

From the initial equation, the equation (3.3) is given as

$$\begin{aligned} f^{n+1}(x_i) - f^{n}(x_i) &= r[f^{n+1}(x_{i-1}) - 2f^{n+1}(x_i) + f^{n+1}(x_{i+1})] \\ f^{n}(x_i) &= f^{n+1}(x_i) - rf^{n+1}(x_{i-1}) + 2rf^{n+1}(x_i) - rf^{n+1}(x_{i+1}) \\ \therefore f^{n}(x_i) &= -rf^{n+1}(x_{i-1}) + (1+2r)f^{n+1}(x_i) - rf^{n+1}(x_{i+1}) \end{aligned} \quad (3.10)$$

when i = 1,2,3.…

From the equation (3.10), use the matrix to solve the equation by substituting the value of i in each equation and will get;

$$\begin{aligned} i = 1, \quad & f^{n}(x_1) = -rf^{n+1}(x_0) + (1+2r)f^{n+1}(x_1) - rf^{n+1}(x_2) \\ i = 2, \quad & f^{n}(x_2) = -rf^{n+1}(x_1) + (1+2r)f^{n+1}(x_2) - rf^{n+1}(x_3) \\ i = 3, \quad & f^{n}(x_3) = -rf^{n+1}(x_2) + (1+2r)f^{n+1}(x_3) - rf^{n+1}(x_4) \\ & \vdots \\ i = N-1, \quad & f^{n}(x_{N-1}) = -rf^{n+1}(x_{N-2}) + (1+2r)f^{n+1}(x_{N-1}) - rf^{n+1}(x_N) \end{aligned}$$

We get in the form of matrix as following

$$\begin{pmatrix} (1+2r) & -r & 0 & \cdots & 0 \\ -r & (1+2r) & -r & \ddots & \vdots \\ 0 & -r & (1+2r) & -r & 0 \\ \vdots & \ddots & \ddots & \ddots & \ddots \\ 0 & \cdots & 0 & -r & (1+2r) \end{pmatrix} \begin{pmatrix} f^{n+1}(x_1) \\ f^{n+1}(x_2) \\ f^{n+1}(x_3) \\ \vdots \\ f^{n+1}(x_{N+1}) \end{pmatrix} = \begin{pmatrix} rf^{n+1}(x_0) + f^{n}(x_1) \\ f^{n}(x_2) \\ f^{n}(x_3) \\ \vdots \\ f^{n}(x_{N+1}) \end{pmatrix}$$

In determining the difference will use the Taylor series distribution method as same in explicit method which is given as the equation (3.11)

$$\text{error} \propto O(\Delta t) + O(\Delta x)^2 \quad (3.11)$$

3.2.3 Crank-Nicolson method

It is the method of combination of explicit methods and implicit methods.

We know;

$$r = \frac{D\Delta t}{(\Delta x)^2} \qquad \text{where } r = 2S$$

$$f^{n+1}(x_i) = rf^n(x_{i-1}) + (1-2r)f^n(x_i) + rf^n(x_{i+1}) \quad (3.12)$$

And from the implicit methods in the equation (3.2.10) we have;

$$f^n(x_i) = -rf^{n+1}(x_{i-1}) + (1+2r)rf^{n+1}(x_i) - rf^{n+1}(x_{i+1}) \quad (3.13)$$

Add equation (3.12) and (3.13) we will get;

$$-rf^{n+1}(x_{i-1}) + (2+2r)rf^{n+1}(x_i) - rf^{n+1}(x_{i+1}) = rf^n(x_{i-1}) + (2-2r)f^n(x_i) + rf^n(x_{i+1})$$

Substitute $r = 2S$ And take 2 divided throughout the equation to get;

$$-Sf^{n+1}(x_{i-1}) + (1+2S)f^{n+1}(x_i) - Sf^{n+1}(x_{i+1}) = Sf^n(x_{i-1}) + (1-2S)f^n(x_i) + Sf^n(x_{i+1}) \quad (3.14)$$

when i = 1,2,3,…,N-1

From the equation (3.14) can be solved by using the matrix form by substituting the value of i in each value as follows;

$$i = 1, -Sf^{n+1}(x_0) + (1+2S)f^{n+1}(x_1) - Sf^{n+1}(x_2) = Sf^n(x_0) + (1-2S)f^n(x_1) + Sf^n(x_2)$$

$$i = 2 - Sf^{n+1}(x_1) + (1+2S)f^{n+1}(x_2) - Sf^{n+1}(x_3) = Sf^n(x_1) + (1-2S)f^n(x_2) + Sf^n(x_3)$$

$$i = 3, -Sf^{n+1}(x_2) + (1+2S)f^{n+1}(x_3) - Sf^{n+1}(x_4) = Sf^n(x_2) + (1-2S)f^n(x_3) + Sf^n(x_4)$$

$$\vdots$$

$$-Sf^{n+1}(x_{N-2}) + (1+2S)f^{n+1}(x_{N-1}) - Sf^{n+1}(x_N) = Sf^n(x_{N-2}) + (1-2S)f^n(x_{N-1}) + Sf^n(x_N)$$

$$i = N-1,$$

When we write in matrix;

$$\begin{pmatrix} (1+2S) & -S & 0 & \cdots & 0 \\ -S & (1+2S) & -S & \ddots & \vdots \\ 0 & -S & (1+2S) & -S & 0 \\ \vdots & \ddots & \ddots & \ddots & \ddots \\ 0 & \cdots & 0 & -S & (1+2S) \end{pmatrix} \begin{pmatrix} f^{n+1}(x_1) \\ f^{n+1}(x_2) \\ f^{n+1}(x_3) \\ \vdots \\ f^{n+1}(x_{N+1}) \end{pmatrix} =$$

$$\begin{pmatrix} (1-2S) & S & 0 & \cdots & 0 \\ S & (1-2S) & S & \ddots & \vdots \\ 0 & S & (1-2S) & S & 0 \\ \vdots & \ddots & \ddots & \ddots & \ddots \\ 0 & \cdots & 0 & S & (1-2S) \end{pmatrix} \begin{pmatrix} f^{n+1}(x_1) \\ f^{n+1}(x_2) \\ f^{n+1}(x_3) \\ \vdots \\ f^{n+1}(x_{N+1}) \end{pmatrix}$$

$$+ \begin{pmatrix} S[f^{n+1}(x_0) + f^{n}(x_1)] \\ f^{n}(x_2) \\ f^{n}(x_3) \\ \vdots \\ f^{n}(x_{N+1}) \end{pmatrix}$$

In determining the discrepancy, since it is a combination of explicit methods and implicit methods therefore, the total error is as follows;

$$\text{error} \propto O(\Delta t)^2 + O(\Delta x)^2 \qquad (3.15)$$

3.3 Study of solar eruptions to select the solar event

We study the physical characteristics of solar eruptions including the analysis of the motion of high energy particles from the Sun recorded by ACE spacecraft. The event of interest is selected based on the changes and phenomena which are determined by the level of intensity of particles traveling to Earth. We have selected the solar event on 6th September, 2017 because the eruption was violent and it is the strongest flare in the 24th solar cycle, with the intensity of X-rays of X9.3. The eruption position at S10W30 has a solar wind speed of 575 km/s. We have chosen to analyse the density data of He, N, C, O and Fe particles measured by the ACE spacecraft on 6 September 2017.The physical characteristics of selected event is shown below in Table 4.

Table 4 Physical characteristics of the event on 6 September 2017

Physical characteristics	Details
Solar cycle	24th cycle
Radiation level	X9.3
The eruption began	11:53 UT
End of the eruption time	12.10 UT
Eruption duration	17 Minutes
Eruption position	S10W30
Solar wind speed	575 km/s

The eruption from the sun's surface on 6th September, 2017 of X9.3 which began at 11:53 UT and end at 12:10 UT is calculated for the duration of 17 minutes. The intense particle of X9.3 white light on the right side of the Sun from the eruption at the AR2673 position as shown in the following figure 22.

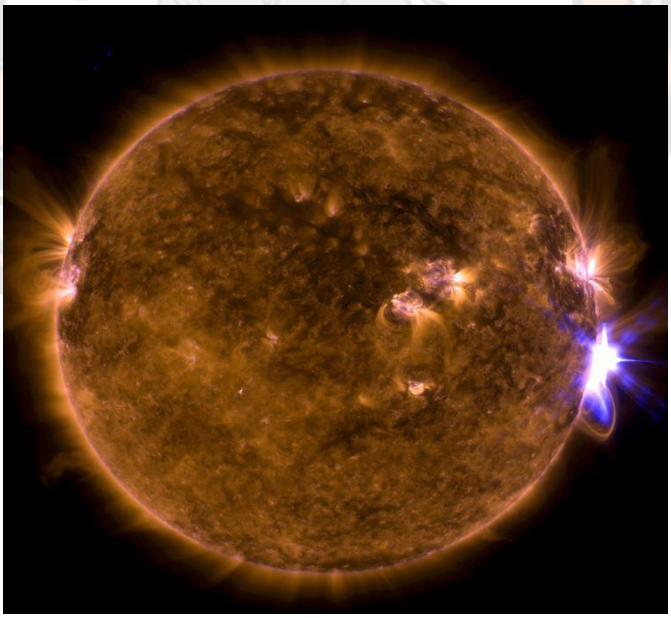

Figure 22 The solar eruption on 6th September, 2017.

Source: https://apod.nasa.gov/apod/ap170914.html

According to the physical characteristics of the study, the preliminary data on the intensity of X-rays from 11:53 – 12:10 UT on 6th September, 2017, it is found that the

eruption took place around 17 minutes on the surface of the Sun. The eruption on the surface from the Sun is observed from the intensity of X-rays measured in units (W/m^2) based on severity level, A, B, C, M and X, measured from the GOES spacecraft on 6th September, 2017with the highest intensity eruption at X9.3 at 12.02 UT. The intensity of X-rays approached 10^{-3} (W/m^2) and also found that the speed of solar wind on 6th September, 2017 varied between 480 km/s and 600 km/s. It is observed that 12.02 UT is the time when most particles are released, with wind speeds of 575 km/s in the following figure 23.

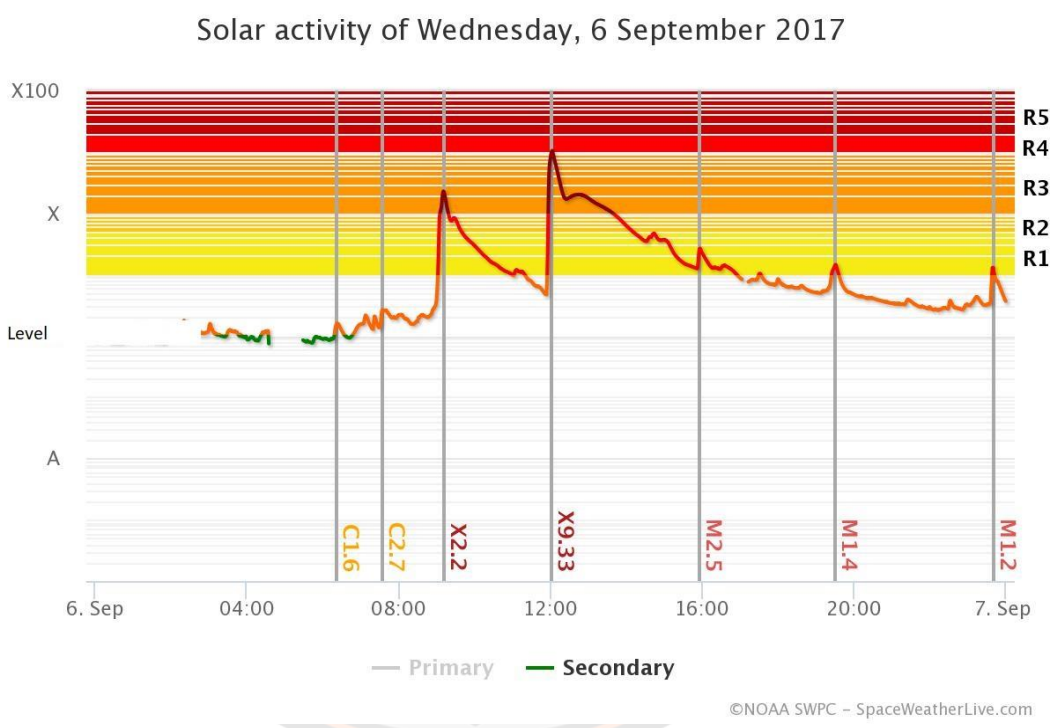

Figure 23 X-ray severity values on 6th September 2017

Source: https://www.spaceweatherlive.com/en/archive/2017/09/06/xray

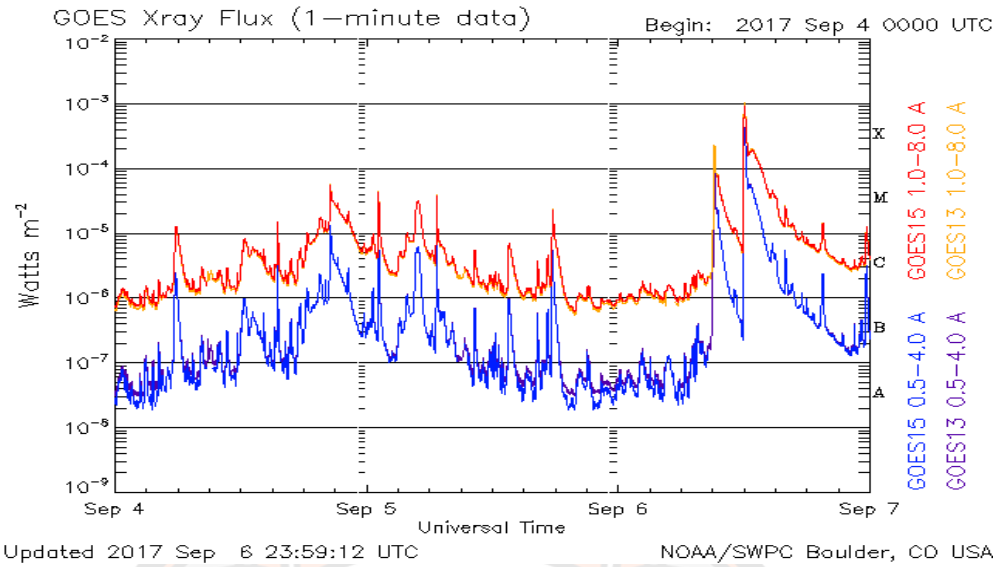

Figure 24 Shows the X-ray emission eruption from 4-6 September 2017.

Source: https://www.spaceweatherlive.com/en/archive/2017/09/06/xray

we classify solar flare according to their X-ray intensity in the wavelength range from 1 to 8 Angstroms. We have the class A, B, C, M and X level. X-class flares are big, they are major events that can trigger planet-wide radio blackouts and long-lasting radiation storms. These measurements are made by GOES, a geostationary satellite.

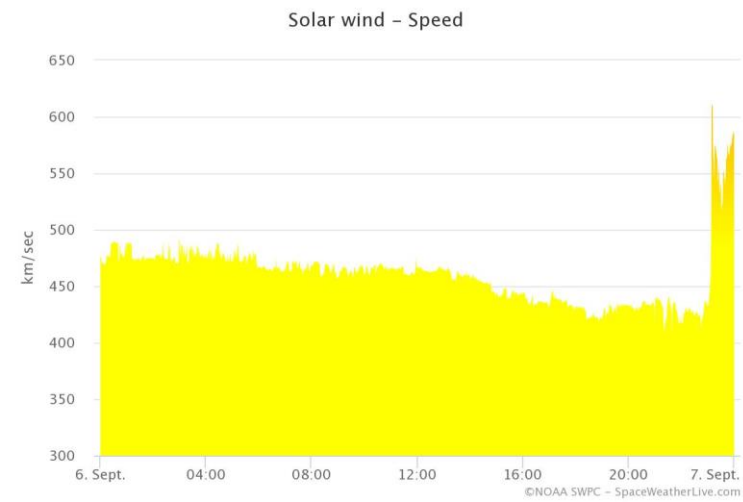

Figure 25 The graph showing the solar wind speed on 6th September 2017.

Source: https://www.spaceweatherlive.com/en/archive/2017/09/06/aurora

The Sun is continuously emitting a stream of charge particles to Earth over a time. Therefore, we have selected particles of helium, carbon, nitrogen, oxygen, and iron particles with an energy almost close to each other. We analyze the flux values of He, C, N, O and Fe particles measured from the SIS instrument on the ACE spacecraft for September 6, 2017.

3.4 Download basic information collected from the ACE spacecraft

The present research is carried out based on the data collected from the website www.srl.caltech.edu/ACE where the information is gathered by spacecraft ACE measured by SIS that allows us to download information about various phenomena that occur on the Sun and in the solar system. The information is downloaded by using the following steps:

3.4.1 Go to website www.srl.caltech.edu/ACE

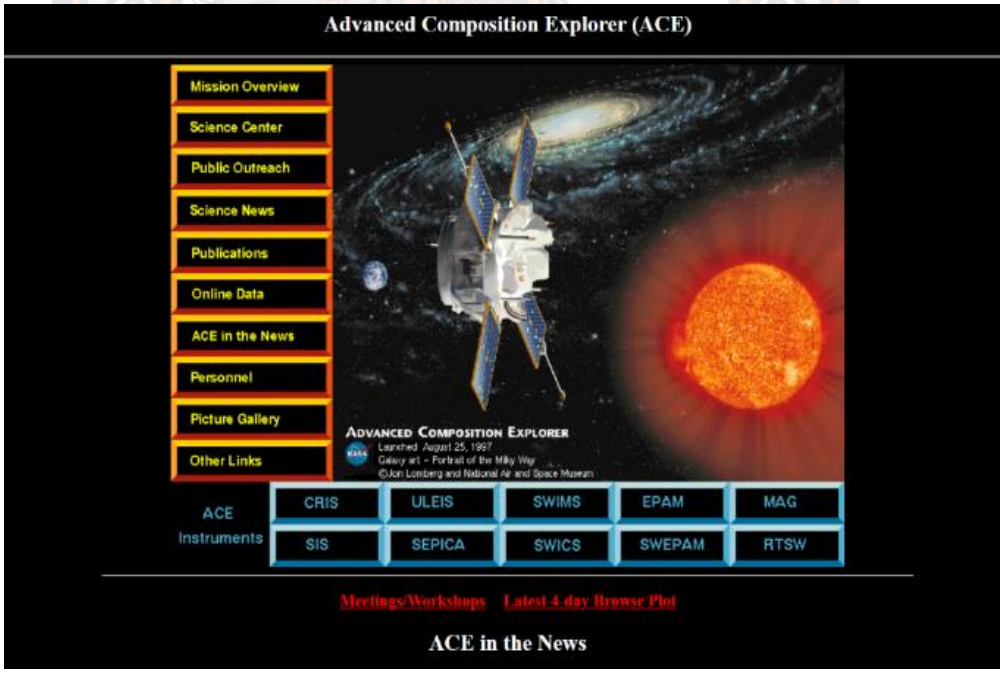

Figure 26 Homepage www.srl.caltech.edu/ACE

Source: http://www.srl.caltech.edu/ACE/

3.4.2 Select Online Data to access the online data download.

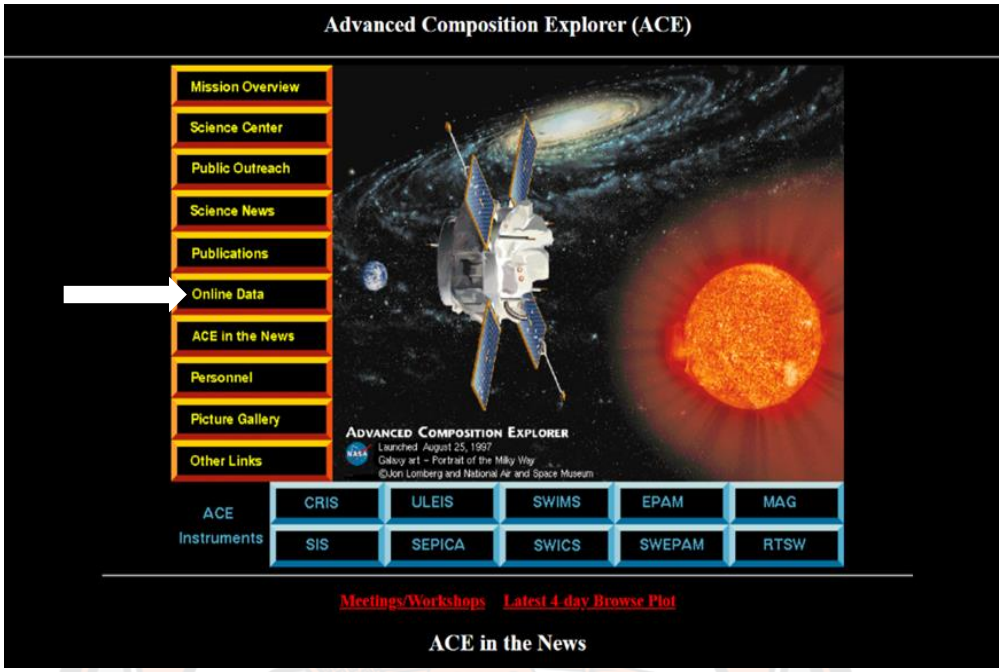

Figure 27 Homepage www.srl.caltech.edu/ACE

Source: http://www.srl.caltech.edu/ACE/

3.4.3 Select Level 2 (Verified) the type of measuring instrument

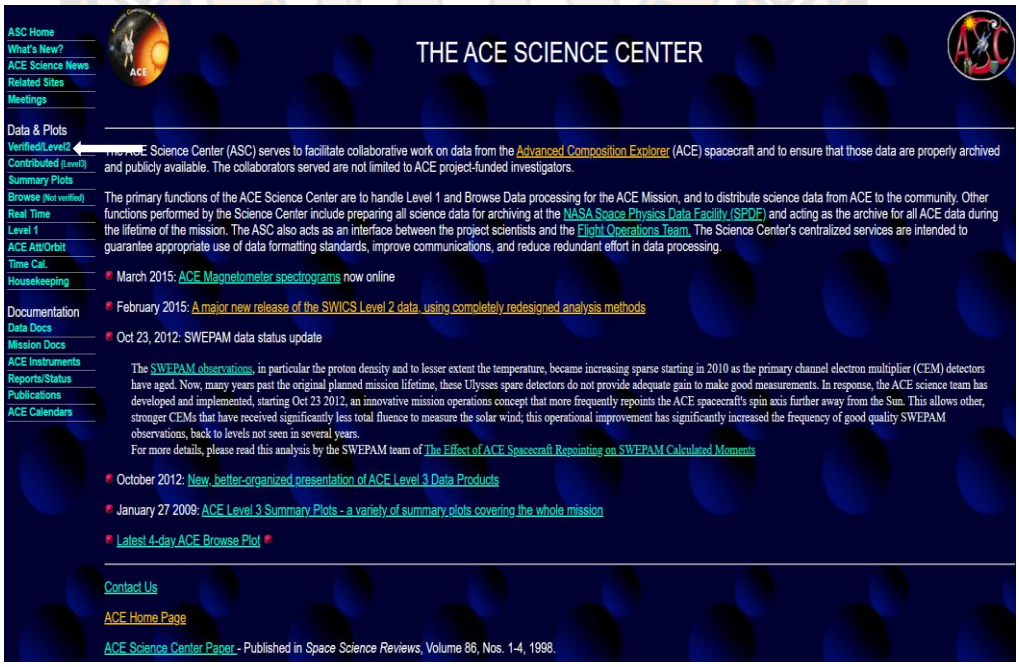

Figure 28 Shows a page for Online Data

Source: http://www.srl.caltech.edu/ACE/ASC/

3.4.4 Select SIS Data to select the data from the instrument SIS

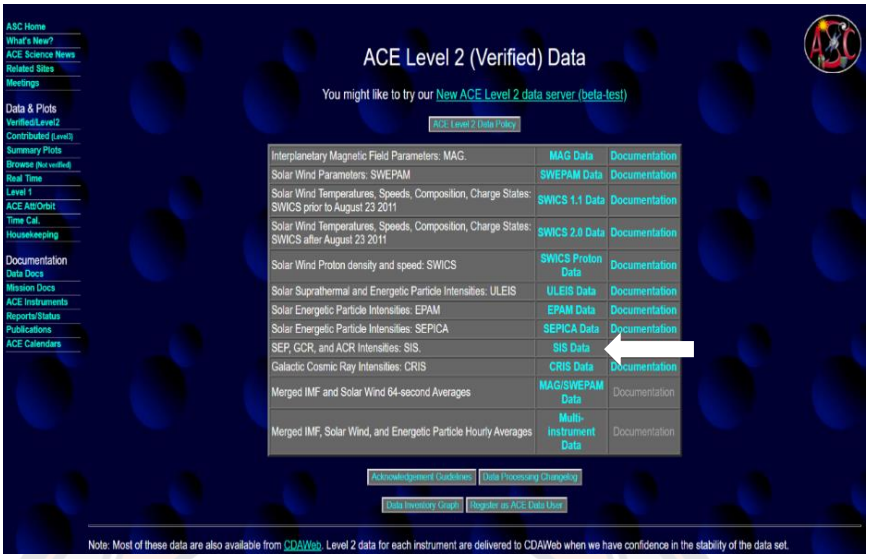

Figure 29 Shows a page level 2 (Verified) measurement tools for research

Source: http://www.srl.caltech.edu/ACE/ASC/level2/index.html

3.4.5 Select SIS Data to select data from the instrument SIS

Choose the date range of the information you need in the Hourly Averages field. This study chose to study the eruption event on 6th September 2017, calculated as the number of days in the year, which is 249 of the year. Then select 247/2017-254/2017 Press GO to download as shown in figure 30.

Figure 30 Shows the date range setting for the data to be studied.

Source: http://www.srl.caltech.edu/ACE/ASC/level2/lvl2DATA_SIS.html

3.4.6 Select the required element for simulation.

To analyze the elements He, C, N, O, Fe. Choose the data to download, including time, particle density and the number of particles per unit time of the various elements. Then specify the desired date range in the Starting and Ending boxes. Select the data format as Text file download and select Retrieve data to download the data.

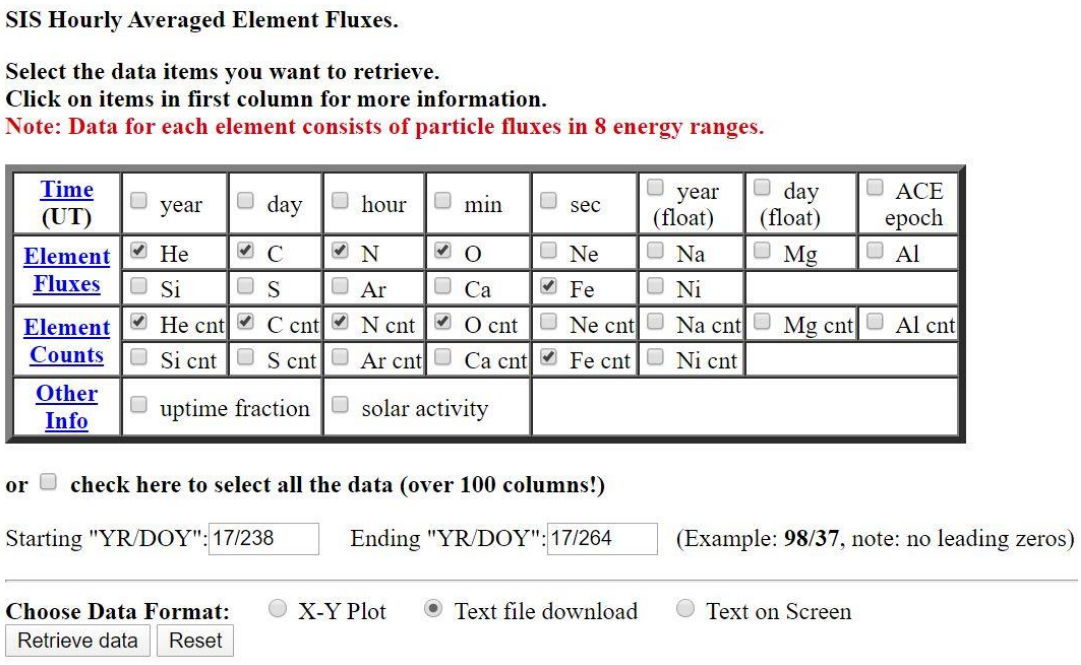

SIS Hourly Averaged Element Fluxes.

Select the data items you want to retrieve.
Click on items in first column for more information.
Note: Data for each element consists of particle fluxes in 8 energy ranges.

Time (UT)	☐ year	☐ day	☐ hour	☐ min	☐ sec	☐ year (float)	☐ day (float)	☐ ACE epoch
Element Fluxes	☑ He	☑ C	☑ N	☑ O	☐ Ne	☐ Na	☐ Mg	☐ Al
	☐ Si	☐ S	☐ Ar	☐ Ca	☑ Fe	☐ Ni		
Element Counts	☑ He cnt	☑ C cnt	☑ N cnt	☑ O cnt	☐ Ne cnt	☐ Na cnt	☐ Mg cnt	☐ Al cnt
	☐ Si cnt	☐ S cnt	☐ Ar cnt	☐ Ca cnt	☑ Fe cnt	☐ Ni cnt		
Other Info	☐ uptime fraction		☐ solar activity					

or ☐ check here to select all the data (over 100 columns!)

Starting "YR/DOY": 17/238 Ending "YR/DOY": 17/264 (Example: **98/37**, note: no leading zeros)

Choose Data Format: ○ X-Y Plot ◉ Text file download ○ Text on Screen

Retrieve data | Reset

Figure 31 Website page that can choose to download only the desired information.

Source:http://www.srl.caltech.edu/cgibin/dib/rundibviewsisl2/ACE/ASC/DATA/level2/sis?sis_data_1hr_2511.hdf!hdfref;tag=1962,ref=3,s=0

The measure data from the SIS instruments on the ACE spacecraft of the He element on 6th September 2017, consisting of particle density and the number of particles per unit time. The data is recorded hourly where the time is in minutes, He1-He8 shows the energy level of helium element from 4.032-34.769 MeV/n and CNT1-CNT2 represents number of particles.

	Time	He1	He2	He3	He4	He5	He6	He7	He8	CNT1	CNT2	CNT3	CNT4	CNT5	CNT6	CNT7	CNT8
2	30	3.28E+00	1.91E+00	8.47E-01	3.24E-01	3.85E-02	-1.00E+03	-1.00E+03	-1.00E+03	2.14E+02	1.37E+02	4.70E+01	3.90E+01	7.00E+00	0.00E+00	0.00E+00	0.00E+00
3	90	2.57E+00	1.40E+00	8.08E-01	2.01E-01	3.07E-02	-1.00E+03	-1.00E+03	-1.00E+03	2.02E+02	1.19E+02	5.60E+01	2.80E+01	7.00E+00	0.00E+00	0.00E+00	0.00E+00
4	150	1.12E+00	5.74E-01	3.58E-01	9.29E-02	1.91E-02	-1.00E+03	-1.00E+03	-1.00E+03	1.59E+02	8.50E+01	4.00E+01	2.20E+01	7.00E+00	0.00E+00	0.00E+00	0.00E+00
5	210	8.14E-01	3.77E-01	1.75E-01	6.79E-02	1.45E-02	-1.00E+03	-1.00E+03	-1.00E+03	1.40E+02	7.00E+01	2.60E+01	2.20E+01	6.00E+00	0.00E+00	0.00E+00	0.00E+00
6	270	7.36E-01	3.82E-01	1.77E-01	7.41E-02	3.84E-03	-1.00E+03	-1.00E+03	-1.00E+03	1.46E+02	8.10E+01	3.00E+01	2.60E+01	2.00E+00	0.00E+00	0.00E+00	0.00E+00
7	330	7.14E-01	3.37E-01	1.35E-01	3.14E-02	9.94E-03	-1.00E+03	-1.00E+03	-1.00E+03	1.30E+02	6.40E+01	2.00E+01	1.00E+01	4.00E+00	0.00E+00	0.00E+00	0.00E+00
8	390	6.56E-01	3.22E-01	7.87E-02	3.42E-02	5.21E-03	-1.00E+03	-1.00E+03	-1.00E+03	1.35E+02	7.10E+01	1.40E+01	1.40E+01	3.00E+00	0.00E+00	0.00E+00	0.00E+00
9	450	8.83E-01	4.50E-01	1.82E-01	4.67E-02	6.22E-03	-1.00E+03	-1.00E+03	-1.00E+03	1.70E+02	9.30E+01	3.20E+01	1.60E+01	3.00E+00	0.00E+00	0.00E+00	0.00E+00
10	510	8.58E-01	3.27E-01	1.21E-01	3.84E-02	7.42E-03	-1.00E+03	-1.00E+03	-1.00E+03	1.58E+02	6.90E+01	2.10E+01	1.40E+01	3.00E+00	0.00E+00	0.00E+00	0.00E+00
11	570	8.49E-01	3.95E-01	1.79E-01	4.83E-02	5.25E-03	-1.00E+03	-1.00E+03	-1.00E+03	1.58E+02	7.80E+01	2.80E+01	1.60E+01	3.00E+00	0.00E+00	0.00E+00	0.00E+00
12	630	1.07E+00	3.50E-01	1.64E-01	2.66E-02	5.30E-03	-1.00E+03	-1.00E+03	-1.00E+03	1.71E+02	6.00E+01	2.30E+01	8.00E+00	2.00E+00	0.00E+00	0.00E+00	0.00E+00
13	690	1.05E+00	4.71E-01	2.03E-01	5.37E-02	2.68E-03	-1.00E+03	-1.00E+03	-1.00E+03	1.54E+02	7.20E+01	2.50E+01	1.40E+01	1.00E+00	0.00E+00	0.00E+00	0.00E+00
14	750	1.20E+00	5.23E-01	2.13E-01	7.38E-02	8.36E-03	-1.00E+03	-1.00E+03	-1.00E+03	1.56E+02	7.50E+01	2.40E+01	1.70E+01	3.00E+00	0.00E+00	0.00E+00	0.00E+00
15	810	1.48E+00	4.82E-01	2.14E-01	6.91E-02	1.45E-02	-1.00E+03	-1.00E+03	-1.00E+03	1.76E+02	6.50E+01	2.20E+01	1.50E+01	4.00E+00	0.00E+00	0.00E+00	0.00E+00
16	870	1.37E+00	6.26E-01	3.41E-01	8.88E-02	1.69E-02	-1.00E+03	-1.00E+03	-1.00E+03	1.77E+02	8.40E+01	3.60E+01	2.00E+01	7.00E+00	0.00E+00	0.00E+00	0.00E+00
17	930	1.28E+00	3.60E-01	2.72E-01	5.48E-02	3.11E-02	-1.00E+03	-1.00E+03	-1.00E+03	1.61E+02	5.10E+01	3.00E+01	1.30E+01	1.00E+01	0.00E+00	0.00E+00	0.00E+00
18	990	1.24E+00	5.38E-01	1.28E-01	6.97E-02	3.59E-02	-1.00E+03	-1.00E+03	-1.00E+03	1.67E+02	8.00E+01	1.40E+01	1.70E+01	1.30E+01	0.00E+00	0.00E+00	0.00E+00
19	1050	1.15E+00	3.99E-01	2.43E-01	7.15E-02	1.85E-02	-1.00E+03	-1.00E+03	-1.00E+03	1.56E+02	5.80E+01	2.70E+01	1.80E+01	7.00E+00	0.00E+00	0.00E+00	0.00E+00
20	1110	1.35E+00	5.79E-01	3.21E-01	7.16E-02	3.42E-02	-1.00E+03	-1.00E+03	-1.00E+03	1.66E+02	8.00E+01	3.30E+01	1.60E+01	1.10E+01	0.00E+00	0.00E+00	0.00E+00
21	1170	1.18E+00	6.04E-01	2.06E-01	8.22E-02	4.51E-02	-1.00E+03	-1.00E+03	-1.00E+03	1.36E+02	7.40E+01	2.00E+01	1.70E+01	1.40E+01	0.00E+00	0.00E+00	0.00E+00
22	1230	1.77E+00	6.96E-01	4.06E-01	1.38E-01	6.09E-02	-1.00E+03	-1.00E+03	-1.00E+03	1.71E+02	7.20E+01	3.50E+01	2.40E+01	1.60E+01	0.00E+00	0.00E+00	0.00E+00
23	1290	1.87E+00	1.23E+00	4.55E-01	9.69E-02	3.25E-02	-1.00E+03	-1.00E+03	-1.00E+03	1.50E+02	1.06E+02	3.00E+01	1.40E+01	7.00E+00	0.00E+00	0.00E+00	0.00E+00
24	1350	2.84E+00	1.77E+00	7.73E-01	2.19E-01	5.11E-02	-1.00E+03	-1.00E+03	-1.00E+03	1.57E+02	1.06E+02	3.50E+01	2.20E+01	8.00E+00	0.00E+00	0.00E+00	0.00E+00
25	1410	2.41E+00	1.41E+00	6.64E-01	2.45E-01	4.74E-02	-1.00E+03	-1.00E+03	-1.00E+03	1.86E+02	1.27E+02	4.50E+01	3.30E+01	1.10E+01	0.00E+00	0.00E+00	0.00E+00
26	1470	3.28E+00	2.41E+00	1.11E+00	4.52E-01	1.11E-01	-1.00E+03	-1.00E+03	-1.00E+03	2.65E+02	2.14E+02	7.90E+01	6.80E+01	2.50E+01	0.00E+00	0.00E+00	0.00E+00

Figure 32 Shows an example of the He element downloaded from SIS.

3.5 Procedure for preparing data from the spacecraft for simulation

In this research, we collect the data measured by SIS instrument on the ACE spacecraft and to calculate the initial values necessary for the program to simulate particle motion. Which consists of the following values;

3.5.1 Determination of the data error due to spacecraft

The data measured from the spacecraft will be inaccurate therefore, the measured data will be used to find the data error due to the spacecraft (σ_{stat}). The data error is equal to the density of the particles or the flux of the particles divided by the square root of the number of particles per unit time.

$$\sigma_{stat} = \frac{\text{flux}}{\sqrt{\text{counts}}} \qquad (3.16)$$

Where; σ_{stat} is the data error due to spacecraft.

flux is the density of particles over time in unit area.

count is the number of particles.

Table 5 Shows an example of data measured from the SIS instruments on the ACE spacecraft of helium particle erupted on 6th September 2017

Time (min)	He1 (particles/(s-cm^2 -sr-MeV/n)	Counts 1 (no of particle)	Error
30	3.28	214	0.22422
90	2.57	202	0.18083
150	1.12	159	0.08882
210	0.814	140	0.0688
270	0.736	146	0.06091
330	0.714	130	0.06262
390	0.656	135	0.05646
450	0.883	170	0.06772
510	0.858	158	0.06826
570	0.849	158	0.06754
630	1.07	171	0.08183

Then we use the flux and time values to draw a graph showing the relationship between time in minutes along x-axis and the y-axis as the flux in particles/(s-cm^2-sr-MeV/n) to find the initial values required to simulate the motion, such as the particle density at the maximum start time and the time when the particle density is reduced by half.

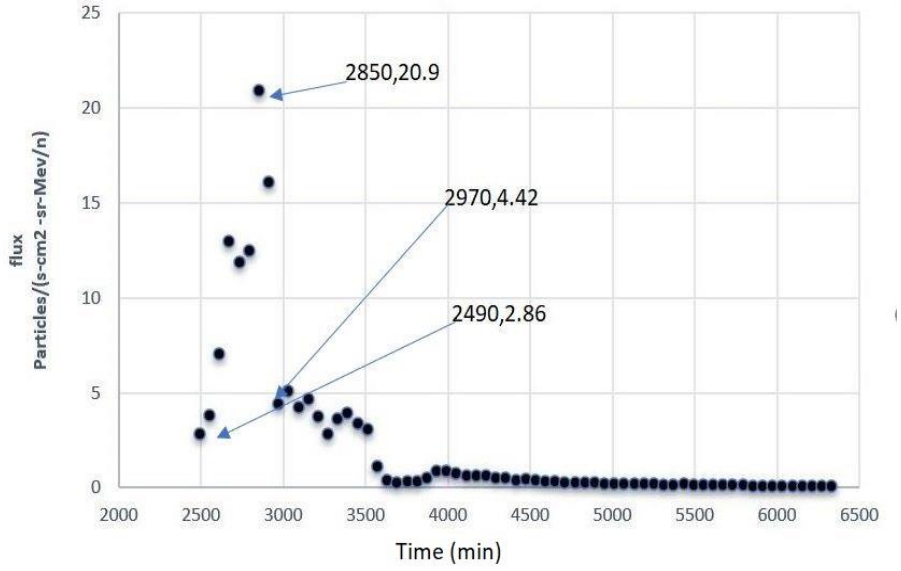

Figure 33 The density of He particles related with time.

From the figure 33, we can see that the particle density of the helium element at the energy level of 4.032 MeV/n, with the particles started to increase at 2490 minutes, peak at 2850 minutes and halved by 2970 minutes.

3.5.2 Determination of the true mass of each particle.

$$\text{Real mass} = \frac{(931.502 \frac{\text{MeV}}{c^2})\,A}{Z} \tag{3.17}$$

where Z is the mass number.

A is the atomic mass.

Real mass is the true mass of the particle (m_0).

1. Calculate real mass values of He particle.

$$\text{Real mass of helium} = \frac{(931.502)(4.0026)\frac{\text{MeV}}{c^2}}{4}$$

$$\text{Real mass of helium} = 932.107\ \frac{\text{MeV}}{c^2}$$

2. Calculate real mass values of C particle.

$$\text{Real mass of Carbon} = \frac{(931.502)(12.011)\frac{\text{MeV}}{c^2}}{12}$$

$$\text{Real mass of Carbon} = 932.355\frac{\text{MeV}}{c^2}$$

3. Calculate real mass values of N particle.

$$\text{Real mass of Nitrogen} = \frac{(931.502)(14.0067)\frac{\text{MeV}}{c^2}}{14}$$

$$\text{Real mass of Nitrogen} = 931.948\frac{\text{MeV}}{c^2}$$

4. Calculate real mass values of O particle.

$$\text{Real mass of Oxygen} = \frac{(931.502)(15.9994)\frac{\text{MeV}}{c^2}}{16}$$

$$\text{Real mass of Oxygen} = 931.467\ \frac{\text{MeV}}{c^2}$$

5. Calculate real mass values of Fe particle.

$$\text{Real mass of iron} = \frac{(931.502)(55.845)\frac{\text{MeV}}{c^2}}{16}$$

$$\text{Real mass of iron} = 928.934\ \frac{\text{MeV}}{c^2}$$

3.5.3 Determination of the average energy value for each energy level (E_K)

Table 6 Energy value of element He

Range Helium	Emin (MeV/n)	Emax (MeV/n)	Sqrt (Emin*Emax) (MeV/n)
0	3.43000	4.74000	4.03215
1	4.74000	6.13000	5.39038
2	6.13000	7.29000	6.68489
3	7.29000	9.72000	8.41777
4	9.72000	13.5900	11.4932
5	13.5900	17.9600	15.6229
6	17.9600	29.3500	22.9592
7	29.3500	41.1900	34.7696

Source:http://www.srl.caltech.edu/ACE/ASC/level2/sis_energy_levels/SIS_ebands.txt

From the average maximum energy and minimum energy, each energy level will be

$$\text{Average energy } (E_k) = \sqrt{E_{Min} + E_{Max}} \qquad (3.18)$$

3.5.4 Determination of the distance of the magnetic field lines drawn by the solar wind (R)

From the equation $$R = \frac{v_{sw} \times 0.002291}{\cos(\text{s/c latitude})} \qquad (3.19)$$

Where R is the distance of the magnetic field drawn by the solar wind.

v_{sw} is the solar wind speed (1 km/s=0.00291 AU/min).

3.5.5 Determination of the distance between the position of the spacecraft and the Sun (USERR)

From the equation $$USERR = \frac{1AU}{1+0.0017\cos\left[\left(\frac{DOY-2}{365}\right)\times 360\right]} \quad (3.20)$$

Where USERR is the distance between the position of the spacecraft and the Sun (AU).

DOY is the day that the eruption occurred, the number of days is counted in one year.

3.5.6 Determination of the momentum of energy levels for each element

To simulation of particle motion, we have to study the distribution of particles in each momentum. The data that we get from the spacecraft is data of the energy level values. Therefore, we can calculate the momentum from the following equation.

$$P = \sqrt{(E_k + m_0)^2 - m_0^2} \quad (3.21)$$

where E_k is the average energy of each energy level (MeV/n).

p is the momentum (MeV/c).

m_o is the true mass of each element (kg).

3.5.7 Determination of the ratio of solar wind speed to light speed

The ratio of the solar wind speed to light speed is calculated as

$$v_{sw} = \beta c$$

$$\beta = \frac{v_{sw}}{c} = \frac{P}{E_k + m_0} \quad (3.22)$$

Where β ratio of solar wind speed to light speed.

v_{sw} solar wind speed (AU/min).

c speed of light equal to 0.1202 AU/min.

3.5.8 Determination of the Spectrum

$$\text{Spectrum of each energy level} = \frac{\text{maximum flux at energy level N}}{\text{maximum flux at energy level 1}} \quad (3.23)$$

Where N = 1,2,3,4,5,6,7 &8

3.5.9 Determination of the constant value for the particle decay.

Since the decomposition of high energy particles from the Sun has a tendency of continuous decay which is in accordance with the power law as in the equation.

$$\frac{dE}{dN} \alpha E^{-\gamma} \quad (3.24)$$

Where; E is the energy of particles (MeV/n).

N is the number of particles in each energy level.

γ is the constant deceleration rate of the particle in each energy level.

The deceleration of that particle can be determined from the slope of the graph between the log momentum value and the log spectrum value $\log\left(\frac{dE}{dN}\right)$as shown in Figure 19.

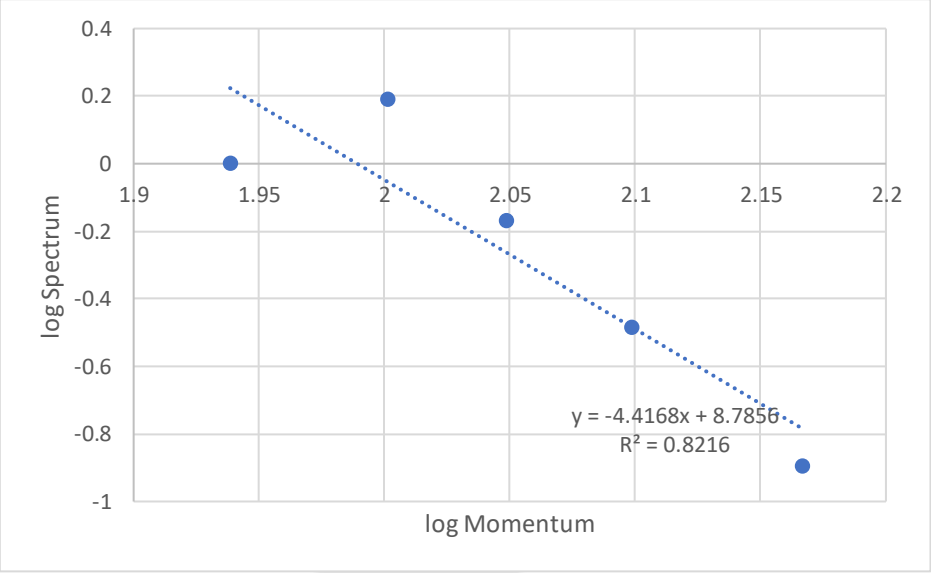

Figure 34 The graph shows the relationship between momentum log values and flux spectrum log values of He Particle.

As shown in Figure 34 the relationship between the log momentum and log spectrum (flux ratios) in which the linear slope of the particle's energy decreases at each energy level. So, it can be used as a default value in the next particle motion simulation.

3.5.10 Determination of the maximum distance of particles in each energy level from the relationship

From the equation $v_{max} = \beta c$

$$S = v_{max}\, t \qquad (3.25)$$

Where; v_{max} is the maximum speed of each power level (AU/min).

β is the ratio of solar wind speed to light speed.

t is the time that the particle has to move (min).

S is the distance traveled by a particle (AU).

c is the speed of light equal to 0.1202 (AU/min).

Table 7 Shows the values in the data preparation process for the element Fe.

E (MeV/n)	m_0 (MeV/c²)	P (MeV/c)	B	V (AU/min)	log P	flux He	spectrum	log spectrum	S (AU)
13.0021	928.924	55.965	0.165580609	0.019902789	2.193026185	0.0013158	1.000	0	114.640066
18.4613	928.924	186.116	0.196452144	0.023613548	2.269783294	0.0003473	0.264	-0.578473	136.0140351
23.7958	928.924	211.602	0.222102645	0.026696738	2.325518801	0.0000402	0.031	-1.514888	153.7732104
30.9023	928.924	241.592	0.251703983	0.030254819	2.383082615	0.0000122	0.009	-2.033757	174.2677562
43.5443	928.924	287.741	0.295887165	0.035565637	2.459001462	0.0000087	0.007	-2.178888	204.8580703
60.5592	928.924	340.848	0.344470546	0.04140536	0		0	0	238.4948717
90.8522	928.924	420.766	0.412605888	0.049595228	0		0	0	285.6685115
140.375	928.924	529.623	0.495299342	0.059534981	0		0	0	342.9214897

The table 7 shows the preparation of iron particles at the energy range from 13.0021 – 140.375 MeV/n.

Where; E is the average energy of the minimum and maximum energy.

m_0 is the true mass (kg).

P is the momentum value (MeV/c).

β is the ratio of solar wind speed to light speed.

V is the velocity of a particle at various energy levels (AU/min).

S is the maximum distance that the particles can move (AU).

3.6 Simulation of particle motion and fitting data

The Ruffolo's transportation equation is a linear partial differential equation. Therefore, a equation is used to calculate by using Finite Difference Method, with the initial condition data being the actual data from the ACE spacecraft. The equation helps to simulate the movement of high energy particles written in C language program on the ubuntu operating system.

$$\frac{\partial F}{\partial t} = -\frac{\partial}{\partial z}\mu v F - \frac{\partial}{\partial z}(1-\mu^2\frac{v^2}{c^2})v_{sw}\sec\psi\, F - \frac{\partial}{\partial \mu}\frac{v}{2L(z)}\left[1+\mu\frac{v_{sw}}{v}\sec\psi - \mu\frac{v_{sw}v}{c^2}\sec\psi\right](1-\mu^2)F$$
$$+\frac{\partial}{\partial \mu}v_{sw}\left(\cos\psi\frac{d}{dr}\sec\psi\right)\mu(1-\mu^2)F + \frac{\partial}{\partial \mu}\frac{\phi(\mu)}{2}\frac{\partial}{\partial \mu}\left(1-\mu\frac{v_{sw}v}{c^2}\sec\psi\right)F +$$
$$\frac{\partial}{\partial p}pv_{sw}\left[\frac{\sec\psi}{2L(z)}(1-\mu^2)+\cos\mu\frac{d}{dr}(\sec\psi)\mu^2\right]F$$

3.7 Fit to compare data

Once the results of the particle motion simulation are obtained, we then compare the data from the spacecraft with the results of particle motion simulation by using the linear least squares fitting technique with the following equation;

$$x^2 = \sum_{i=1}^{n}\left[\frac{y_n - y(x_n)}{\sigma_n}\right]^2 \qquad (3.26)$$

Where; x^2 is the sum of the squares difference of the amount of data n.

y_n is the real data from the spacecraft in the time flux data file of particles (fitdata.dat).

$y_{(x_n)}$ is the data from the simulation of particle motion in a file of counts.dat.

σ_n is the standard deviation of each data point.

n is the amount of data.

We fit the data to simulate the mean free path values with the actual data to find the x^2 value from the 5 neighbouring points which gives the minimum x^2 value from the parabolic trend line as shown in figure 35.

After getting the best mean free path from the average trend line once again, the values obtained will be used to compare the data to get the x^2 values which is used to find final delta lambda.

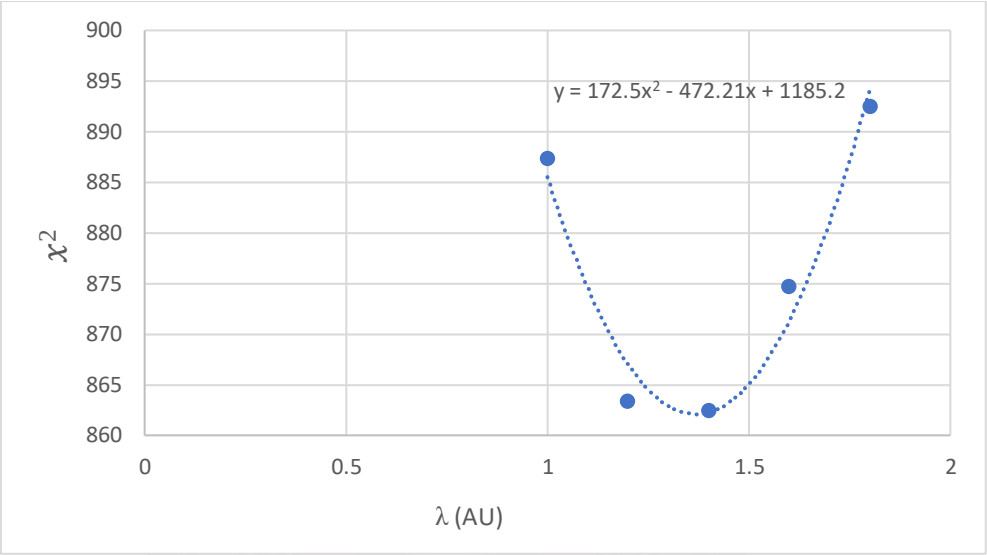

Figure 35 Shows a graph of the relationship between x^2 and the mean free path.

3.8 Determine the period of release of particles

When the appropriate mean free path is obtained, the result of fitting data will get the function of particle release time which can be used to draw graphs to determine the injection time where the y-axis is the injection function and the x-axis is the particle release time, as shown in Figure 36. In this research we use the FWHM method to determine the final injection time of the particle.

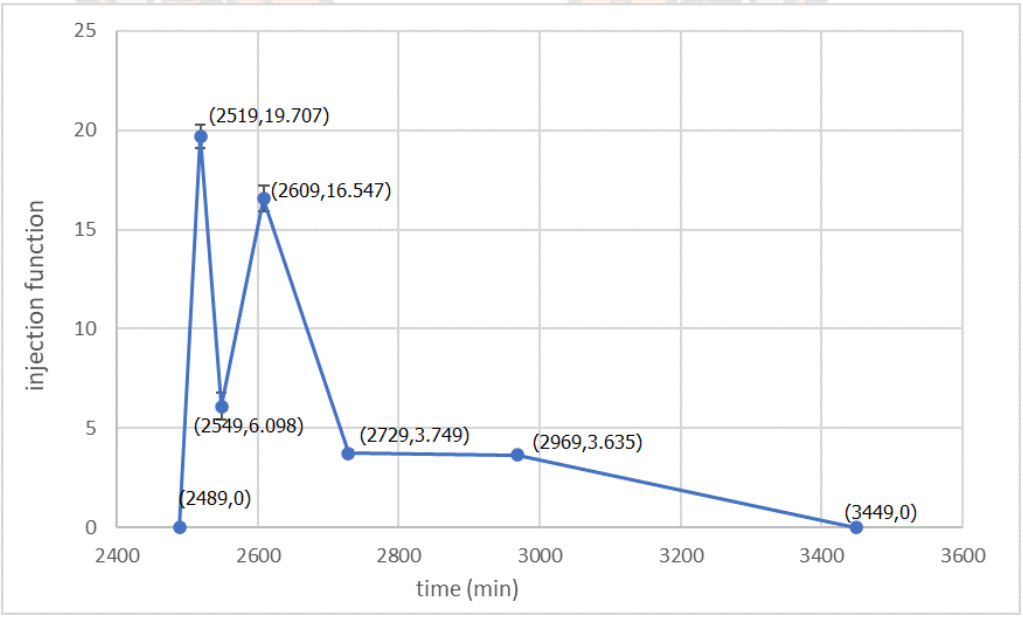

Figure 36 Shows the injection profile of helium at an energy level of 4.032 MeV/n.

The graph will look similar to the triangle. We can find the injection time of particle release using the FWHM method as follows:

1. Find the half value from the highest point of the release triangle (Half Maximum)

$$\text{Half Maximum} = \frac{y_2}{2} = \frac{19.707}{2} = 9.854$$

1. Find the time period t_1 and t_2

From the first linear graph

$y = 0.6569x - 1635$ where $y = 9.854$

$x \text{ or } t_1 = \frac{(9.854+1635)}{0.6569} = 2503.9633$ minutes

From the second linear graph

$y = -0.4536x + 1162.4$ where $y = 9.854$

$x/t_2 = \frac{(9.854-1162.4)}{-0.4536} = 2540.8873$ minutes

Difference in t_1 and t_2 = 36.924 minutes

2. Find the time period t_3 and t_4

From the third linear graph

$y = 0.1741x - 437.8$ where $y = 9.854$

$x/t_3 = \frac{(9.854+437.8)}{0.1741} = 2571.2436$ minutes

From the fourth linear graph

$y = -0.1067x + 294.8$ where $y = 9.854$

$x/t_4 = \frac{(9.854-294.8)}{-0.1067} = 2670.5388$ minutes

Difference in $t_3$and t_4 = 99.2952 minutes

3. Final release time

Sum of difference in t_1 and t_2 with difference in $t_3$and t_4 which is

36.924 + 99.2952 = 136.2192 minutes

Therefore, the release period of helium particles at the energy level of 4.032 MeV was the duration of 136.2192 minutes.

3.9 Space condition analysis

The Sun is continuously erupting the charge particles in the form of solar flare, corona mass ejection or solar storms which affect the Earth. So, we conducted a study of space conditions during the solar eruption in September 2017. There were 28 eruptions of M-level and 4 X-level from 6-10 September 2017. We have found that there was rapid expansion of dark spots on the AR2673 on 6th September, 2017 was the most violent, X9.3, and on September 10, 2017, there was X8.2, which is the second most violent in the 24th cycle.

Table 8 Data for the solar eruption in September

Eruption day	Began time (UT)	End time (UT)	Active Region	Corona Mass Ejection
6/10/2017	8:48	9:59	2673	Not found
	11:53	12:10	2673	Type II
7/10/2017	10:11	10:18	2673	Type IV
	14:20	14:55	2673	Type II
8/10/2017	7:40	7:58	2673	Not found
10/10/2017	15:35	16:31	2673	Type II, IV

The observed CME spreads forward to the Earth and reaches Earth's magnetosphere in the morning of September 7, 2017. On 6th September 2017 at 12:24 UT there was a second CME from the same active region targeting to the Earth. It is the shock wave of the second CME to reach Earth's magnetosphere in the afternoon of September 8.

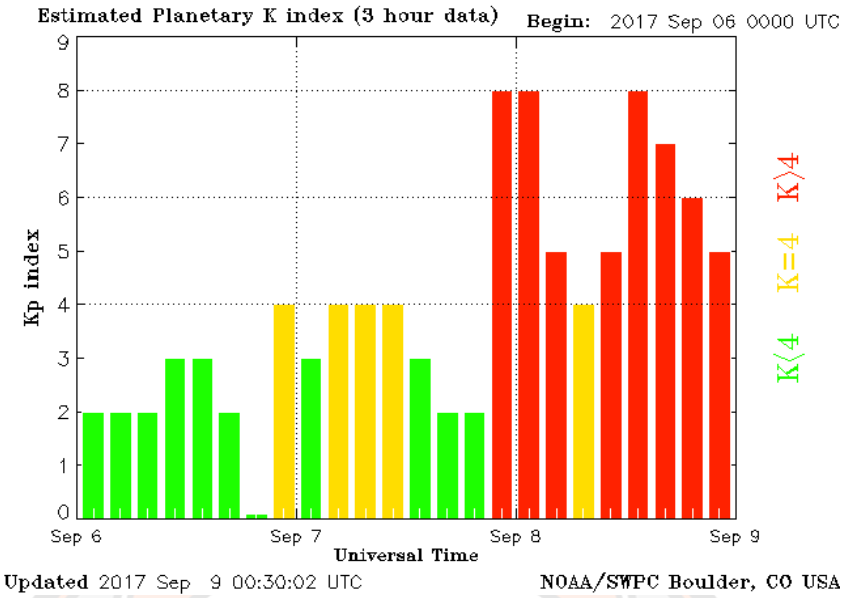

Figure 37 shows the kp index value on 6-8 September 2017.

Source: https://www.spaceweatherlive.com/en/archive/2017/09/08/kp.html

On 6th September 2017, the value of kp index = 4 is found, which is not at the level that affects the satellite navigation system or the radio communication system. Which can be compared according to the level as shown in the following table 9.

Table 9 The potential impact of solar activity on the kp index

Kp index	Severity Level	The effect
9	most intense	The electricity distribution system cannot supply electricity. The transformer is damaged. Problems of receiving and sending satellite signals and tracking satellite positions. The low-frequency radio navigation system will be unusable for many hours.
8	very intense	The power supply is not working correctly. Satellite tracking problems. The disturbed low-frequency radio navigation system
7	intense	Satellite and low frequency radio wave navigation systems may occasionally crash and cause the Aurora phenomenon in the 50 degree latitude region
6	moderate	High frequency radio propagation in high latitudes will reduced signals. Cause the Aurora phenomenon in the 55 degree latitude zone
5	little	Little effect on satellite operation Cause the Aurora phenomenon in the high latitudes

Source: https://www.weather.rtaf.mi.th/climate/SpaceWeather/

CHAPTER IV

RESULT ANALYSIS

This research studied about the movement of high energy particles from the Sun to Earth for the solar event on 6th September 2017. The research is carried out based on the data that is recorded by the SIS instruments on the spacecraft. We analyzed high energy particles of helium, carbon, nitrogen, oxygen and iron at various energy levels. The motion of high energy particles from the Sun are simulated by using Ruffolo 1998 transport equation in C^{++} programming to solve numerical equations on ubuntu operating system.

4.1 The simulation result for the SEP propagation

In the simulation of particle motion, the output results are stored in the file to be used in fitting procedure later. The simulation results of the distribution of carbon particles over time at different energy levels from 7.443– 28.883 MeV/n is shown in figure 38. It is clear from the graph that the particle of higher energy has less flux and takes less distribution time as compared to the low energy particle. The particles with high energy come to the Earth faster than the particles with low energy.

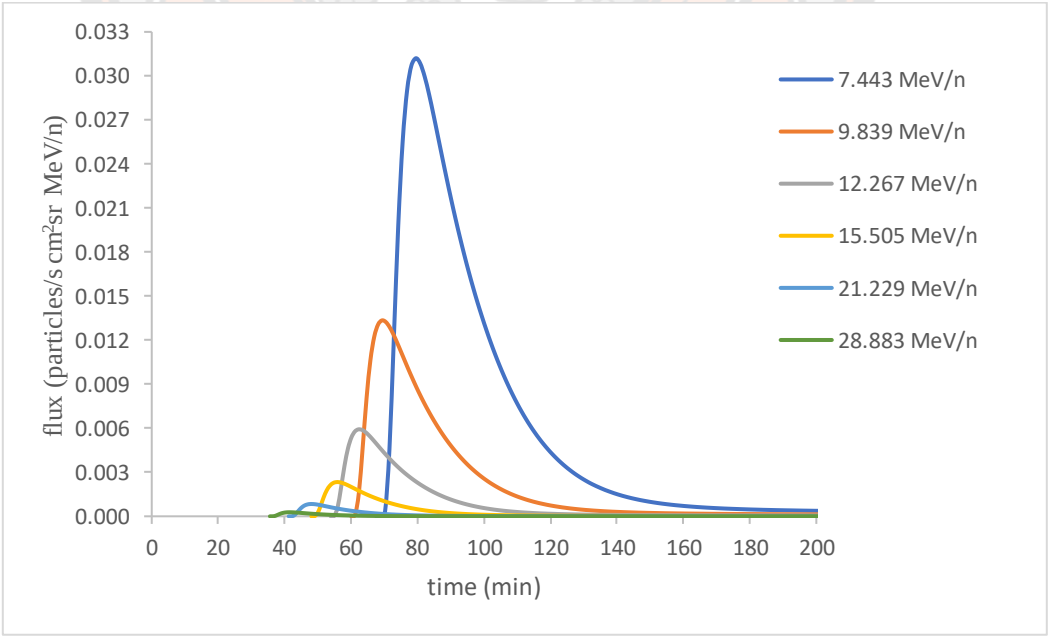

Figure 38 The simulation results of carbon particles distribution over time at different energy levels from 7.443– 28.883 MeV/n.

4.2 Distribution simulation of particles over time at average mean free path(λ).

In the simulation of the particle motion, carbon particle is simulated by the distribution of the particles over time with the various mean free path (λ), which is the distance of particle traveled along the irregular magnetic field lines before it is scattered by the unstable magnetic field lines. The simulation results are given in figure 39.

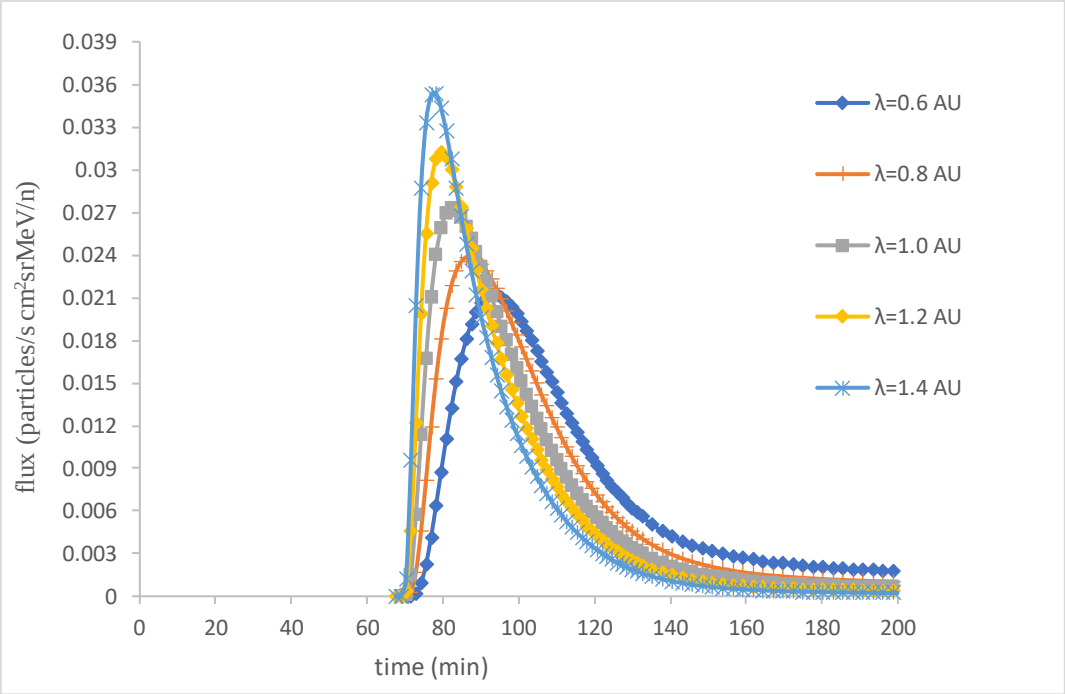

Figure 39 Simulation result of carbon particle distribution at various mean free path on a 12.267 MeV/n energy level.

The carbon particle of flux over time at various mean free paths at the energy level of 12.267 MeV/n is shown in Figure 39. It is clear from the graph that the particles with a high mean free path travels faster to Earth than the particles with a lower mean free path and also particles with a high mean free path were scattered less than a particle with a low mean free path. The particle distribution with low mean free path is diffused wider at peak more than the high mean free path.

4.3 Comparison fitting between the spacecraft data and simulation result.

We can find the injection function of particle moving from the Sun to the Earth by fitting process. The figure 40, 41,42 and 43 represents the data from the spacecraft, simulation result of particle propagation with the best mean free path, the data comparison between the spacecraft and the simulation result from fitting process and injection function of the helium at 4.03 MeV/n.

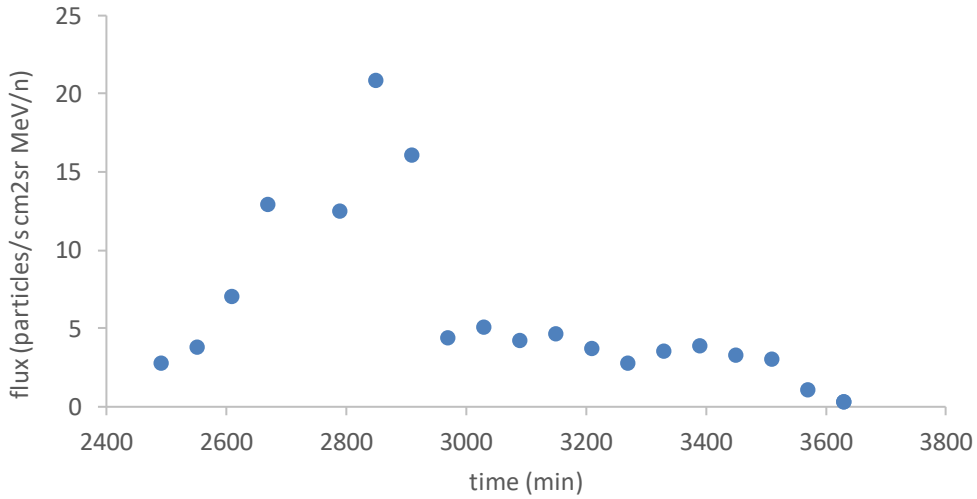

Figure 40 Shows the spacecraft data of He at 4.032 MeV/n for the solar event on 6th September, 2017.

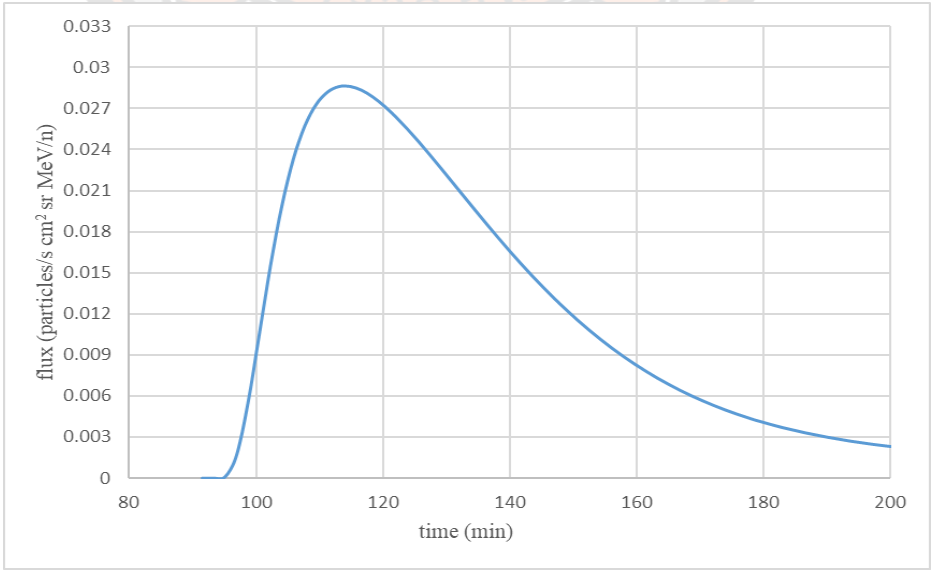

Figure 41 Shows the simulation result of He at 4.032 MeV/n for the solar event on 6th September, 2017.

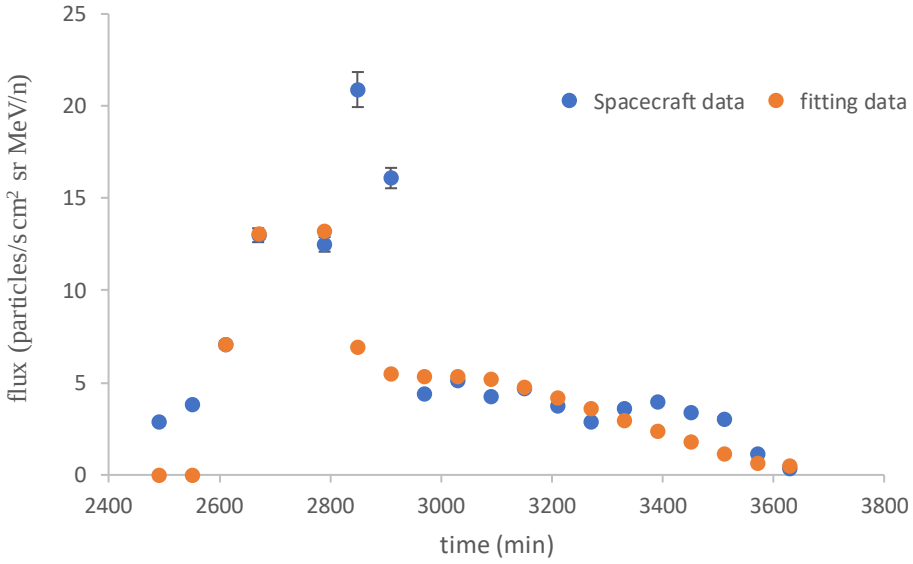

Figure 42 Shows the simulation result of He at 4.032 MeV/n for the solar event on 6th September, 2017.

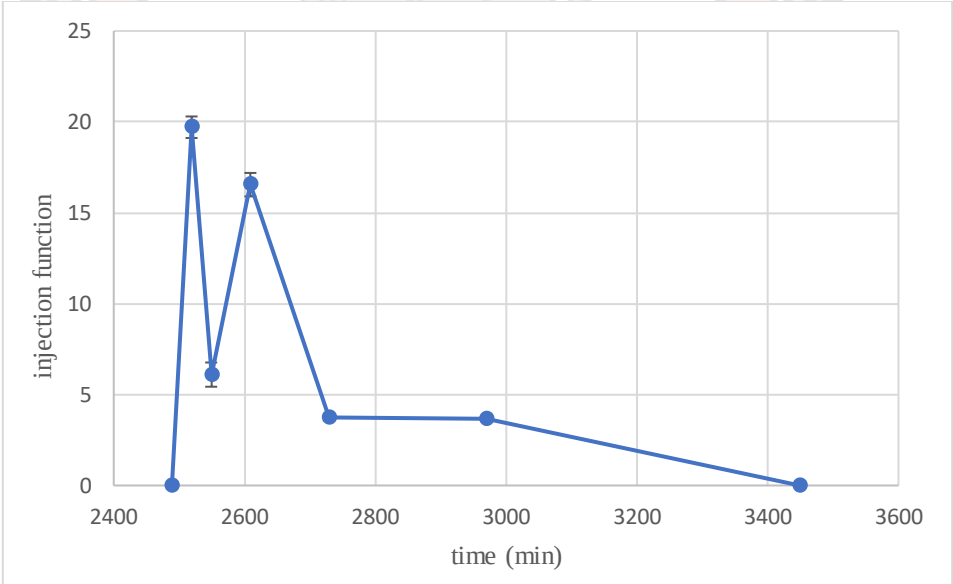

Figure 43 Shows the injection profile of He at 4.032 MeV/n for the solar event on 6th September, 2017.

The figure 44, 45,46 and 47 represents the data from the spacecraft, simulation result of particle propagation with the best mean free path, the data comparison between the spacecraft and the simulation result from fitting process and injection function of the carbon at 7.443 MeV/n.

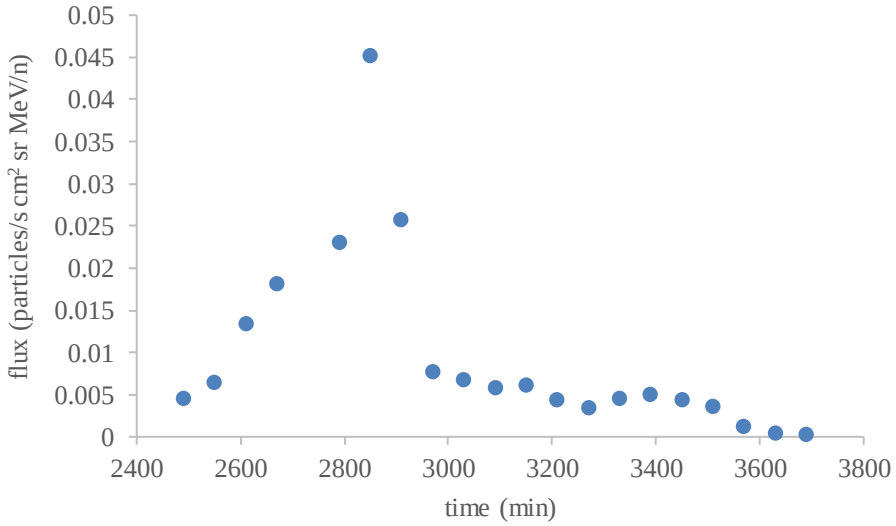

Figure 44 Shows the spacecraft data of C at 7.443 MeV/n for the solar event on 6th September, 2017.

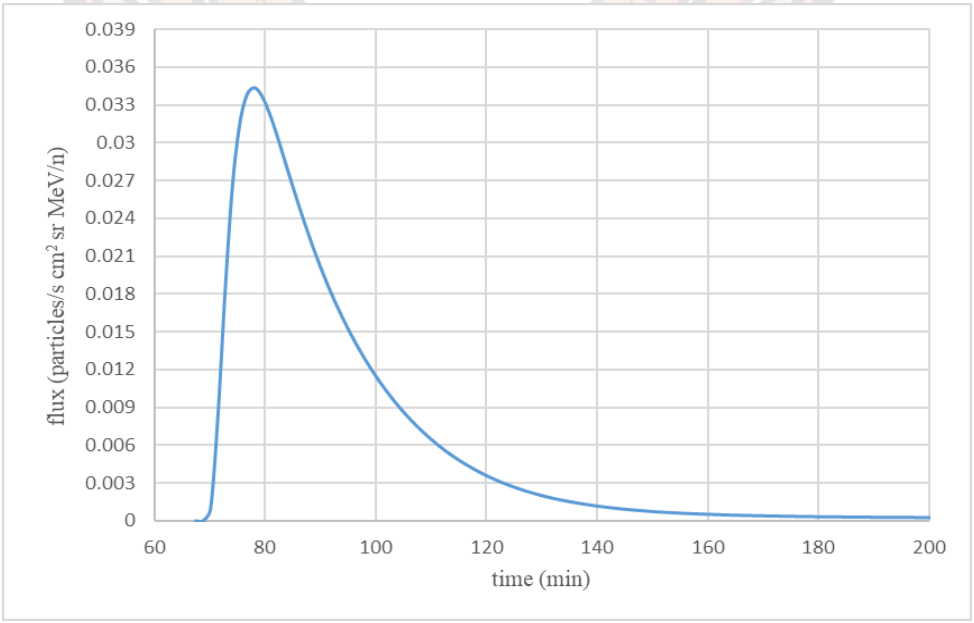

Figure 45 Shows the simulation result of C at 7.443 MeV/n for the solar event on 6th September, 2017.

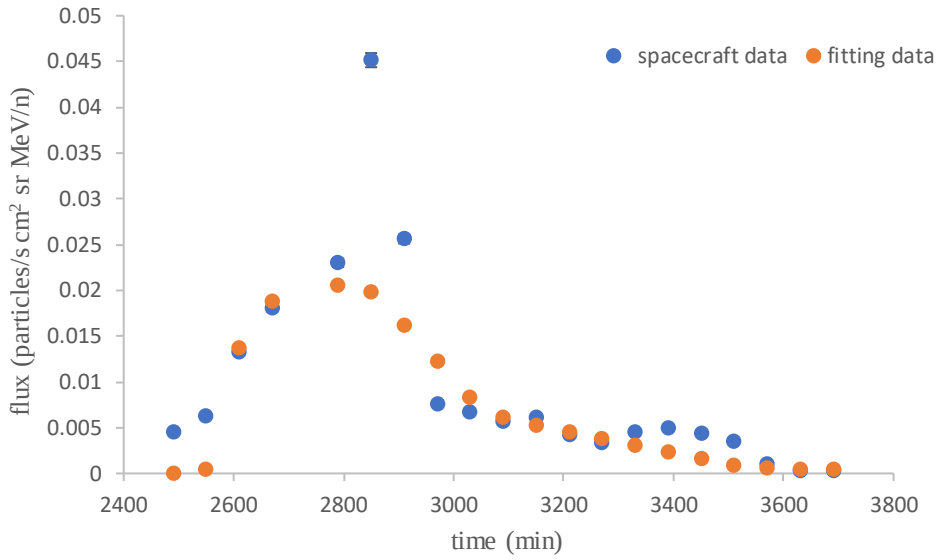

Figure 46 Shows the fitting result of C at 7.443 MeV/n for the solar event on 6th September, 2017.

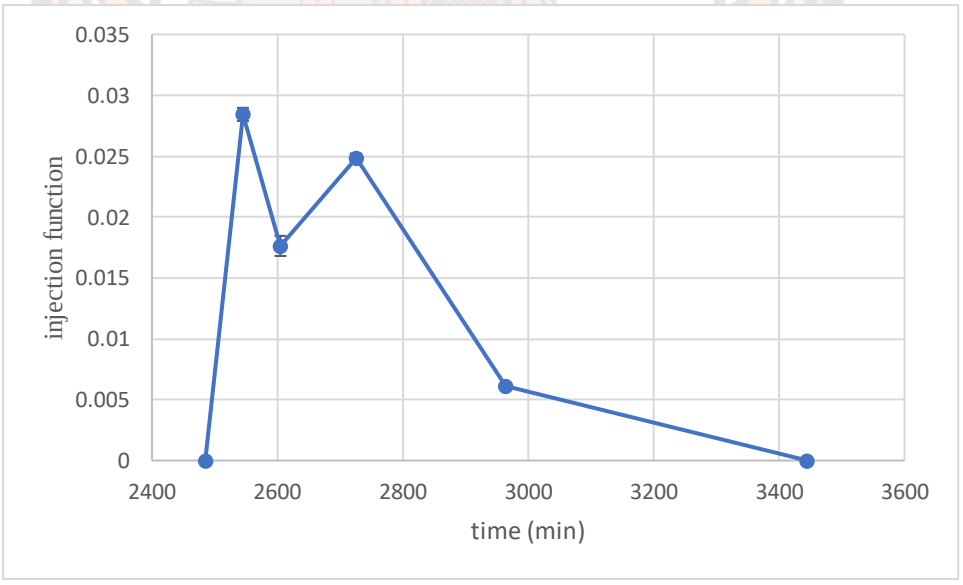

Figure 47 Shows the injection profile of C at 7.443 MeV/n for the solar event on 6th September, 2017.

The figure 48,49,50 and 51 represents the data from the spacecraft, simulation result of particle propagation with the best mean free path, the data comparison between the spacecraft and the simulation result from fitting process and injection function of the oxygen at 8.538 MeV/n.

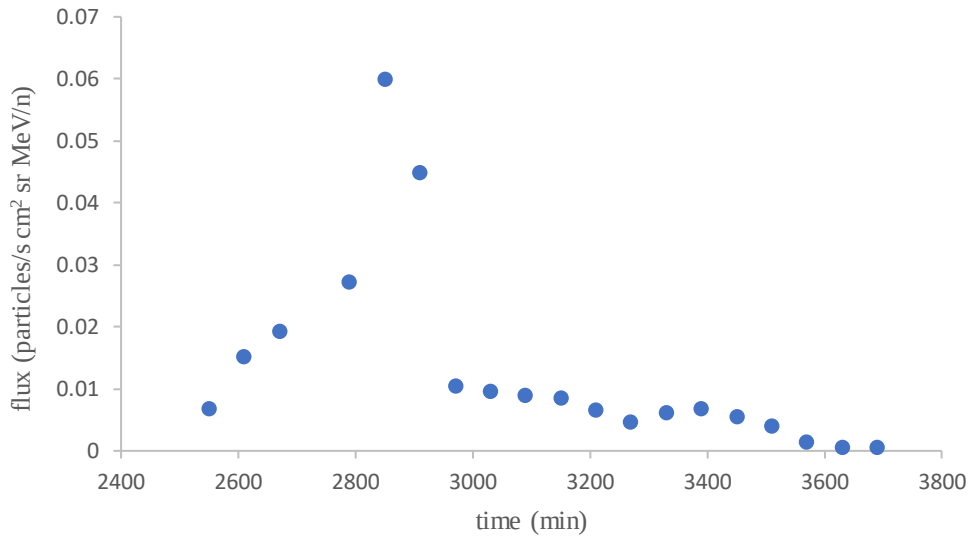

Figure 48 Shows the spacecraft data of O at 8.538 MeV/n for the solar event on 6th September, 2017.

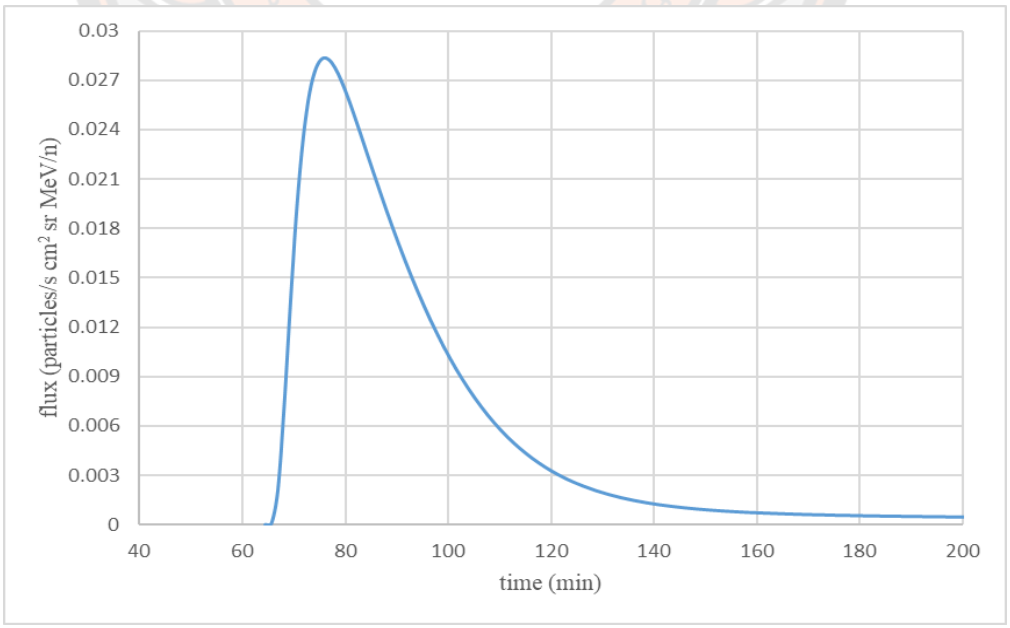

Figure 49 Shows the simulation result of O at 8.538 MeV/n for the solar event on 6th September, 2017.

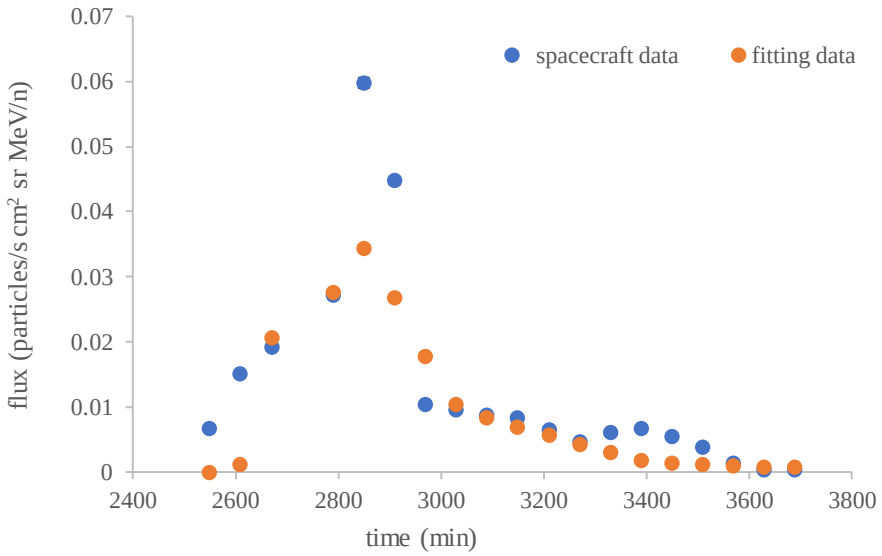

Figure 50 Shows the fitting result of O at 8.538 MeV/n for the solar event on 6th September, 2017.

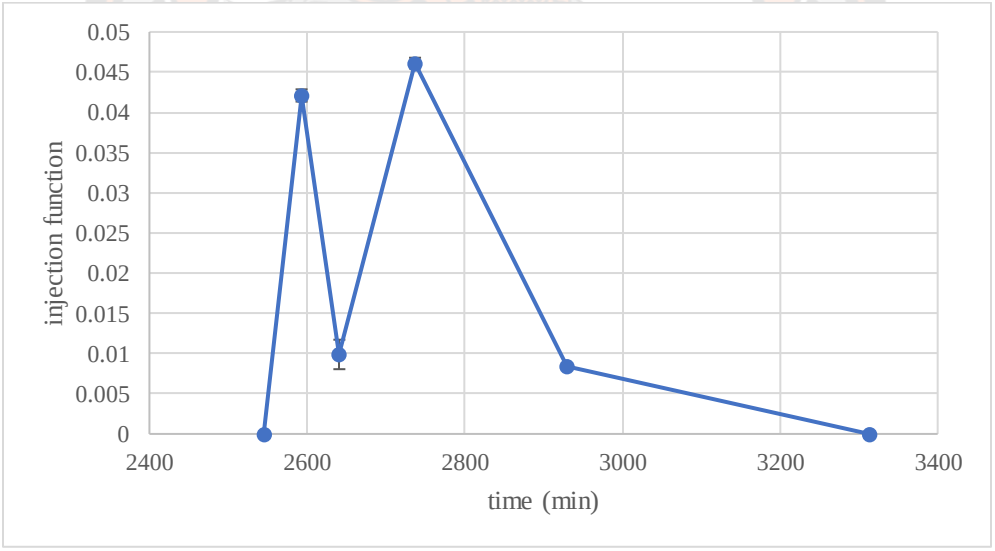

Figure 51 Shows the injection profile of O at 8.538 MeV/n for the solar event on 6th September, 2017.

The figure 52,53,54 and 55 represents the data from the spacecraft, simulation result of particle propagation with the best mean free path, the data comparison between the spacecraft and the simulation result from fitting process and injection function of the nitrogen at 8.009 MeV/n.

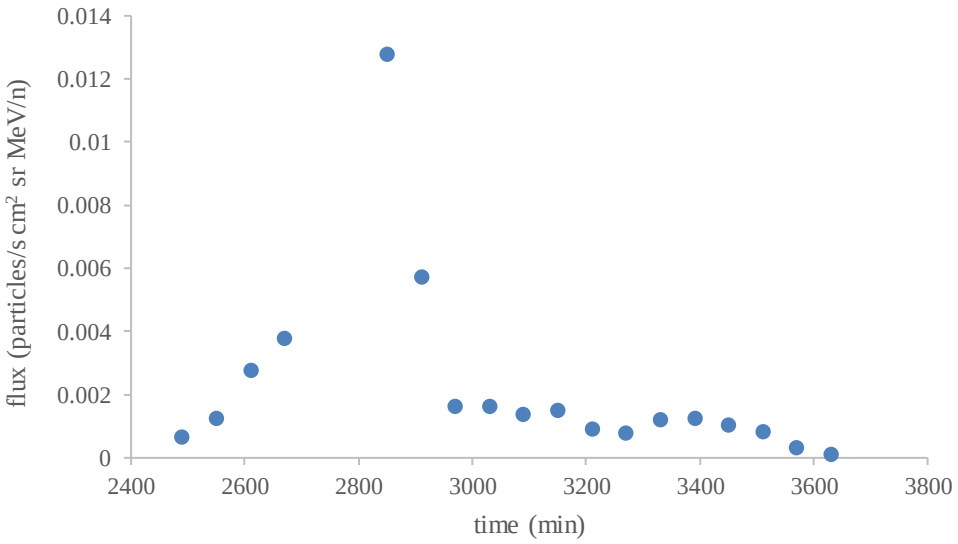

Figure 52 Shows the spacecraft data of N at 8.009 MeV/n for the solar event on 6th September, 2017.

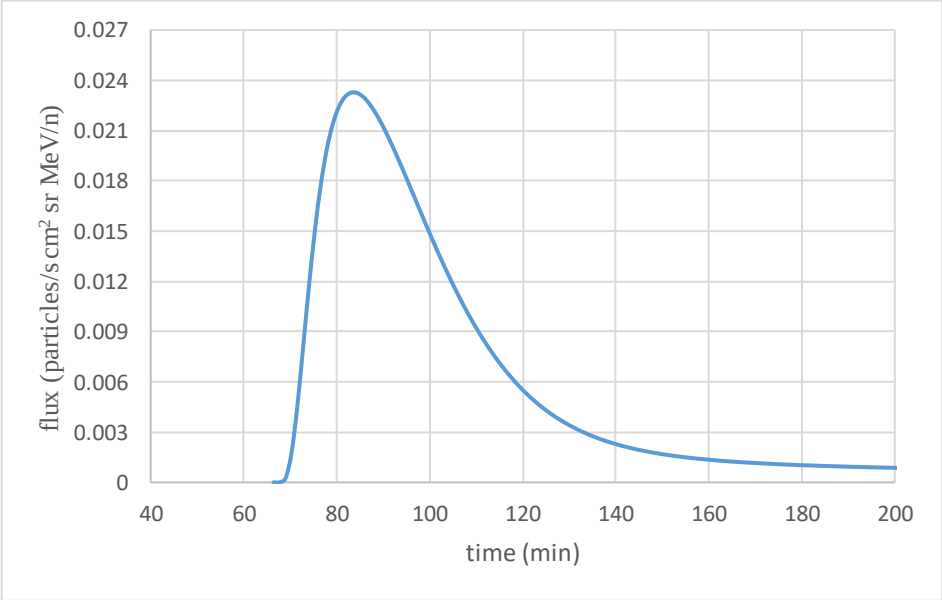

Figure 53 Shows the simulation result of N at 8.009 MeV/n for the solar event on 6th September, 2017.

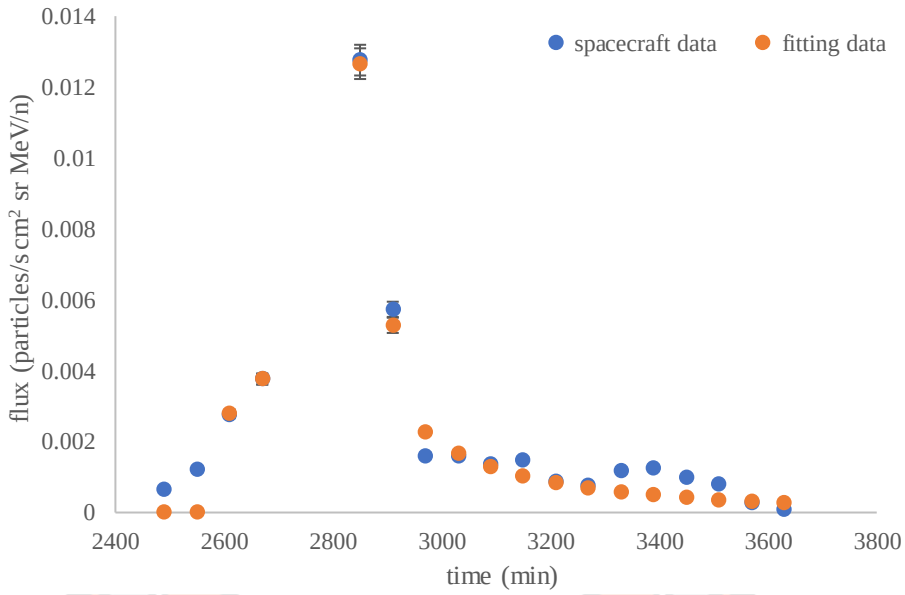

Figure 54 Shows the fitting result of N at 8.009 MeV/n for the solar event on 6th September, 2017.

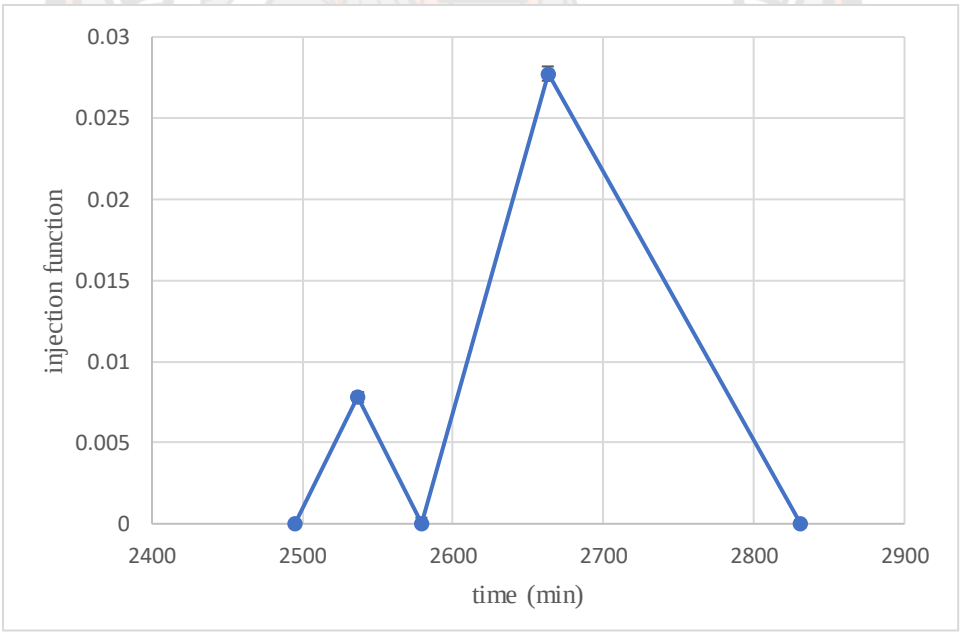

Figure 55 Shows the injection profile of N at 8.009 MeV/n for the solar event on 6th September, 2017.

The figure 56, 57,58 and 59 represents the data from the spacecraft, simulation result of particle propagation with the best mean free path, the data comparison between the spacecraft and the simulation result from fitting process and injection function of the iron at 13.002 MeV/n.

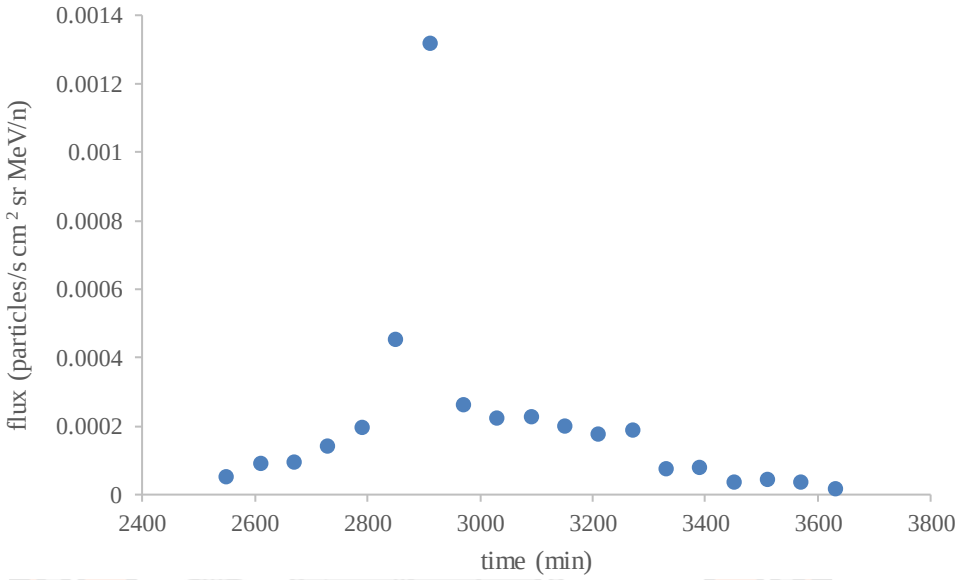

Figure 56 Shows the spacecraft data of Fe at 13.002 MeV/n for the solar event on 6th September, 2017.

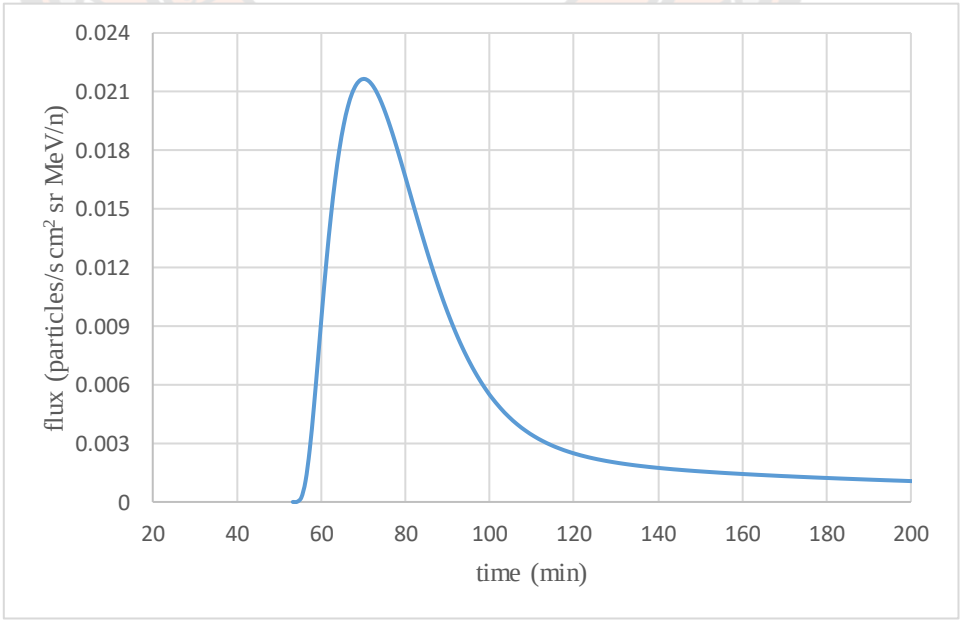

Figure 57 Shows the simulation result of Fe at 13.002 MeV/n for the solar event on 6th September, 2017.

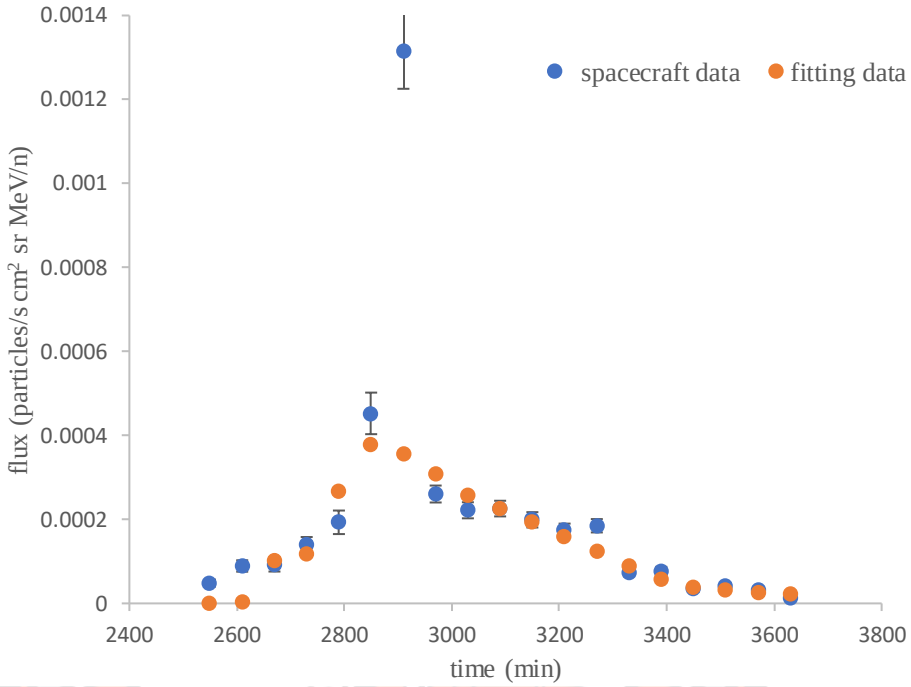

Figure 58 Shows the fitting result of Fe at 13.002 MeV/n for the solar event on 6th September, 2017.

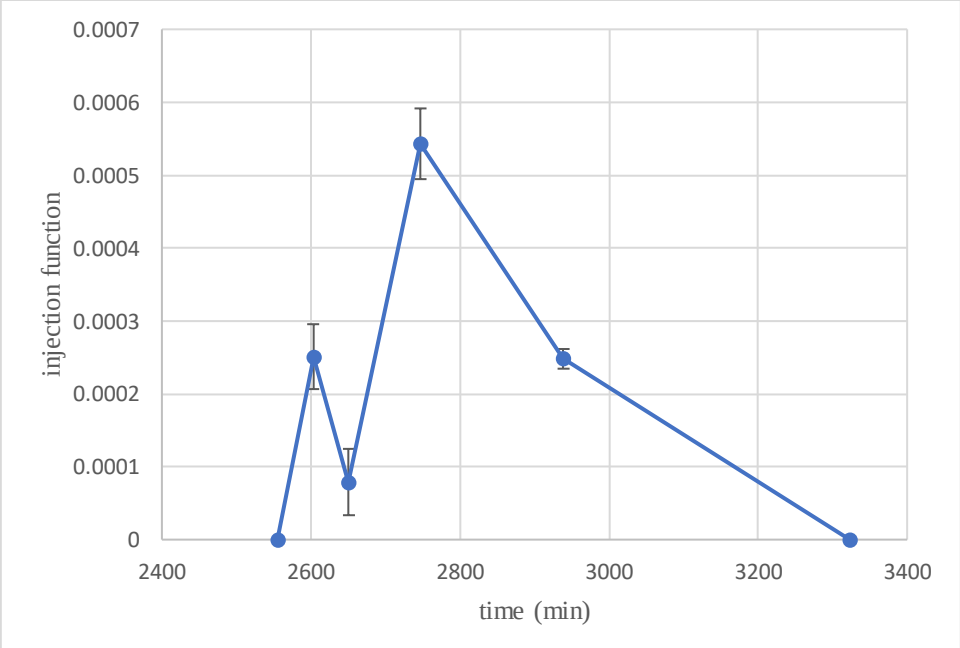

Figure 59 Shows the injection profile of Fe at 13.002 MeV/n for the solar event on 6th September, 2017.

Finally, the fitting result shows the best mean free path for each particle at various energy level in AU and the release time of particle from the Sun to the Earth in minute by the FWHM technique for solar event on 6th September,2017 as shown in table 10.

Table 10 The simulation results of helium, carbon, oxygen, nitrogen and iron.

Element	Energy (MeV/n)	Mean free path (AU)	Release time (min)
Helium	4.032	1.408 ± 0.042	136
	5.390	0.914± 0.076	198
	6.685	1.531± 0.097	171
	8.418	1.532± 0.121	359
	11.493	0.475± 0.143	113
Carbon	7.443	1.350± 0.044	415
	9.839	1.369± 0.053	379
	12.267	1.199± 0.106	233
	15.505	1.795± 0.166	361
	21.229	0.827± 0.106	115
	28.883	1.454± 0.208	39
Oxygen	8.538	1.069± 0.079	281
	11.427	1.717± 0.053	161
	14.293	1.199± 0.106	743
	18.104	0.999± 0.097	128
	24.839	0.863± 0.153	74
	33.847	1.448± 0.496	103
	49.832	0.960± 0.371	232
Nitrogen	8.009	0.805± 0.033	614
	10.660	0.740± 0.085	372
	13.317	0.508± 0.077	141
	16.854	0.657± 0.121	86
	23.096	0.904± 0.022	339
Iron	13.002	0.647± 0.149	330
	18.461	0.371± 0.196	741

The simulation result showed that the helium particles at the energy level of 4.032-11. 493 MeV/n has the mean free path of 0. 475 - 1.532 AU. The middle elements such as carbon, nitrogen and oxygen of energy level from 7.443 – 28.883, 8.009 - 23.096, and 8.538 - 49.832 MeV/n which have the best mean free path from 0.827-1.795, 0.508 - 0.904, and 0.863- 1.717 AU respectively. The time period for releasing high energy particles from the Sun is in the range of 39-743 minutes. From the result it shows that the duration of the release of high energy particles from the Sun decreases as the energy level of the particles increases. The solar energetic particle with the high energy roughly has high mean free path, in which the diffusion of particle will be less, so the injection time of particle will be less than the particle with low energy.

The result from the table 10 of best mean free path and injection time of various energy level is shown in figure 60 and 61.

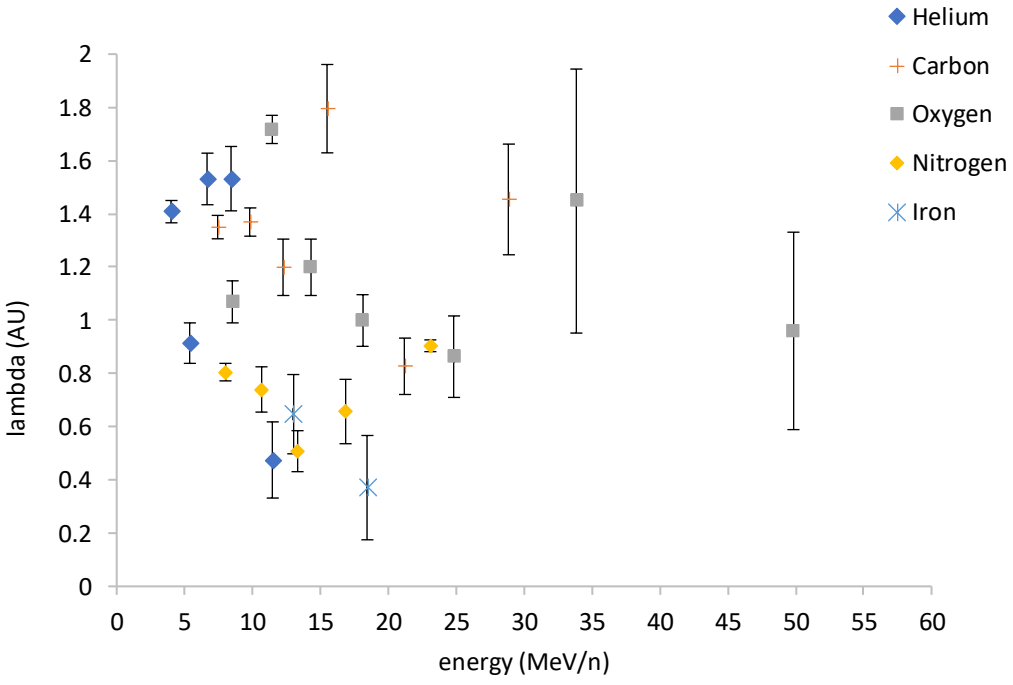

Figure 60 Best mean free path of He, C, O, N and Fe at various energy range of the solar event on September 6,2017.

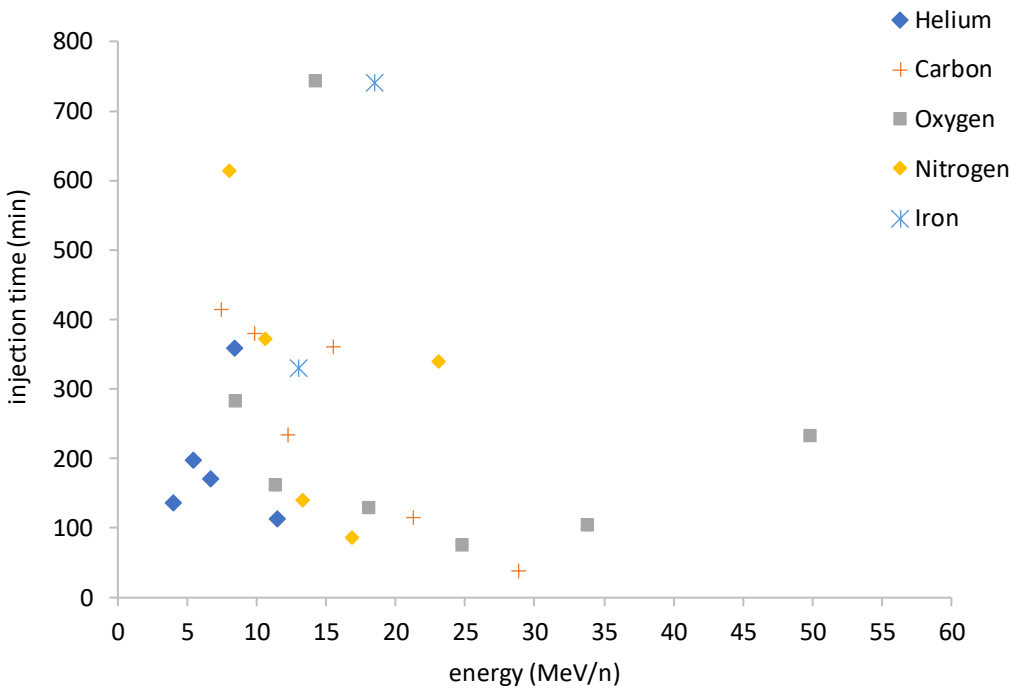

Figure 61 Injection time of He, C, O, N and Fe at various energy range of the solar event on September 6,2017.

CHAPTER V
CONCLUSION

This research is carried out by studying the physical characteristics of solar eruption including the analyzing of the motion of high energy particles from the Sun by using the distribution data obtained from the SIS Instrument on the Advanced Composition Explorer spacecraft. The event of interest is selected based on the changes and phenomena which are determined by the level of intensity of particles traveling to earth. The study is mainly focused on the solar event on 6th September 2017, because it is a violent event based on the X-rays intensity of X9.3 at 12:02 UTC which is the strongest solar flare of the 24th solar cycle. The eruption started at 11:53 UT and ended at 12:10 UT for a duration of 17 minutes. It has erupted at position of S10W30 with a solar wind speed of 575 km/s.

The research analyzed the helium, carbon, oxygen, nitrogen and iron elements and simulated particle motion with Ruffolo transport equation written in the C programming on the Ubuntu operating system. The transport equation of SEPS (solar energetic particles) was solved by the numerical technique of finite different method. The injection duration of mean free path (λ) of the solar event is calculated by using the technique of FWHM method and the results obtained from the simulation of solar energetic particles are compared with actual value of data from the spacecraft.

From the simulation results, it is found that the mean free path (λ) of the selected solar energetic particles is approximately from 0.475 - 1.795 AU. The best mean free path of helium, carbon, nitrogen, oxygen and iron are 0. 475 - 1.532 AU, from 0.827-1.795 AU, 0.508 - 0.904 AU, 0.863- 1.717 AU and 0.371 – 0.647 AU respectively. When the particles are moving along the magnetic field lines, a particle with a high mean free path travels to Earth faster than a particle with a lower mean free path. The particles with high mean free path have less scattering or diffusion than particles with lower mean free path. The eruption on 6th September 2017 was followed by corona mass ejection, causing the acceleration of particles in space. The coronal mass injection was detected at the end time of this flare that affects in increasing the injection time. This solar event occurs at 11:53 – 12:10 UT, and we found the CME effect in space at 12:01 UT and 12:02 UT with radio type IV and type II respectively.

The time for releasing high energy particles from the Sun to Earth is in the range of 39-743 minutes, while the injection time of SEPs from X-ray duration is 17 minutes. Therefore, it takes longer time to travel from the Sun to Earth than the heavier and more energetic particles. The injection time of helium from the fitting result are fluctuating, whereas the middle elements such as carbon, nitrogen and oxygen's injection time is found to be decreased as the energy level increases. Particles with high energy travel to Earth faster than particles with low energy. The error of these results depends on the number of the detected particles from spacecraft. So, the detected particle at highest energy is less which it makes the high error. The number of high-energy particles count is less than those with low energy level.

The simulation and fitting result are longer than the injection time on the Sun, as the effect of CME and the number of the detected particles affecting the injection time. We can see the effect of this flare to the Earth by the kp- index of this flare is 4, that means it does not affect the Earth. Where kp-index describes the disturbance of the Earth's magnetic field caused by the solar wind. The study of space conditions found that the eruption did not affect the world. The value of kp -index has increased to 8 on 7^{th} and 8^{th} September, 2017 due to another solar event occurred from same sunspot region where aurora was appeared in United States, France, Kazakhstan, Australia and many other countries and affected satellites, GPS, and power grids.

The graph that is obtained from the neutron monitor is correspond to data from the ACE spacecraft and it takes a time approximately one and half day before it gets effect of solar flare. The number of particles that detect by neutron monitor will decrease because of solar flare and particles from the other sources.

REFERENCES

Augusto, C., Navia, C., de Oliveira, M., Nepomuceno, A., Fauth, A., Kopenkin, V., & Sinzi, T. (2018). Relativistic Proton Levels from Region AR 12673 (GLE# 72) and the Heliospheric Current Sheet as a Sun–Earth Magnetic Connection. Publications of the Astronomical Society of the Pacific, 131(996), 024401.

California Institute of Technology. (2007,November 28). The Solar Isotope Spectrometer. Retrieved from http://www.srl.caltech.edu/ACE/CRIS_SIS/sis.html

Earthquake Prediction. (2017,July 2). What is Coronal Mass Ejection? (CME). Retrieved from http://www.earthquakepredict.com/2017/07/what-is-coronal-mass-ejection-cme.html

Learning center for Earth Science and Astronomy. (2020, November 10). The Sun. Retrieved from http://www.lesa.biz/astronomy/solar-system/sun

Paluk, P., Khumlumlert, T., Kanlayaprasit, N., & Aiemsa-ad, N. (2017). The solar energetic particle propagation of solar flare events on 24 th solar cycle. Paper presented at the Journal of Physics. Conference Series (Online).

Pande, B., Pande, S., Chandra, R., & Mathpal, M. C. (2018). Solar flares, CMEs and solar energetic particle events during solar cycle 24. Advances in Space Research, 61(2), 777-785.

Ruffolo, D., Khumlumlert, T., & Youngdee, W. (1998). Deconvolution of interplanetary transport of solar energetic particles. Journal of Geophysical Research: Space Physics, 103(A9), 20591-20602.

Ruffolo, D., Tooprakai, P., Rujiwarodom, M., Khumlumlert, T., Wechakama, M., Bieber, J. W., . . . Pyle, R. (2006). Relativistic solar protons on 1989 October 22: Injection and transport along both legs of a closed interplanetary magnetic loop. The Astrophysical Journal, 639(2), 1186.

Sharing Earth Observation Resources. (2020, November 13). ACE (Advanced Composition Explorer). Retrieved from https://directory.eoportal.org/web/eoportal/satellite-missions/content/-/article/ace

Space place. (2020, November 11). What is solar cycle? Retrieved from https://spaceplace.nasa.gov/solar-cycles/en/

Su, Y. (2007). Magnetic Shear in Two-ribbon Solar Flares. Purple Mountain Observatory Nanjing.

Tassev, Y., Velinov, P. I., Tomova, D., & Mateev, L. (2017). Analysis of Extreme Solar Activity in Early September 2017: G4–Severe Geomagnetic Storm (07÷ 08.09) and GLE72 (10.09) in Solar Minimum. Compt. rend. Acad. bulg. Sci, 70(10), 1437-1444.

APPENDIX

Appendix A: Comparison fitting between the spacecraft data and simulation result

The figure 1,2,3 and 4 represents the data from the spacecraft, simulation result of particle propagation with the best mean free path, the data comparison between the spacecraft and the simulation result from fitting process and injection function of the helium at 8.428 MeV/n.

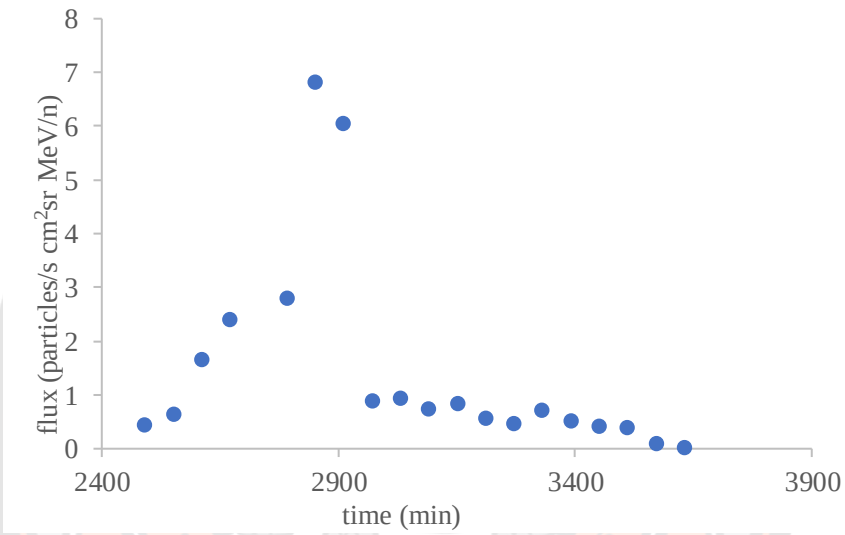

Figure 1 Shows the spacecraft data of He at 8.428 MeV/n for the solar event on 6th September, 2017.

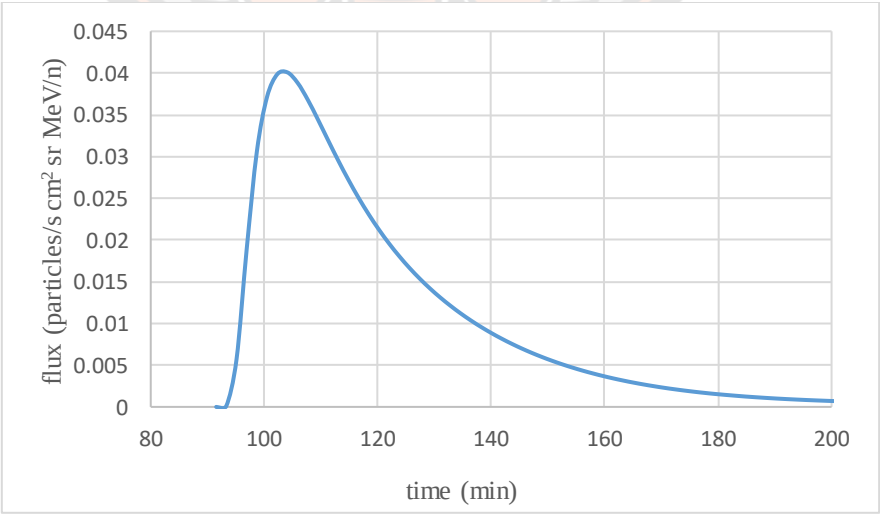

Figure 2 Shows the simulation result of He at 8.428 MeV/n for the solar event on 6th September, 2017.

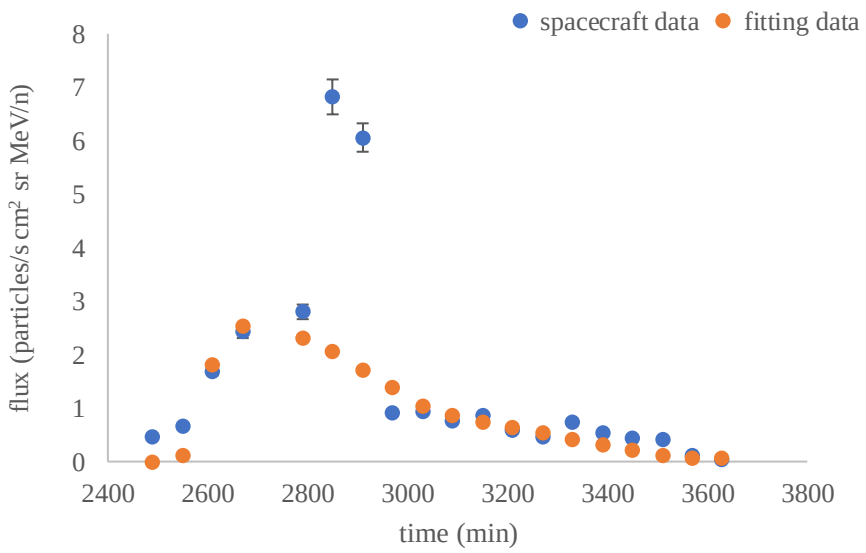

Figure 3 Shows the fitting result of He at 8.428 MeV/n for the solar event on 6th September, 2017.

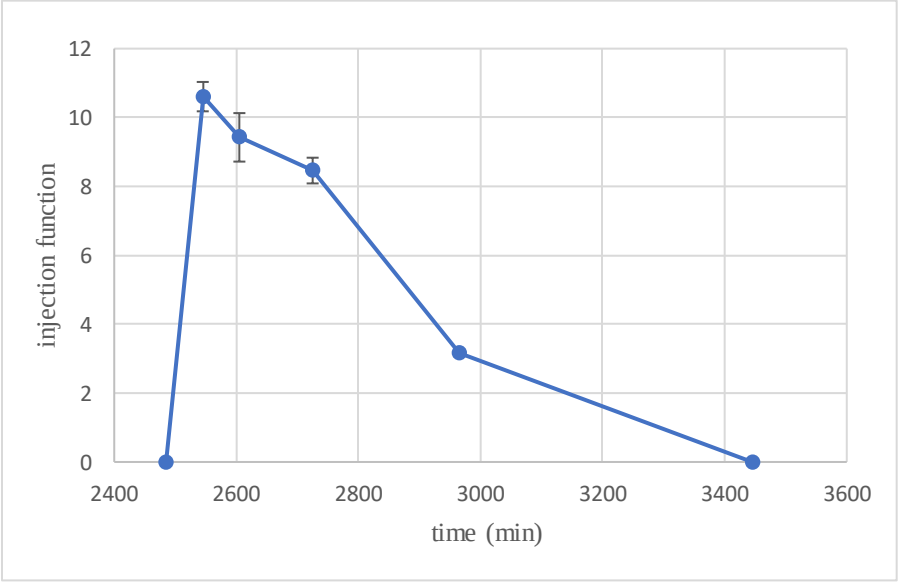

Figure 4 Shows the injection profile of He at 8.428 MeV/n for the solar event on 6th September, 2017.

The figure 5,6,7 and 8 represents the data from the spacecraft, simulation result of particle propagation with the best mean free path, the data comparison between the spacecraft and the simulation result from fitting process and injection function of the carbon at 9.839 MeV/n.

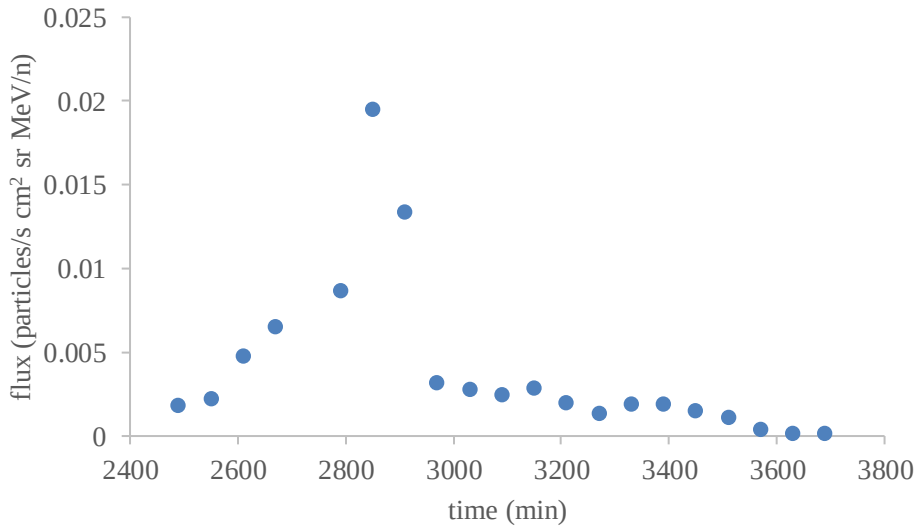

Figure 5 Shows the spacecraft data of C at 9.839 MeV/n for the solar event on 6th September, 2017.

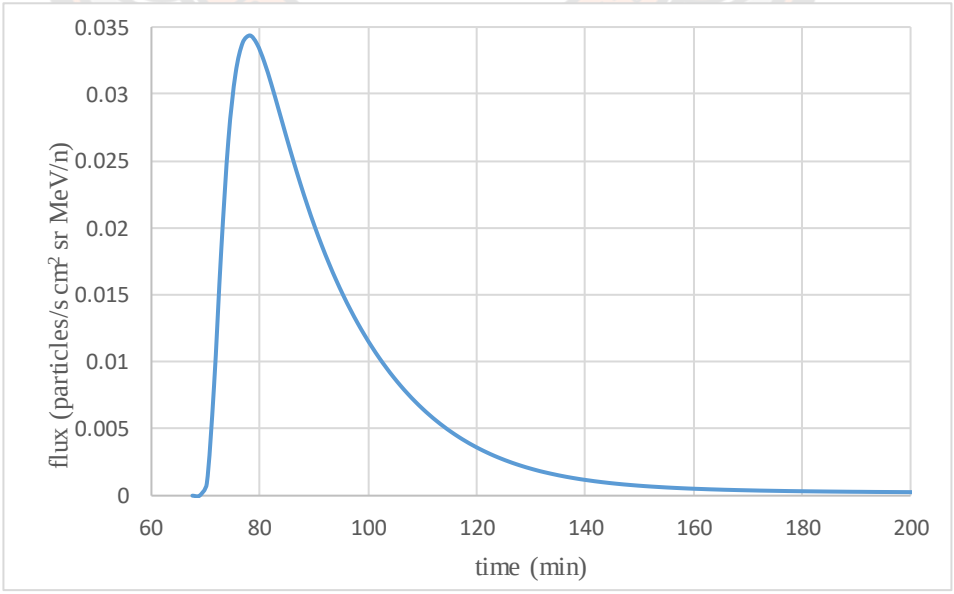

Figure 6 Shows the simulation result of C at 9.839 MeV/n for the solar event on 6th September, 2017.

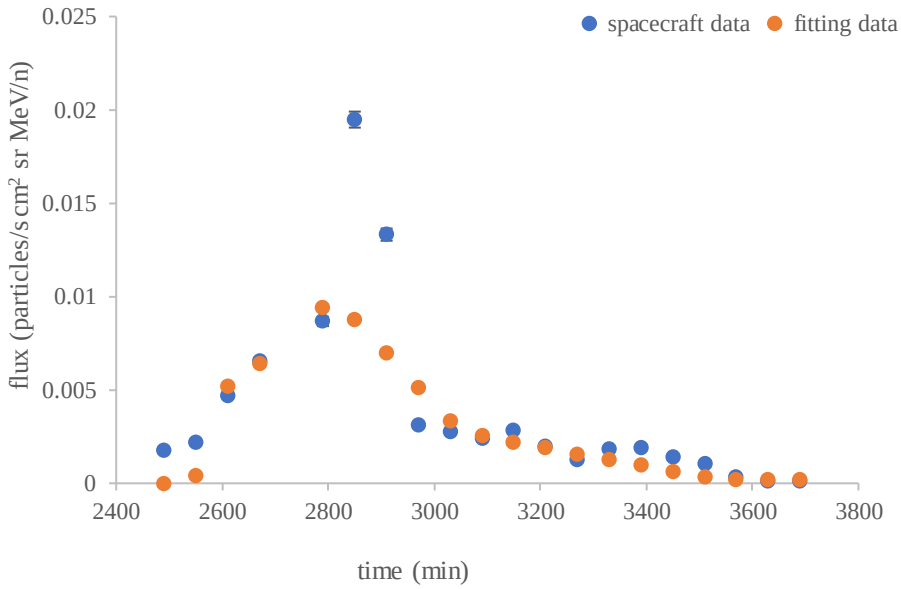

Figure 7 Shows the fitting result of C at 9.839 MeV/n for the solar event on 6th September, 2017.

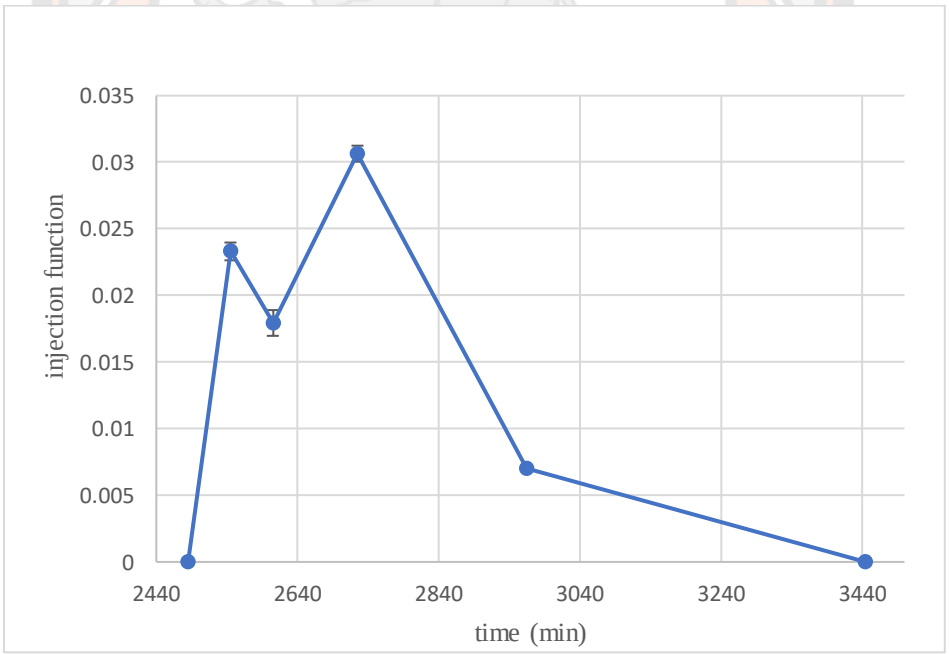

Figure 8 Shows the injection profile of C at 9.839 MeV/n for the solar event on 6th September, 2017.

The figure 9,10,11 and 12 represents the data from the spacecraft, simulation result of particle propagation with the best mean free path, the data comparison between the spacecraft and the simulation result from fitting process and injection function of the oxygen at 14.293 MeV/n.

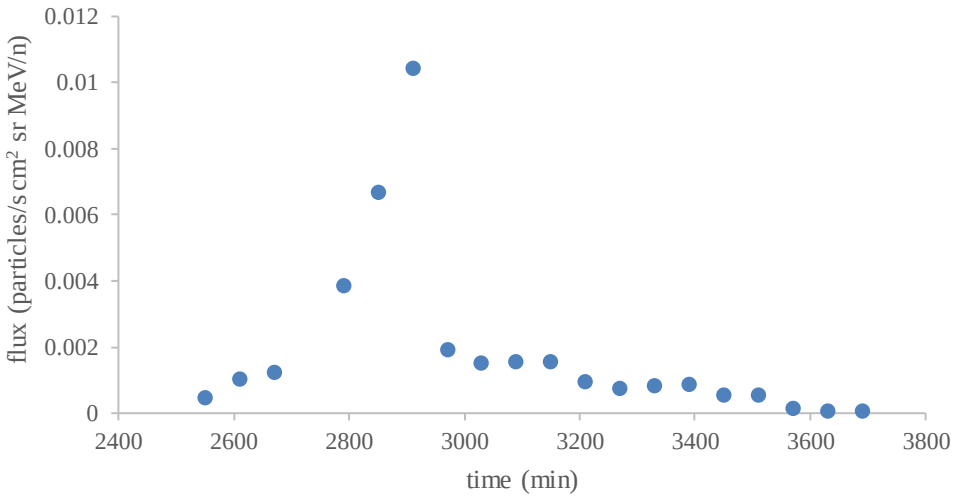

Figure 9 Shows the spacecraft data of O at 14.293 MeV/n for the solar event on 6th September, 2017.

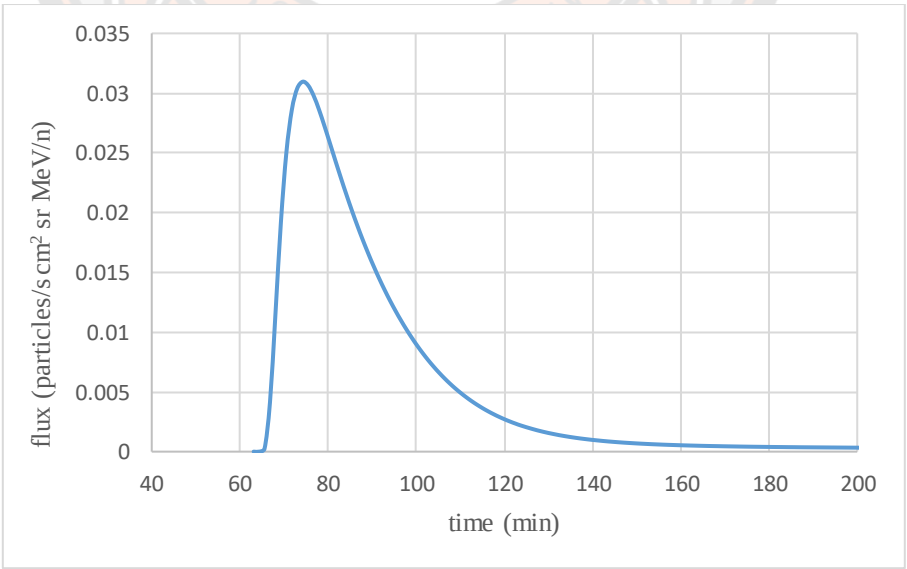

Figure 10 Shows the simulation result of O at 14.293 MeV/n for the solar event on 6th September, 2017.

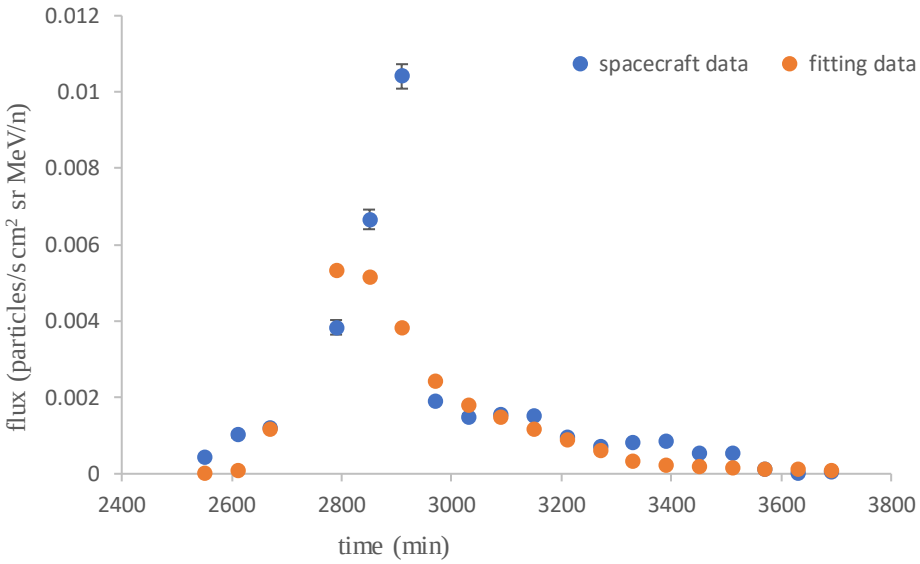

Figure 11 Shows the fitting result of O at 14.293 MeV/n for the solar event on 6th September, 2017.

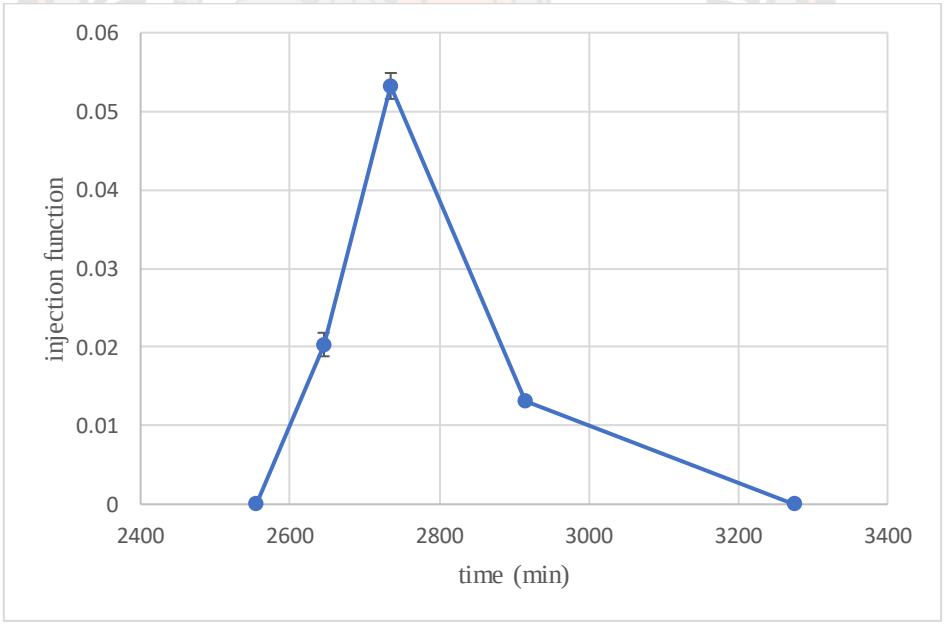

Figure 12 Shows the injection profile of O at 14.293 MeV/n for the solar event on 6th September, 2017.

The figure 13,14,15 and 16 represents the data from the spacecraft, simulation result of particle propagation with the best mean free path, the data comparison between the spacecraft and the simulation result from fitting process and injection function of the nitrogen at 16.854 MeV/n.

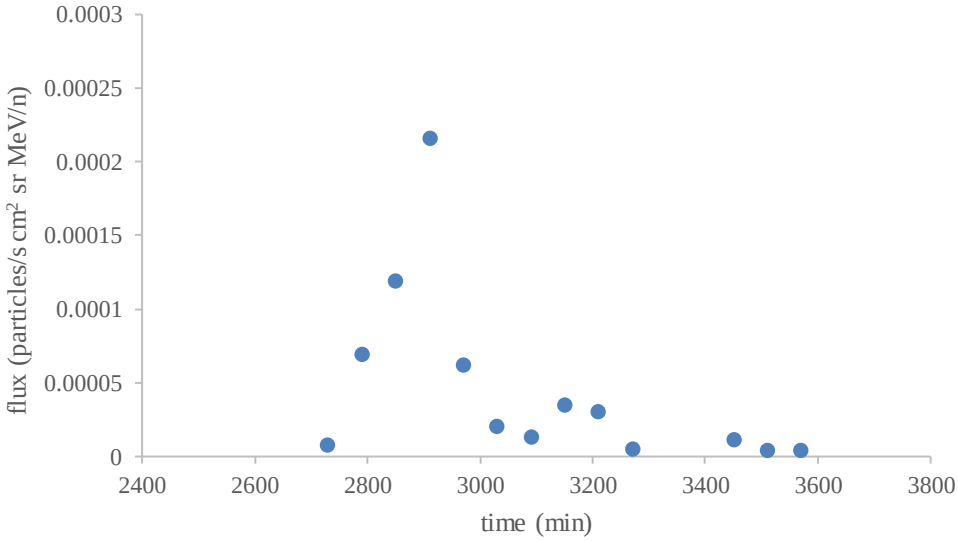

Figure 13 Shows the spacecraft data of N at 23.096 MeV/n for the solar event on 6th September, 2017.

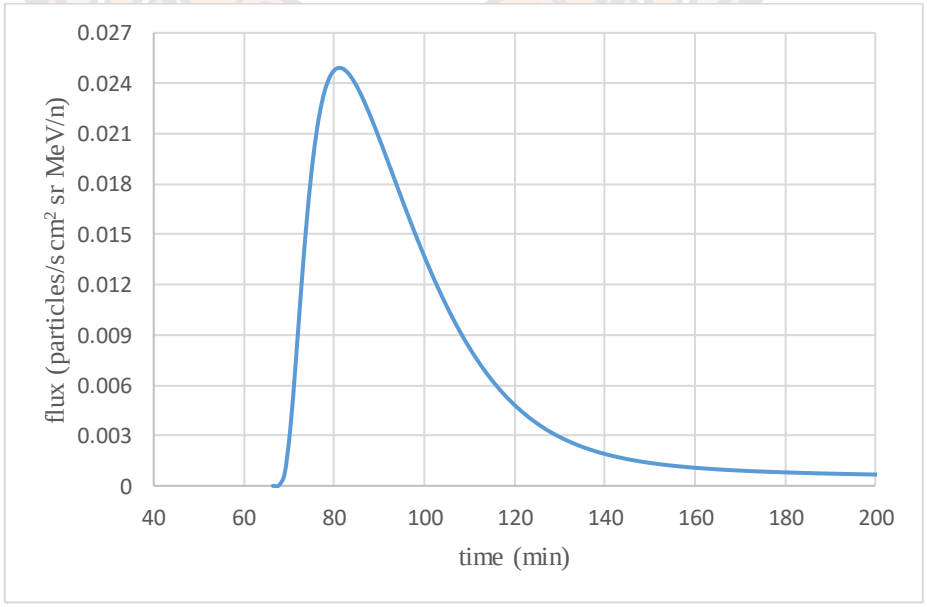

Figure 14 Shows the simulation result of N at 23.096 MeV/n for the solar event on 6th September, 2017.

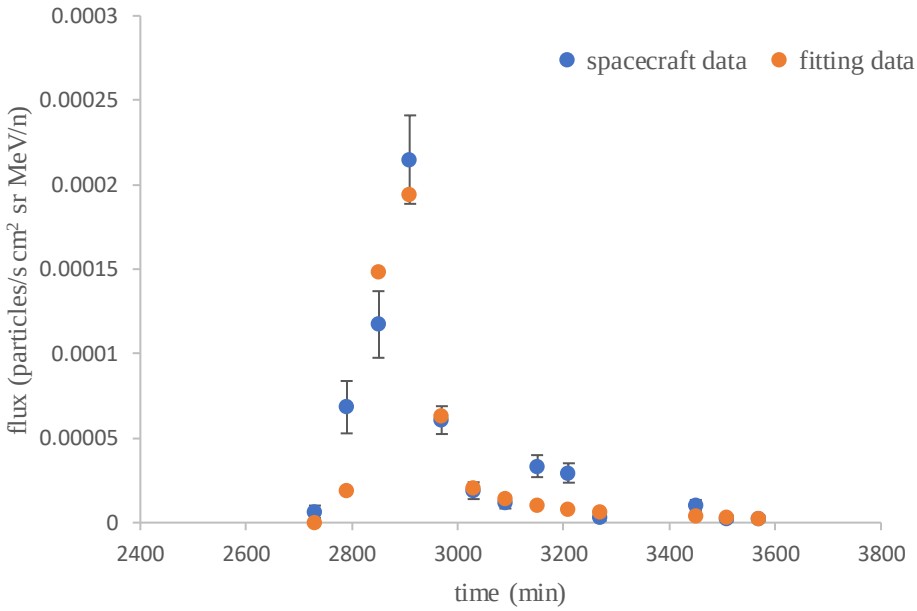

Figure 15 Shows the fitting result of N at 23.096 MeV/n for the solar event on 6th September, 2017.

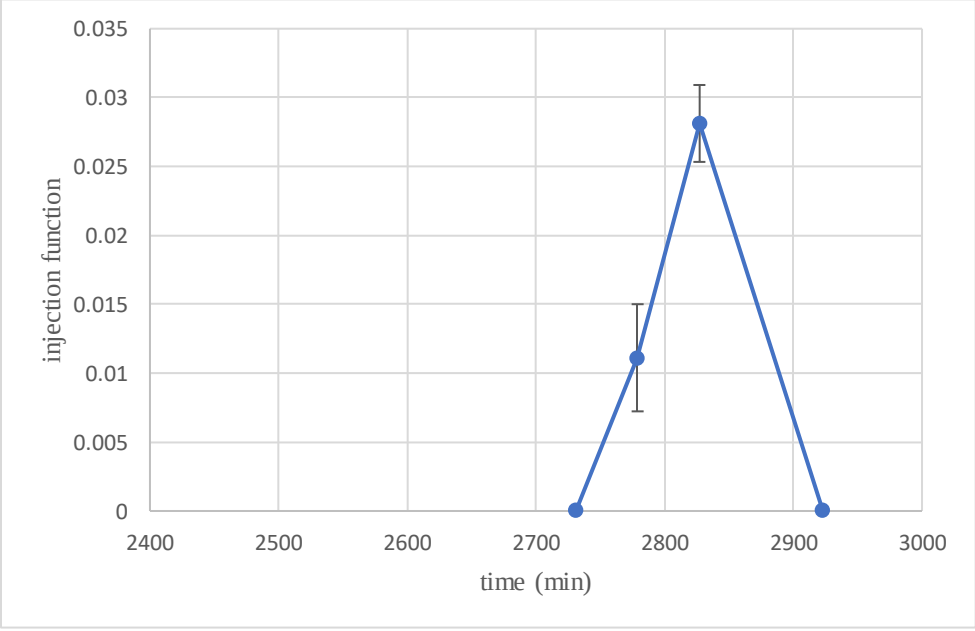

Figure 16 Shows the injection profile of N at 23.096 MeV/n for the solar event on 6th September, 2017.

The figure 17,18,19 and 20 represents the data from the spacecraft, simulation result of particle propagation with the best mean free path, the data comparison between the spacecraft and the simulation result from fitting process and injection function of the iron at 18.461 MeV/n.

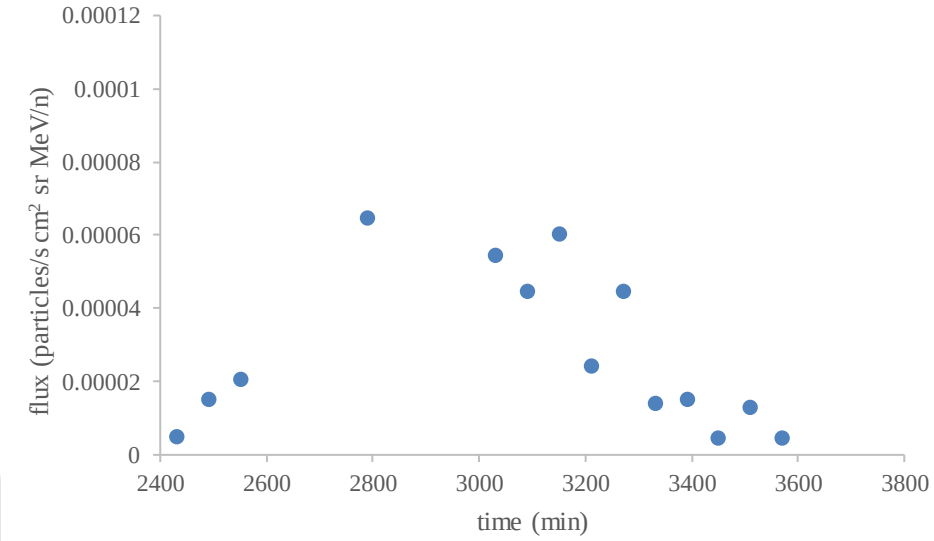

Figure 17 Shows the spacecraft data of Fe at 18.461 MeV/n for the solar event on 6th September, 2017.

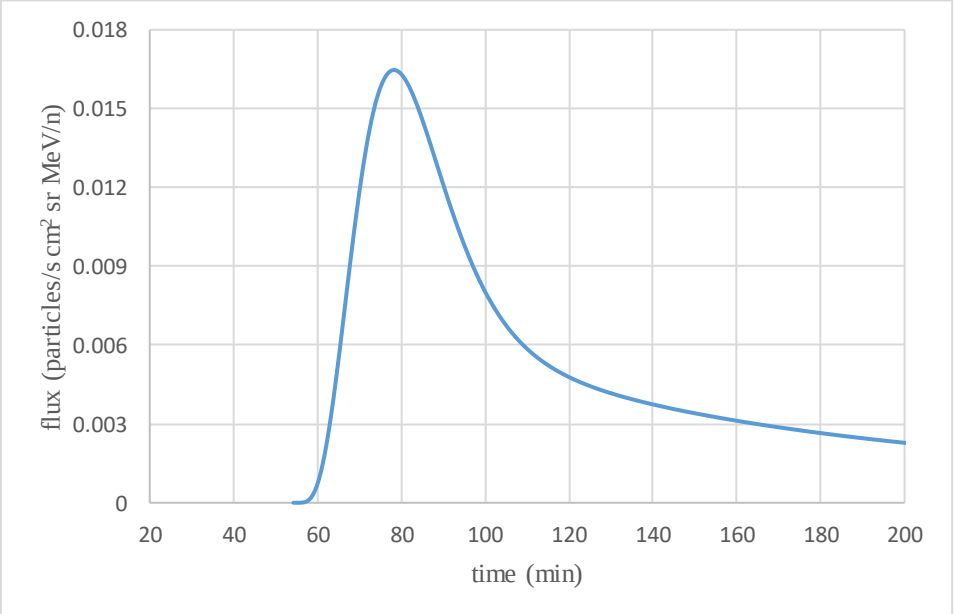

Figure 18 Shows the simulation result of Fe at 18.461 MeV/n for the solar event on 6th September, 2017.

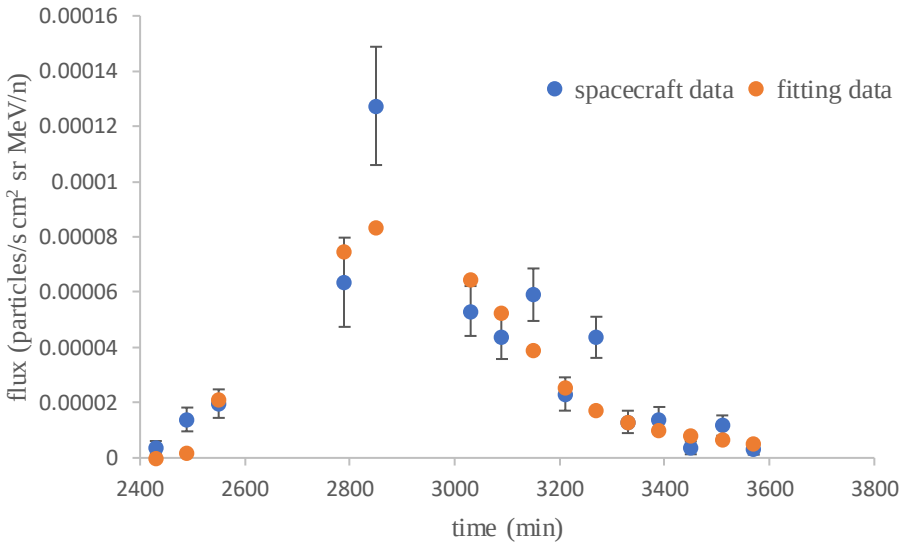

Figure 19 Shows the fitting result of Fe at 18.461 MeV/n for the solar event on 6th September, 2017.

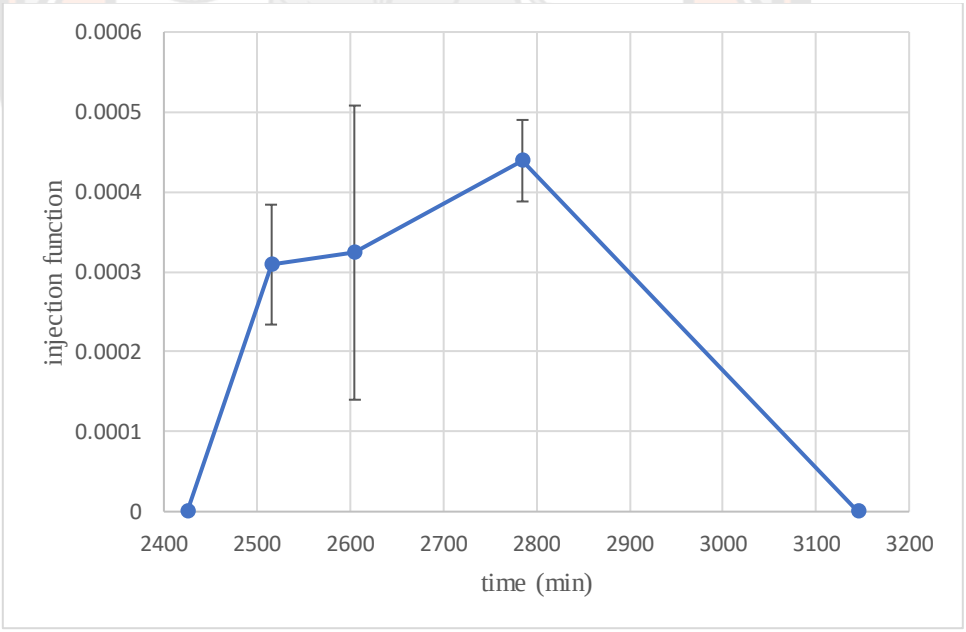

Figure 20 Shows the injection profile of Fe at 18.461 MeV/n for the solar event on 6th September, 2017.

Appendix B: Neutron monitor data

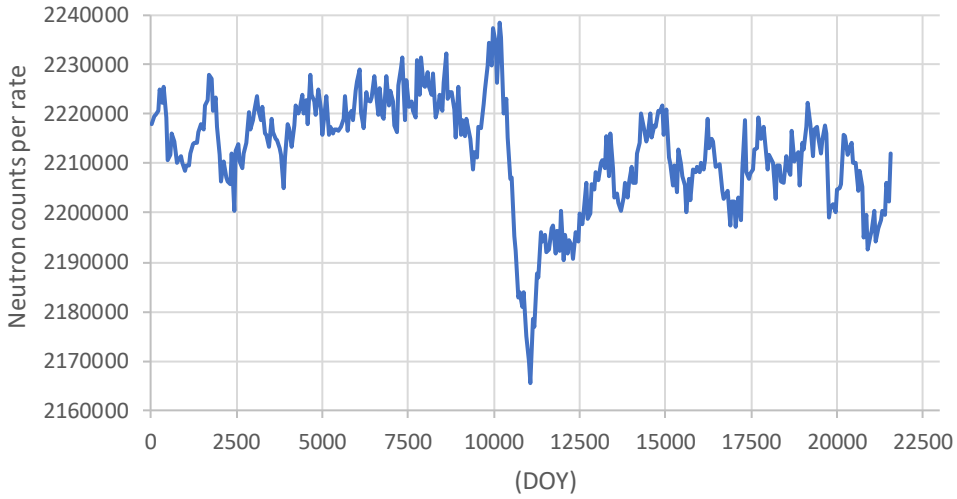

Figure 21 Shows the counts of neutron monitor particle from Sirindhorn Neutron Monitor station on Doi Inthanon, Chiang Mai, Thailand on 1-15 September,2017.

Figure 22 Shows the picture of Princess Sirindhorn Neutron Monitor at Chiang Mai.